NANOCHEMISTRY FOR BIOMEDICAL SENSORS AND CONTRAST AGENTS

By

Thomas D. Horvath

A dissertation submitted in partial fulfillment
of the requirements for the degree of
Doctor of Philosophy
(Chemistry)
In The University of Michigan
2008

Doctoral Committee:

Professor Raoul Kopelman, Chair
Professor Michael D. Morris
Professor Roseanne J. Sension
Associate Professor Nils G. Walter
Associate Professor Jens-Christian Meiners

Learning is about those that have come before us, and try so desperately to teach us the way, even when we are unwilling to learn. Teaching is about trying to show those that follow, and learn to have the patience when they are so desperately trying to not be taught.

Paul S. Horvath (May 13, 1939 – February 18, 2005)
Adelaide E. Horvath (January 29, 2004)

To Susan and Addie; I thank you for understanding.

Acknowledgements

I would like to thank Al Potratz, Kirk Barnes, Dr. Donald Phillips, Dr. Ross Nord, Dr. Roger Hayes, Dr. Timothy Brewer, Dr. Heather Holmes, and Dr. Raoul Kopelman. I would also like to thank my committee members, Dr. Michael Morris, Dr. Roseanne Sension, Dr. Chris Meiners, and Dr. Nils Walter. Without your support and understanding I most certainly would not have made the journey to this point of my academic career.

I would like to express my gratitude to Dr. Brandon McNaughton, Dr. Jeffery Anker, Dr. Rodney Agayan, Dr. Matt King, and (soon to be) Dr. Gwangseong Kim. We have spent countless hours talking about science, good and bad, applicable and not, and usually over a cup of joe. I thank you!

I would like to thank Dr. Maria Moreno, Dr. Eric Monson, and Dr. Sunil Dourado for guidance during the "early years", and Dr. Shai Ashkenazi for the fruitful collaboration.

To my friends Nate & Stacey, Mike & Hannah, Dave & Ashley, Ted & Judy, Todd & Kim, Doug, Johnny, and Steve – for giving me the support, advice, and encouragement to complete what I started many years ago. I thank you.

My most heartfelt thanks and words of gratitude are reserved for my wife Susan and my daughter Adelaide. With the hugs and kind words that you both provide, I feel as though I can accomplish anything. I appreciate the patience and understanding you both have exhibited with me during my pursuit of the Ph.D. Thank you for all the good times that we have shared and will share in the future. I cannot think of two other people on this planet that I would rather spend time with. Thanks for everything.

TABLE OF CONTENTS

LIST OF FIGURES

LIST OF TABLES

ABSTRACT

NANOCHEMISTRY FOR BIOMEDICAL SENSORS AND CONTRAST AGENTS

by

Thomas D. Horvath

Chair: Raoul Kopelman

The primary focus of the work described in this dissertation is the coupling of PEBBLE (Photonic Explorers for Biomedical use by Biologically Localized Embedding) nanosensors with new sensing technologies.

Included in this body of work is the application of fluorescence anisotropy based measurements to PEBBLE nanosensors, in order to measure analyte concentrations. The advantage of the fluorescence anisotropy technique is that it is a self-referencing measurement; therefore the process of designing fluorescence based nanosensors is streamlined. Separate measurements were performed on poly (acrylamide) PEBBLEs with embedded Calcium Green and Newport Green indicator dyes in order to sense $Ca^{2+}_{(aq.)}$ and $Zn^{2+}_{(aq.)}$, respectively. A sol-gel PEBBLE with the embedded $[Ru(dpp)_3]^{2+}$ indicator dye was used to make O_2 measurements in a sealed gas-tight optical cell.

A second sensing technique investigated utilizes a new photoacoustic based sensing method that utilizes the pH-sensitive fluorescent indicator dye SNARF-5F. In the experiment, the photoacoustic response of a series of solutions, with the indicator dye dissolved in buffers that ranged in pH from 6 to 9, was consistent with the trend that one would expect based on the absorption of the SNARF-5F dye as a function of pH. This proof-of-principle experiment demonstrates the possibility of creating an *in vivo* nanoplatform for sensing analyte concentrations in whole, intact tissue using photoacoustic detection.

A silver nanoprism colloid was investigated as a potential Surface-Enhanced Raman Scattering (SERS) substrate, with the analyte 4-mercaptopyridine (4-MPy). This analyte was chosen as a test molecule because it could be utilized to develop a SERS based pH nanosensor with the nanoprism colloid. It had been discovered that, while the poly (vinyl pyrrolidone) (PVP) organic capping agent interfered with the acquisition of the SERS signal on the nanoprism colloid, this approach is feasible.

CHAPTER 1

**INTRODUCTION TO NANOTECHNOLOGY AND THE DEVELOPMENT OF THE
PEBBLE NANOSENSORS**

The field of nanotechnology is related to the length scale of a nanometer, with one nanometer being defined as a meter being divided into one billion equally spaced divisions (1×10^{-9} m). Although it is impossible to imagine how small a nanometer is, one can kind of approximate this length scale as being approximately equal to 1/75,000 of the thickness of a human hair. The term nanotechnology was created to represent the multidisciplinary field of science where nanoscale particles and devices with interesting properties are created by scaling functional materials down to the nanometer size scale. These particles and devices are considered nanoscale materials when the length, width, and thickness of the material are on the size scale of a few 10's of nanometers up to approximately 100 nm.

Examples of nano-scale particles with all three dimensions in the nanometer length scale are semiconductor

quantum dots, spherical metallic colloids, and polymeric particles such as poly(acrylamide) spheres (PAA). When two dimensions are in the nanometer length scale, a particle with a high aspect ratio is the result. Examples of these high aspect ratio nanoparticles are single and double walled carbon nanotubes, and silver nanowires.

An explosion in research and development for nanoscale based materials research occurred with the establishment of the National Nanotechnology Initiative (NNI: www.nano.gov) in 2001. Since the development of the NNI, research and development in nanoscale particles and devices have been utilized to define new fields of study in nanomedicine and nano-bio analytical chemistry.

A primary driving force in the emerging field of nanomedicine is the National Cancer Institute's (NCI: www.nano.cancer.gov) Alliance for Nanotechnology in Cancer. The NCI's interest in nanoplatform based therapies stems from the technology's ability to deliver multifunctional components to tumors *in vivo* using these tiny particles that can be designed to increase circulation time, evade bio-fouling of the particle surface, and limit immune response of the body by the inclusion of a poly (ethylene glycol) (PEG) coating on the surface of the device[1,2]. Areas of interest in nano-based cancer research include

drug delivery[3,4], photodynamic therapy[5], cancer therapeutics[6], and *in vivo* imaging contrast agents[7].

With the advances in the field of nanomedicine, the field of nano-bio analytical chemistry is being co-developed to supplement existing technologies in the discovery of the root causes of disease states in patients.

New sensors utilizing the Localized Surface Plasmon Resonance (LSPR) of metallic nanoparticles are utilized to sense the presence of biological molecules in a sample[8]. These sensors exhibit a shift in the LSPR in the presence of the analyte due to a change in the dielectric environment local to the metallic nanoparticle. Selectivity of the sensor can be built into the technology by the attachment of an antibody to an organic linker that is attached to the metallic nanoparticle. This antibody is specific for the biological analyte that will be detected in the sample.

Another type of nanoparticle based sensor is based on the Surface-Enhanced Raman Scattering (SERS) phenomenon that was originally measured in 1974 by Fleischmann[9]. The surface-enhanced effect for the Raman scattering of pyridine, based on both electromagnetic and chemical enhancement by the presence of a roughened silver electrode, was not recognized as a new phenomena until 1977

3

when both Jeanmarie[10] and Albrecht[11] published concurrent reports. Ultrasensitive detection of biomolecules such as glucose and hemoglobin on metallic colloidal particles, and biomarker detection *in vitro* with SERS nanotags has been reviewed in Qian, *et al.*[12].

A series of fluorescent based nanosensors have been developed to measure biologically relevant ions, and small biomolecules in the intracellular environment[13,14]. These PEBBLE (Photonic Explorers for Biomedical use by Biologically Localized Embedding) nanosensors have been designed with an encapsulating matrix such as poly(acrylamide) (hydrophilic dyes, diameter of 20-30 nm), silica (for dissolved gas sensing, diameter of 100-600 nm), ormosil (diameter of 100 nm), and decyl methacrylate (for hydrophobic ionophores and fluorescent pH dyes, diameter of 250 nm) liquid polymer to provide an external interface for the organic or inorganic sensing dye molecules[15]. This interface acts to protect the chemistry of the indicator from cellular metabolism within the cell, and also protects the cell from the potential toxic effects of the indicator dye. The encapsulating interface also provides a compartment where the dye molecules are free from translocation or cellular sequestering by organelles. The interface also provides a surface to attach targeting

4

agents so that the PEBBLE nanosensor can be targeted to attach to specific locations within the cell, or specific cell types. For *in vivo* applications the PEBBLE can also be "cloaked" from bio-fouling, and to increase circulation time in the body by adding poly (ethylene glycol) to the exterior of the nanoparticle.

PEBBLES have been designed around ion specific indicator dyes to sense intracellular concentrations of ionic analytes such as H^+, Ca^{2+}, Na^+, K^+, Zn^{2+}, Mg^{2+}, and Cl^-, and biologically relevant gases such as NO and O_2[15]. The optically based, fluorescent detection of glucose is only possible through an indirect sensing method that couples the O_2 sensitive ruthenium dye complex, $\{(Ru[dpp(SO_3Na)_2)]_3)Cl_2\}$ with the enzyme glucose oxidase in the close confines of the PEBBLE nanoplatform[16].

Fluorescence based measurements using PEBBLE nanosensors need to have reference dyes that can take into account fluctuations in the excitation source. The inclusion of a fluorescence based internal reference complicates the design of the PEBBLE nanosensor because of the potential of spectral overlap between the indicator dye and the reference standard that are both encapsulated in the same particle. Also, the reference standard must not have a signal response, either to the analyte of interest, or the

experimental conditions for which the indicator dye will probe the analyte concentration. If either the indicator or reference dyes photo-bleach, then an errant result would be measured.

Chapter 2 introduces the application of steady-state fluorescence anisotropy for the detection of Zn^{2+}, Ca^{2+}, and dissolved O_2 concentrations utilizing Newport Green, Calcium Green, and $[Ru(dpp)_3]^{2+}$ PEBBLE nanosensors, respectively. The fluorescence anisotropy technique is a measurement based on both the rotational correlation time of the indicator dye probed, and the excited state lifetime for the dye. Along with the advantages of PEBBLEs described earlier, the physical encapsulation of the indicator dye couples the rotational correlation time of each encapsulated dye to the rotational correlation time of its encapsulating nanoparticle. Under experimental conditions where the rotational correlation time for a suspension of PEBBLE nanosensors remains constant, a change in the fluorescence anisotropy response for a dye embedded in a PEBBLE nanosensor will change due to an addition of analyte because of a change in the excited state lifetime. For example, an increase in the excited state lifetime for the indicator dye allows the ensemble of PEBBLE nanosensors to rotate to a larger degree before they fluoresce, and the

6

measured fluorescence anisotropy for the encapsulated dyes will decrease.

Although frequency modulation experiments have been utilized to measure analyte concentrations with PEBBLE nanosensors without the need for reference dyes[17], fluorescence anisotropy based measurements were attractive at the time of these studies (2001) because of the high cost associated with fluorescence lifetime based equipment. The steady-state fluorescence anisotropy method of detection is a self-referencing method by definition; therefore an internal reference dye is not needed to make analytical measurements[18]. This simplifies the design and synthesis of PEBBLE nanosensors where spectral overlap of sensing and reference components is a concern. Fluorescence anisotropy is an additive effect, so PEBBLEs could be designed to utilize high anisotropy dyes to extend the sensor response over the dynamic range of the encapsulated indicator dye.

Chapter 3 describes progress towards the development of a SERS based PEBBLE nanosensor that is based on a silica-silver nanoprism core-shell nanoplatform (see Figure 1.1). Silver nanoprisms have been modeled using DDA approximations to have large electromagnetic field enhancements because of the triangular shape of the

7

colloid, and thus have been proposed to be one of the superior SERS substrates with an overall SERS enhancement of up to 10^{+12} [18,19]. The electromagnetic field enhancement is especially strong when the analyte of interest resides in between a dimer of nanoprism colloids that are separated by a distance of 2 nm in either a tip-to-tip or tip-to-tail fashion [19,20].

Experiments were performed to acquire the SERS spectrum for the test analyte 4-mercaptopyridine (4-MPy). This analyte is ideal for SERS experiments because its SERS spectrum is well characterized, the molecule has a thiol moiety that lends itself to silver colloid adsorption, and the hetero-nitrogen atom in the pyridine ring has several SERS bands that shift in response to pH changes [21-23]. The goal of these experiments was the development of a sensitive SERS based sensor that utilized 4-MPy as the pH indicator that was adsorbed on the silver nanoprism colloid. What was discovered in this work was that care has to be used when utilizing organic capping reagents during the synthesis of colloid substrates due to complications in adsorption of analytes on the colloidal surface.

Chapter 4 describes a proof-of-concept analytical technique that is based on the photoacoustic effect that

was discovered in 1881 by Alexander Graham Bell[24]. In this technique, the absorption of light by an optical absorber causes thermoelastic expansion of the solvent local to the molecule. This thermoelastic expansion in turn launches a pressure wave that is detected with an ultrasound transducer. The level of ultrasound detected is directly related to the optical absorption of the absorbing species in solution.

The photoacoustic sensing experiments described in this work are based on the ultrasound detection of changes in the optical absorption for the pH sensitive indicator dye seminaptharhodafluor-5F (SNARF-5F). In this method, the sonic response of the dye is based on the change in absorption of the dye as a function of pH. The term "sonophore" has been coined for any indicator dye that has an optical response that translates into a photoacoustic response as a function of analyte concentration.

These proof-of-principle experiments show that PEEBLE nanosensors could translate into *in vivo* measurements of analytes by coupling photoacoustic detection with the proper selection of NIR absorbing indicator dyes. Experiments in the literature show evidence that analytes could be measured at a depth of up to 5 cm deep in whole intact tissue, or in live animals[25]. The advantage of

using photoacoustic detection for analytical measurements is that imaging contrast is based on the distribution of optical adsorption, while the spatial resolution is based on ultrasound resolution. Photoacoustic imaging is currently being employed to image vasculature in intact tissue[26], and to image breast tumors because of the large degree of angiogenesis local to the tumor tissue[27].

The photoacoustic research project was pursued in order to develop a new sensing and imaging technique that extends PEBBLE nanosensors to deep tissue *in vivo* imaging applications. To date, gadolinium and iron oxide loaded PAA PEBBLE nanoplatform particles have been created for MRI contrast imaging of brain cancer[28,29]. Also, Indocyanine Green loaded ormosil PEBBLES with the conjugated Her-2 antibody have been created as a photoacoustic imaging contrast agent for a Her-2 breast cancer cells[7]. The goal of the project was to make available new sensing and imaging tools for analytical chemistry and biomedical diagnostics to probe disease states *in vivo*.
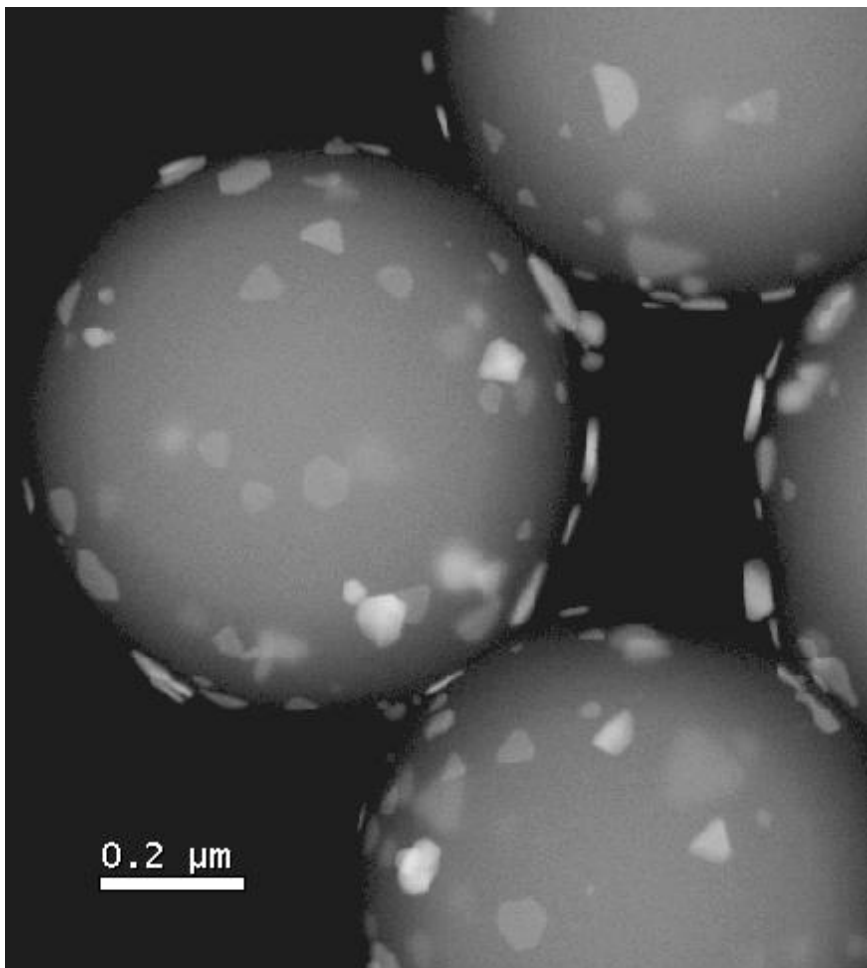
Figure 1.1: Silica-silver nanoprism core-shell PEBBLEs that were imaged with High Angle Annular Dark Field (HAADF) JEOL 2010F TEM electron microscope.

REFERENCES

1. Gu, F., Zhang, L., Teply, B.A., Mann, N., Wang, A., Radovic-Moreno, A.F., Langer, R., Farokhzad, O.C., Precise engineering of targeted nanoparticles by using self-assembled biointegrated block copolymers, Proc. Natl. Acad Sci. USA **2008**, *105*:2586-2591.

2. Otsuka, H., Nagasaki, Y., Kataoka, K., PEGylated nanoparticles for biological and pharmaceutical applications, Advanced Drug Delivery Reviews **2003**, *55*:403-419.

3. Farokhzad, O.C., Langer, R., Nanomedicine: Developing smarter therapeutic and diagnostic modalities, Advanced Drug Delivery Reviews **2006**, *58*:1456-1459.

4. Koo, Y.-E.L., Reddy, G.R., Bhojani, M., Schneider, R., Philbert, M.A., Rehemtulla, A., Ross, B.D., Kopelman, R., Brain cancer diagnosis and therapy with nanoplatforms, Advanced Drug Delivery Reviews **2006**, *58*:1556-1577.

5. Gao, D., Agayan, R.R., Xu, H., Philbert, M.A., Kopelman, R., Nanoparticles for Two-Photon Photodynamic Therapy in Living Cells, Nano Lett. **2006**, *6*:2383-2386.

6. Kukowska-Latallo, J.F., Candido, K.A., Cao, Z., Nigavekar, S.S., Majoros, I.J., Thomas, T.P., Balogh, L.P., Khan, M.K., Baker Jr., J.R., Nanoparticle Targeting of Anticancer Drug Improves Therapeutic Response in Animal Model of Human Epithelial Cancer, Cancer Res. **2005**, *65*:5317-5324.

7. Kim, G., Huang, S.-W., Day, K.C., O'Donnell, M., Agayan, R.R., Day, M.A., Kopelman, R., Ashkenazi, S., Indocyanine-green-embedded PEBBLEs as a contrast agent

for photoacoustic imaging, Journal of Biomedical Optics **2007,** *12*:044020-1.

8. Willets, K.A., Van Duyne, R.P., Localized Surface Plasmon Resonance Spectroscopy and Sensing, Annu. Rev. Phys. Chem. **2007.** *58*:267-297.

9. Fleischmann, M., Hendra, P.J., McQuillan, A.J., Raman Spectra of Pyridine Adsorbed at a Silver Electrode, Chem. Phys. Lett. **1974,** *26*:163-166.

10. Jeanmaire, D.L., Van Duyne, R.P., Surface Raman Spectroelectrochemistry: Part I. Heterocyclic, Aromatic, and Aliphatic Amines Adsorbed on the Anodized Silver Electrode, J. Electroanalyt. Chem. **1977,** *84*:1-20.

11. Albrecht, M.G., Creighton, J.A., Anomalously Intense Raman Spectra of Pyridine at a Silver Electrode, J. Amer. Chem. Soc. **1977,** *99*:5215-5217.

12. Qian, X.-M., Nie, S.M., Single-molecule and single-nanoparticle SERS: from fundamental mechanisms to biomedical applications, Chem. Soc. Rev. **2008,** DOI: 10.1039/b708839f.

13. Clark, H.A., Hoyer, M., Philbert, M.A., Kopelman, R., Optical Nanosensors for Chemical Analysis inside Single Living Cells. 1. Fabrication, Characterization, and Methods for Intracellular Delivery of PEBBLE Sensors, Anal. Chem. **1999,** *71*:4831-4836.

14. Clark, H.A., Kopelman, R., Tjalkens, R., Philbert, M.A., Optical Nanosensors for Chemical Analysis inside Single Living Cells. 2. Sensors for pH and Calcium and the Intracellular Application of PEBBLE Sensors, Anal. Chem. **1999,** *71*:4837-4843.

15. Buck, S.M., Koo, Y.E.L., Park, E., Xu, H., Philbert, M.A., Brasuel, M.A., Kopelman, R., Optochemical

nanosensor PEBBLEs: photonic explorers for bioanalysis with biologically localized embedding., Current Opionion in Chemical biology **2004,** *8*:540-546.

16. Hao, X., Aylott, J.W., Kopelman, R., Fluorescent nano-PEBBLE sensors designed for intracellular glucose imaging., The Analyst **2002,** *127*:1471-1477.

17. Chen-Esterlit, Z., Aylott, J., Kopelman, R., Development of Oxygen and pH Optical Sensors Using Phase Modulation Technique, Proc. SPIE (Int. Soc. Opt. Eng.) **1999,** *3540*:19-27.

18. Lakowicz, J.R., (2006). Principles of Fluorescence Spectroscopy, 3rd edition, New York, NY, Springer.

19. Hao, E., Schatz, G.C., Electromagnetic fields around silver nanoparticles and dimers, J. Chem. Phys. **2004,** *120*:357-366.

20. Hao, E., Schatz, G.C., Hupp, J.T., Synthesis and Optical Properties of Anisotropic Metal Nanoparticles, J. Fluor. **2004,** *14*:331-341.

21. Hu, J., Zhao, B., Surface-Enhanced Raman Spectroscopy on the structure changes of 4-mercaptopyridine adsorbed on silver substrates and silver colloids, Spectrochimica Acta Part A. **2002,** *58*:2827-2834.

22. Baldwin, J.A., Vlćková, B., Andrews, M.P., Butler, I.S., Surface-Enhanced Raman Scattering of Mercaptopyridines and Pyrazinamide Incorporated in Silver Colloid-Adsorbate Films, Langmuir **1997,** *13*:3744-3751.

23. Jung, H.S., Kim, K., Kim, M.S., Raman spectroscopic investigation of the adsorption of 4-mercaptopyridine on a silver-sol surface, Journal of Molecular Structure **1997,** *407*:139-147.

24. Bell,A.G., Production of sound by radiant energy., Phil. Mag. **1881**, *11*:156-158.

25. Ku, G., Wang, L.V., Deeply penetrating photoacoustic tomography in biological tissues enhanced with an optical contrast agent., Opt. Lett. **2005**, *30*:507-509.

26. Konstantin, M., Wang, L.V., High-resolution photoacoustic vascular imaging in vivo using a large-aperture acoustic lens., Proc. SPIE, Photons Plus Ultrasond: Imaging and Sensing **2005**, *5697*:7-14.

27. Oraevsky, A.A., Andreev, V.A., Karabutov, A.A., Fleming, D.R., Gatalica, Z., Singh, H., Esenaliev, R.O., Laser Opto-Acoustic Imaging of the Breast: Detection of Cancer Angiogenesis., Proc. SPIE **1999**, *3597*:352-363.

28. Moffat, B.A., Reddy, G.R., McConville, P., Hall, D.E., Chenevert, T.L., Kopelman, R.R., Philbert, M., Weissleder, R., Rehemtulla, A., Ross, B.D., A novel polyacrylamide magnetic nanoparticle contrast agent for molecular imaging using MRI, Mol. Imaging **2003**, *2*:324-332.

29. Ross, B., Rehemtulla, A., Reddy, R., Kim, G., Behrend, C., Buck, S., Schneider, R.J., Philbert, M.A., Weissleder, R., Kopelman, R., Photonic and magnetic nanoexplorers for biomedical use: from subcellular imaging to cancer diagnostics and therapy, Nanobiophotonics and Biomedical Applications **2004**, *5331*:76-83.

CHAPTER 2

USE OF STEADY-STATE FLUORESCENCE ANISOTROPY WITH PEBBLE NANOSENSORS FOR CHEMICAL ANALYSIS

2.1 INTRODUCTION

In medical and biochemical research, when the domain of the sample is reduced to micrometer regimes, *e.g.*, living cells or their sub-compartments, the real-time measurement of chemical and physical parameters with high spatial resolution and negligible perturbation of the sample becomes extremely challenging. One of the challenges of designing chemical sensors (optical, electrochemical, etc.) is the minimization of chemical interference between sensor and sample. This may be achieved through the use of inert biocompatible matrices, or the attachment of an anti-bio-fouling agent such as poly (ethylene glycol) (PEG) to the sensor surface. However, when it comes to the penetration of individual live cells with an optical sensor, even the introduction of a sub-micron pulled optical fiber sensor tip can cause biological damage and resultant biochemical consequences. In contrast, individual molecular probes

(free sensing dyes) are sufficiently small to avoid physical damage to the cell, but usually suffer from chemical interference between the chemical probe and cellular components.

Recently developed PEBBLE sensors (Photonic Explorers for Biomedical use by Biologically Localized Embedding) are nanoscale spherical devices consisting of sensing molecules entrapped in a chemically inert matrix such as: poly (acrylamide) (PAA) organic hydrogel[1,2], poly(decyl methacrylate) (PDMA)[3], sol gel (silica) inorganic/organic hybrid[4], or an organically modified silicate nanobottle (Ormosil)[5] (see Figure 2.1A-B). This protective coating places a barrier between the molecular probes and the cellular material, thus eliminating interferences such as protein binding and/or membrane/organelle sequestration that alter the dye response. Conversely, the nanosensor matrix (the barrier) also provides protection for the cellular contents, enabling the use of dyes that could potentially be toxic to cells (e.g. single oxygen production). This yields a non-invasive analytical tool for determining concentrations of a given analyte within an individual cell. The PEBBLEs provide a fluorescence technique that is both quantitative and ratiometric through the inclusion of reference dyes. PEBBLEs have been used to

17

measure analytes such as H^+ [6], Ca^{2+} [6], K^+ [7], O_2 [4,5], Zn^{2+} [8], Na^+ [9], Mg^{2+} [10], Cl^- [11], NO [12], and glucose[13].
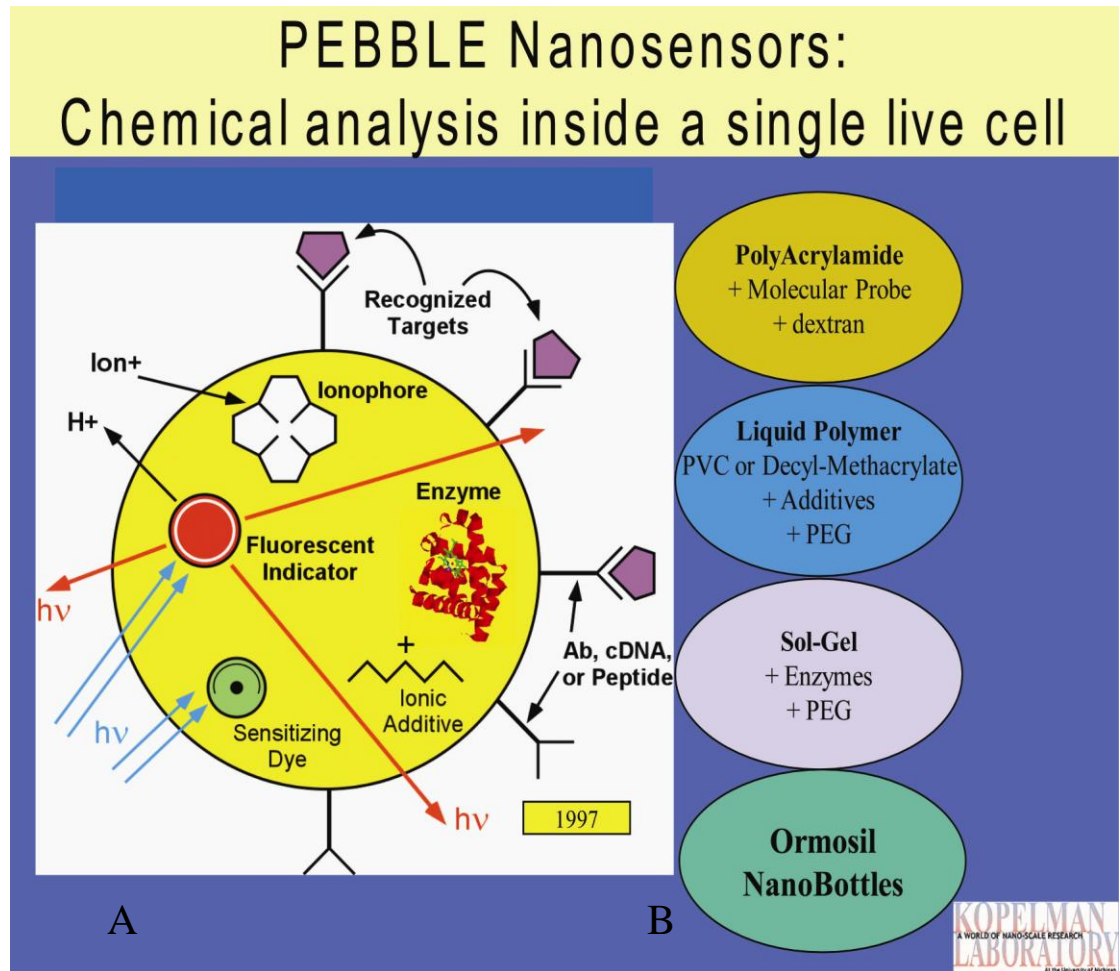
Figure 2.1: (A.) Diagram of PEBBLE nanosensor and all of the sensing components that can either be embedded within, or attached to the surface of the particle matrix. (B.) Diagrams of the four PEBBLE platforms that can be used to encapsulate different sensing dyes.

Figure 2.1A is a schematic that shows all the permutations of the PEBBLE biosensor. In applications

where the analyte has a fluorescent indicator available, the indicator dye and a reference dye can be embedded into the PEBBLE. This is known as direct sensing, where the analyte interacts directly with the indicator dye, either enhancing or quenching the fluorescent emission of the dye. In this case, the indicator dye response is directly dependent on the concentration of analyte present in the sample matrix local to the PEBBLE. The reference dye response is independent of the analyte concentration, and is used to account for fluctuations in the intensity based on systemic changes, such as laser fluctuations or PEBBLE concentration changes[14].

Typically, when the PEBBLE is designed to use the direct sensing modality, a PAA or sol-gel matrix is utilized (see Figure 2.1B). The PAA nano-platform has been utilized to make PEBBLEs with sensing indicators, and magnetic contrast agents such as gadolinium chelate or iron oxide for their use as MRI contrast agents[15,16]. This sensing method has been developed to make PEBBLEs for sensing H^+, Ca^{2+}, Mg^{2+}, Zn^{2+}, and O_2.

The PAA nano-platform has also been utilized for indirect sensing of glucose in cells[13]. At the core of this PEBBLE is the enzyme glucose oxidase (GOx) coupled with the O_2 sensitive ruthenium dye complex, Ru(II)-tris(4,7-diphenyl-

1,10-phenanthroline disulfonic acid disodium salt)chloride
{(Ru[dpp(SO$_3$Na)$_2$)]$_3$)Cl$_2$}. This particle is designed so that
the (Ru[dpp(SO$_3$Na)$_2$)]$_3$)Cl$_2$ and the GOx are located in close
proximity to each other within the PEBBLE. In this scheme,
the (Ru[dpp(SO$_3$Na)$_2$)]$_3$)Cl$_2$ detects the local change in oxygen
concentration as it is depleted by the oxidation of glucose
via GOx.   The Ru[dpp(SO$_3$Na)$_2$)]$_3$)Cl$_2$} indicator dye has its
fluorescence quenched in the presence of oxygen, so as the
oxygen is depleted because of the oxidation of glucose,
then the fluorescence of the indicator increases. This is
a case where the PEBBLE nanosensor makes the indirect
measurement of glucose possible because of the close
proximity of the ruthenium based indicator dye and the GOx
enzyme within the PEBBLE matrix.

The sol-gel based PEBBLE has been utilized for the
sensing of O$_2$ using the ruthenium dye complex Ru(II)-
tris(4,7-diphenyl-1,10-phenanthroline)chloride   ([Ru-
(dpp)$_3$]$^{2+}$) (GFS Chemicals, Inc., Columbus, OH, USA). This
PEBBLE is based on the same mechanism described for the
glucose sensor in that the fluorescence of the ([Ru-
(dpp)$_3$]$^{2+}$) complex is diminished in the presence of O$_2$.

A new method for sensing analyte concentrations in our
lab has been the combination of steady-state fluorescence
anisotropy with PEBBLEs.   Fluorescence anisotropy is a

technique that measures the change in the polarization of the fluorescence emission of a fluorophore relative to the excitation polarization. For example, in the case of steady-state fluorescence anisotropy sensing, the binding of the analytes to the molecular probes will increase the lifetime of the excited state. This will in turn allow the molecular probes, as an ensemble, to be able to rotate to a larger degree before emission, and thus the anisotropy for the probe would decrease. Several mechanisms of depolarization include: change of rotational diffusion of the fluorophore in the solvent, reduction of max anisotropy ($r=0.4$) due to a change of the angle β between the excitation and emission dipoles for the fluorophore due to changes in solvent environment, and changes to the lifetime of the excited state of the fluorophore. Note that in the studies of the dye and PEBBLE response to analyte the rotational correlation time is not changing, and the dye is embedded in a stable encapsulating environment, so a change in steady-state fluorescence anisotropy is reflective of a change in fluorescence lifetime.

Previous work has shown the effectiveness of this method with free dyes in solution and in bulk sensor membranes[17-21]. One advantage of using PEBBLEs for these studies is that the fluorophore's rotational environment is stabilized

by the encapsulation of the dye in the PEBBLE matrix. This allows for a very consistent anisotropy signal in the presence of such interferents as proteins, peptides, and other species present in cellular environments that could potentially change the anisotropy signal of the fluorophore in bulk solution or membranes. An added advantage of steady-state fluorescence anisotropy is that it can provide quantitative detection of analytes utilizing inexpensive instrumentation relative to the high cost of time-resolved fluorescence lifetime equipment.

2.2 EXPERIMENTAL BACKGROUND AND SETUP

The diagrams in Figure 2.2 exhibit the polarization configurations necessary in the determination of the anisotropy of a sensor solution. To measure this depolarization of fluorophores, the polarization of the excitation beam must be precisely controlled, and then the polarization components of the emission must be measured relative to that of the excitation. More specifically, with the excitation polarizer in the vertical orientation, the emission will be measured in both the vertical and horizontal orientations. This gives parallel and

perpendicular emission intensity components relative to the

polarization of the excitation denoted as I_{VV} and I_{VH}.
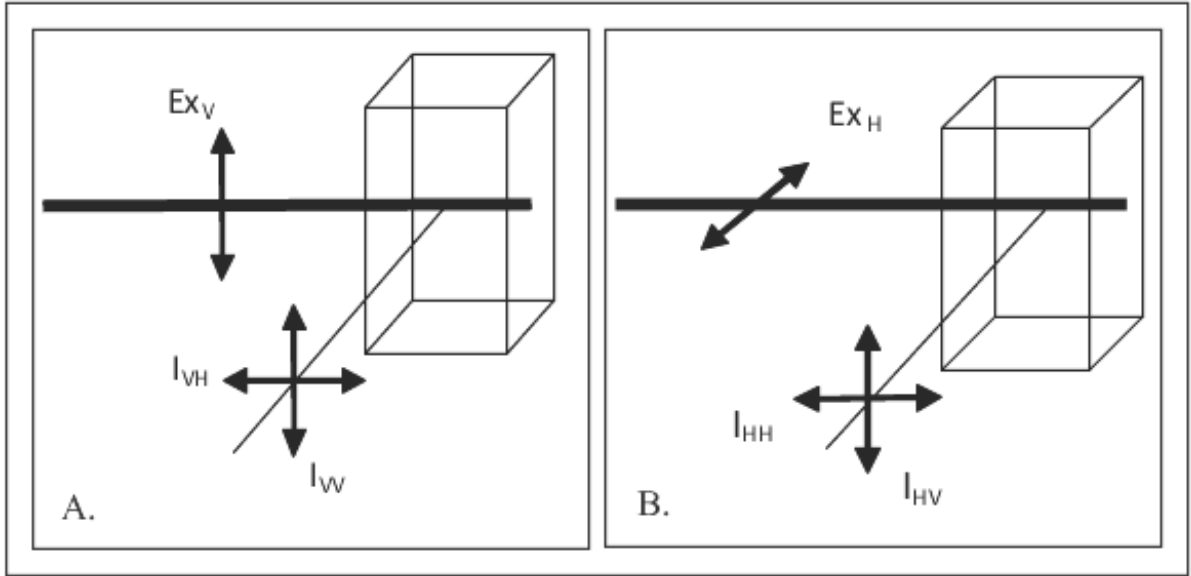
Figure 2.2: (A.) System polarizer configuration used to measure the anisotropy of the free dye sensors, and PEBBLE biosensors at various analyte concentrations. (B.) System configuration for determination of the G factor.

Based on these measurements the anisotropy is then calculated by Equation 2.1:

$$r = \frac{(Ivv - G * Ivh)}{(Ivv + 2 * G * Ivh)}$$

Eq. 2.1

Where the G factor ($G = I_{HV} / I_{HH}$) is a measure of the system sensitivity to the emission polarization in the horizontal and vertical orientations.   With the excitation polarizer

set in the horizontal configuration, the emission polarizations that are measured are perpendicular to the excitation in both the horizontal and vertical orientations (see Figure 2.2 (B.)). Thus, a difference in the intensities measured for the different emission polarizations is purely due to instrumental biases.

For a spherical PEBBLE nanosensor suspended in a homogeneous isotropic media that is rotating freely, the fluorescence anisotropy decay of the embedded indicator dye molecules is described by the exponential decay:

$$a = a_o * e^{\left(-\frac{t}{\tau_p}\right)}$$

Eq. 2.2

Where t is the time elapsed after excitation of the fluorophore, and τ_p is the rotational correlation time of the PEBBLE[22]. The term a_o describes the fluorescence anisotropy after excitation of the fluorophore before the PEBBLE has had a chance to rotate. The decay in the signal is a direct result of depolarization of the emission relative to the polarization of the excitation for the subset of PEBBLEs in the ensemble that had adsorption dipoles parallel to that of the excitation. If the angle β between the absorption and emission dipoles for the embedded indicator dyes is 0, and the dipoles are collinear

24

and the maximum value for the steady state fluorescence anisotropy would be 0.4 [18]. If the angle β is greater than 0, then a_o is reduced.

In some applications this technique is useful as a quantitative detection method for the PEBBLE nanosensors. Unlike fluorescent intensity based measurements, it is not necessary to have an internal reference fluorophore within the PEBBLE to compensate for issues such as excitation source fluctuations or changes in the number of PEBBLEs being monitored due to diffusion of the nanosensors. This is a result of the anisotropy measurements being internally normalized, which stems from the definition of fluorescence anisotropy shown in Equation 2.1. If in a particular orientation some environmental factor causes a fluctuation in the fluorescence intensity, the influence will be represented in both terms of the ratio, and the anisotropy measurement will be insensitive to the fluctuation.

At the heart of the practical apparatus for the steady-state anisotropy measurements is an argon ion continuous wave (CW) laser that is operated with the emission at 488 nm (Figure 2.3). In order to limit saturation of the photodiode detector, the intensity of the excitation is attenuated by a series of neutral density filters placed in the beam path. The excitation polarizer utilized in the

experimental apparatus is a Glann-Thompson polarizer. This
excitation polarizer can be rotated to change the system
configuration in order to make measurements for the steady-
state fluorescent anisotropy (Figure 2.2 (A.)) or the
empirical G factor determination (Figure 2.2 (B.)). The
fluorescence from the molecular probes in the sample is
collected in a perpendicular configuration from the
excitation beam ("L" format; see (18)). The emission
polarizer lies in the collected beam path, which can be
rotated into both the vertical and horizontal orientations,
is used to make the intensity measurements for the
different polarizations. Next in the emission path are the
long pass filters that are used to block scattered
excitation photons from the samples. The last component in
the apparatus is a lens that focuses the light onto the
avalanche photodiode, which is in turn connected to the
photon counter.
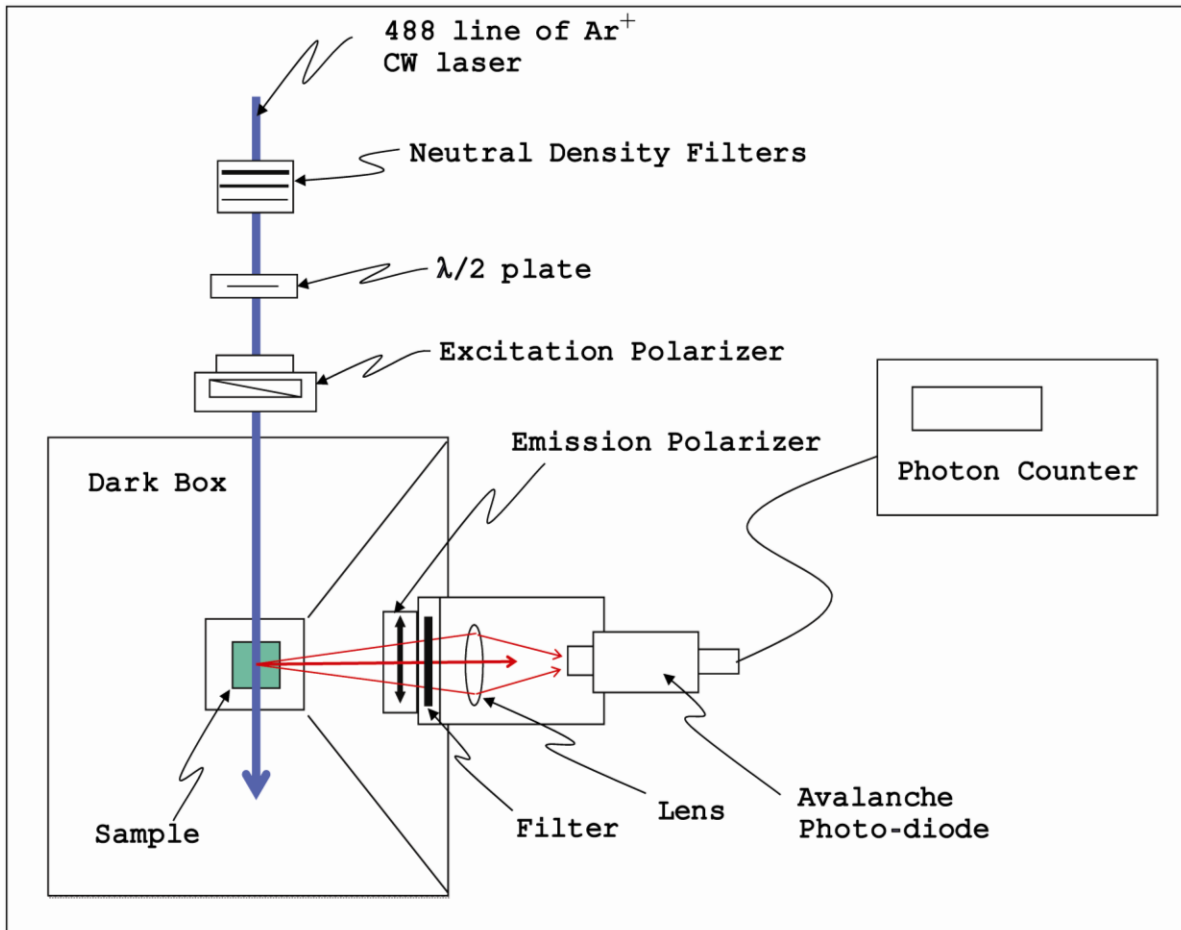
Figure 2.3: Experimental apparatus used to determine fluorescence anisotropy for both PEBBLE and free dye samples.

2.3 EXPERIMENTAL METHODS

2.3.1 PAA PEBBLE preparation

The preparation for these inert nanosensors utilizes the combination of two solutions in an oil-and-water

microemulsion[2,8].   Once the polymerization is initiated, the reaction yields 20 to 200 nm PAA PEBBLEs with the indicator dye embedded within the particle matrix.

The polymerization solution that is prepared fresh for each synthesis contains the acrylamide monomer and N',N'-methylenebis-(acrylamide) cross-linker (both from Sigma-Aldrich, St. Louis, MO, USA) dissolved in a 10 mM phosphate buffer (BRL Life Sciences, Gaithersburg, MD, USA) solution near pH 7.4.   The indicator dye, in this case the dextran linked Calcium Green, or the Newport Green (both from Molecular Probes, Eugene, OR), and internal reference dye (typically Texas Ted with Dextran for the Newport Green ratiometric PEBBLE, and sulforhodamine 101 for Calcium Green PEBBLEs) for the PEBBLE synthesis would also be dissolved in the polymerization solution.

The second solution contains hexane, and the surfactants dioctyl sulfosuccinate sodium salt (AOT) (Sigma-Aldrich, St. Louis, MO, USA), and polyoxyethylene (4) lauryl ether (Brij 30) (Sigma-Aldrich, St. Louis, MO, USA).   The hexane (Fisher, Fairlawn, NJ, USA) is purged of oxygen, by bubbling N_2 (99.99% dry, Cyrogenic Gases, Detroit, MI, USA), prior to adding the surfactants.   This solution is added to a round bottom flask that is sealed from atmosphere using a

rubber septum, and the reaction is completed under N$_2$ atmosphere.

The emulsion is formed by adding the polymerization solution, in dropwise fashion, to a hexane and surfactant solution. The oil-and-water mixture is stirred using a magnetic stirrer until the solution becomes cloudy as the emulsion is formed. Then the initiator solution is added to start the free-radical polymerization of the acrylamide and the cross-linker N',N'-methylenebis-(acrylamide). The initiator solution is either a 10% sodium bisulfate solution (Sigma-Aldrich, St. Louis, MO, USA), or a combination of a 10% ammonium persulfate solution (Sigma-Aldrich, St. Louis, MO, USA) and N,N,N',N'-tetramethylethylenediamine (TEMED) (Sigma-Aldrich, St. Louis, MO, USA).

Upon completion of the reaction, the hexane is removed by rotary evaporation, and the particles are precipitated using ethanol. The surfactant, unreacted monomer, and dye is washed off of the PEBBLE suspension by repeated washings with ethanol (200 proof, Pharmco Products Inc., Brookfield, CT, USA) in the Amicon Ultra-Filtration system (Millipore Corp., Bedford, MA, USA) using a 100 kDA filter. All aqueous solutions in this work were prepared with 18 MΩ

deionized (DI) water purified by a Barnstead 1 Thermolyne Nanopure II system.

2.3.2 Sol-Gel PEBBLE preparation

In this reaction, an ethanolic solution of tetraethyl orthosilicate (TEOS) (Sigma-Aldrich, St. Louis, MO, USA), the indicator dye ($[Ru(dpp)_3]^{2+}$), and a reference dye is stirred in a plastic reaction vessel[4,16]. If it is necessary to cloak the PEBBLEs in a poly(ethylene glycol) (PEG) coating, then PEG MW 5000 monomethyl ether (Sigma-Aldrich, St. Louis, MO, USA) can be added to this reaction mixture as well. The PEBBLEs that are formed as a result of this reaction are on the size scale of 100-600 nm, and the ($[Ru(dpp)_3]^{2+}$) indicator dye is embedded in the silica network.

The hydrolysis of the TEOS is initialized by the addition of the 30% Ammonium Hydroxide solution (Sigma-Aldrich, St. Louis, MO, USA) in a dropwise fashion. In this reaction, the ammonia is the catalyst that starts the hydrolysis reaction, and the water is a reactant. The reaction mixture is stirred at room temp for a period of about 1 hour. Once that time is up, the reaction is stopped by flooding the reaction vessel with ethanol.

30

The PEBBLEs are washed by repeated additions of ethanol, and the unreacted reagents are filtered off by the Amicon Ultra-Filtration system, using a 100 kDA filter. The PEBBLEs are further rinsed with 500 mL of ethanol to ensure that all unreacted materials are removed from the particles.

2.3.3 Newport Green (zinc) Studies

The Newport Green Dye stock (Molecular Probes, Eugene, OR, USA) was prepared by dissolving 1 mg of the dye in 1 mL of double distilled water. The 4.0 µM dye solution and the 3.0 mM Zn^{2+} stock were prepared in 5.1 mM 3-morpholinopropanesulfonic acid (MOPS) buffer (Fluka BioChemika, Switzerland) at pH 7.13.

A 3.0 mg/mL Newport Green PAA PEBBLE sensor suspension was prepared in 2 mL of DI water. The 3.0 mM zinc solution was prepared by diluting the appropriate volume of 10.99 mM $ZnCl_2$ (Sigma-Aldrich, St. Louis, MO, USA) solution in DI water to give 2 mL of stock solution.

2.3.4 Calcium Green Studies

In order to measure the anisotropies for the 10,000 molecular weight (mw) dextran linked Calcium Green-1 probe (Molecular Probes, Eugene, OR, USA), a commercial calcium buffer kit (Molecular Probes, Eugene, OR, USA) was purchased. Included in the kit is a published method for obtaining an 11-point calibration curve using the Calcium Green molecular probe[23]. In this method, a zero μM free calcium stock was prepared by diluting 1.2 μL of the 1 mg/mL Calcium Green with dextran solution in 1.5 mL of zero μM free calcium buffer for a total concentration of 2 μM dye in solution. The high calcium stock solution was prepared by diluting 3.6 μL of the 1 mg/mL Calcium Green with dextran stock in 4.5 mL of the 39 μM free calcium buffer for a 2 μM dye concentration. The samples were made by mixing the low and high calcium buffers with 2 μM Calcium Green with dextran dye in predetermined proportions according to the published method in (23).

The buffered suspensions of 10,000 mw dextran linked Calcium Green PAA PEBBLEs were prepared similarly to the free dye solutions. The suspensions were prepared to a

32

final concentration of 3 mg/mL of Calcium Green PEBBLEs in the zero µM and 39 µM free calcium buffered solutions.

2.3.5 Calcium Green Bovine Serum Albumin (BSA) Studies

The Calcium Green free dye solution was made by diluting 1.6 µL of a 25 mg/mL stock of 10,000 mw dextran linked Calcium Green-1 in 1.998 mL of 5.1 mM MOPS buffer, pH 7.13. To this solution, 20 µL of 1.7 mM ethylene glycol tetraacetic acid (EGTA) (Sigma-Aldrich, St. Louis, MO, USA) stock solution was added in order to chelate all of the free calcium for the zero point reading. The low (zero µM free calcium) and high (60 µM calcium) measurements were made before adding any BSA. The samples with Bovine Serum Albumin (BSA) were prepared at concentrations of 0.05 % (w/v) and 0.15 (w/v) % from a 5 % BSA stock solution in 10mM K_2HPO_4 / KH_2PO_4 buffer at pH 7.1. The PEBBLE solutions were made according to the method described for the free dye samples. The final PEBBLE concentration was 3.0 mg/mL.

2.3.6 Ruthenium Sol-Gel PEBBLE (Oxygen) studies

The 0.6 mg/mL Ruthenium PEBBLE solution was prepared with 10mM K_2HPO_4 / KH_2PO_4 buffer at pH 7.1, following previously published methods[6]. The oxygen studies were performed using an airtight optical cell so that the dissolved gases in the sample could be controlled with precise amounts of O_2.

2.3.7 Experimental Conditions

The 488 nm line (16 mW of output power) of an argon ion laser was used as the excitation source for the sensors studied. The intensity of the polarized emission was measured over a 10 second interval using the photon counter. For the Newport Green and Calcium Green studies a 500 nm long pass Schott filter was used to block any scattered photons of the excitation wavelength. For the ruthenium chelate studies a 610 nm long pass Schott filter (RG-610) was used. The empirically determined G factor for the experimental apparatus was measured before each set of experiments, and was found to vary between 0.99 and 1.01 (see Table 2.1).

Sample	Empirical G-factor
Newport Green Free Dye	1.015
Newport Green PEBBLEs	1.019
Calcium Green Free dye	0.995
Calcium Green PEBBLEs	0.993
Calcium Green Free dye – BSA	0.995
Calcium Green PEBBLEs – BSA	0.993
Ruthenium PEBBLEs	1.012

Table 2.1: Empirical G-factor values for the experiments using the optical setup described in Figure 2.2 (B).

2.4 RESULTS AND DISCUSSION

The results described below suggest that the fluorescence anisotropy based measurements of the encapsulated indicator dyes in PEBBLE nanosensors is a functional technique for measuring analyte concentrations. Newport Green is an intensity-based fluorescent indicator that exhibits an increase in emission intensity (corresponding to an increase in the fluorescence lifetime) with increasing zinc concentration. The Newport Green measurements show a decrease in anisotropy with an increase in zinc concentration. This decrease in anisotropy is consistent with the expected increase in the fluorescent lifetime of the Newport Green molecular probe with increasing zinc

35

binding. The fluorescence lifetime increases from $\tau_f = 0.88$ nS for the dye not bound with Zn^{2+} to $\tau_b = 2.93$ nS when the dye has bound Zn^{2+} [24]. The anisotropy calibration curve of both the free Newport Green dye and the Newport Green PEBBLES are shown in Figure 2.4. The calibration curve shows an anisotropy decrease of 0.060 anisotropy units over a usable dynamic range of approximately 0 to 10 μM zinc. For the free dye, an anisotropy decrease of approximately 0.1 anisotropy units is exhibited over a dynamic range of 0 to 15 μM zinc. It is thought that this decrease in sensitivity and reduction of dynamic range is due to the encapsulation of the dye in the PEBBLE matrix. One potential method for increasing the overall anisotropic response of the Newport Green PEBBLE is to add a high anisotropic reference dye to the PEBBLE matrix. This method has potential because of the additive nature of fluorescence anisotropy.
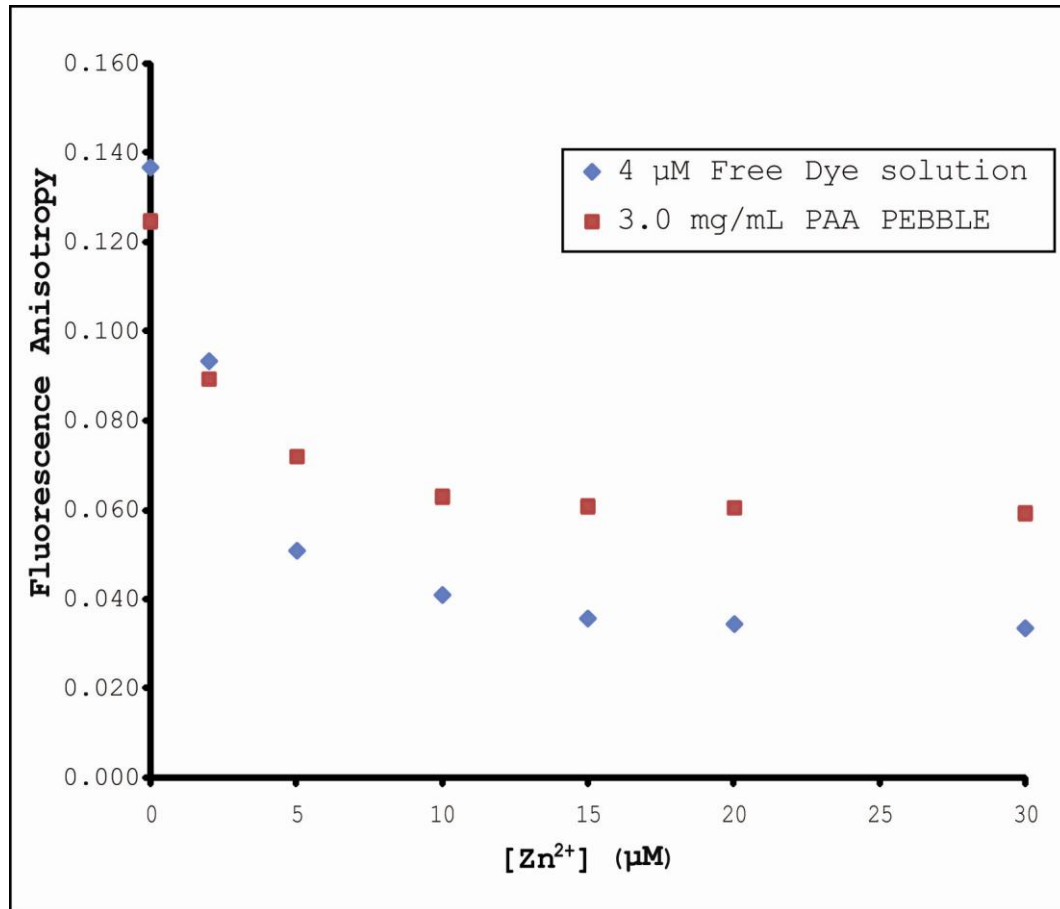
Figure 2.4: Steady-state fluorescence anisotropy calibration curves for both Newport Green PEBBLEs and the free dye. The error for each measurement was less than 2%, so the error bars are smaller than the markers for the data points.

The original work published by Sumner *et al.* describes interference experiments with the Newport Green and Texas Red with Dextran (internal reference dye) PEBBLE Zn^{2+} nanosensor[8]. In these experiments the fluorescence response was tested for the Zn^{2+} sensitive PEBBLE for ionic metals that would be present in the cellular cytosol which includes Na^+, K^+, Mg^{2+}, and Ca^{2+}. The results show that the

change in the fluorescent response of either the free or embedded Newport Green in PEBBLEs was minimal or none due to the presence of cellular concentrations of these ions.

The Calcium Green molecular probes (also an intensity-based dye) also exhibited a decrease in anisotropy as a function of calcium concentration. The fluorescence lifetime of the indicator without bound Ca^{2+} was measured to be τ_f = 1.6 nS, and the fluorescence lifetime increases to τ_f = 3.6 nS for bound Ca^{2+} [25]. Figure 2.5 shows the calibration curves for both the Calcium Green linked to dextran free dye (10,000 mw) and the PEBBLE nanosensors containing the same dye. The anisotropy decrease in the dextran linked Calcium Green dye is approximately 0.045 anisotropy units is exhibited across the usable dynamic range from 0 to 1.5 µM calcium. For the calcium Green PEBBLEs, the drop in the anisotropy exhibited across the same dynamic range is approximately 0.040 anisotropy units.

Work has been published in the literature for a study of the specificity of Ca^{2+} indicators against Zn^{2+} in solution[26]. What was discovered is that the Calcium Green-1 indicator had a fluorescent response to Zn2+ in solution. This indicators response to Zn^{2+} still occurred in high concentrations of Ca^{2+}.
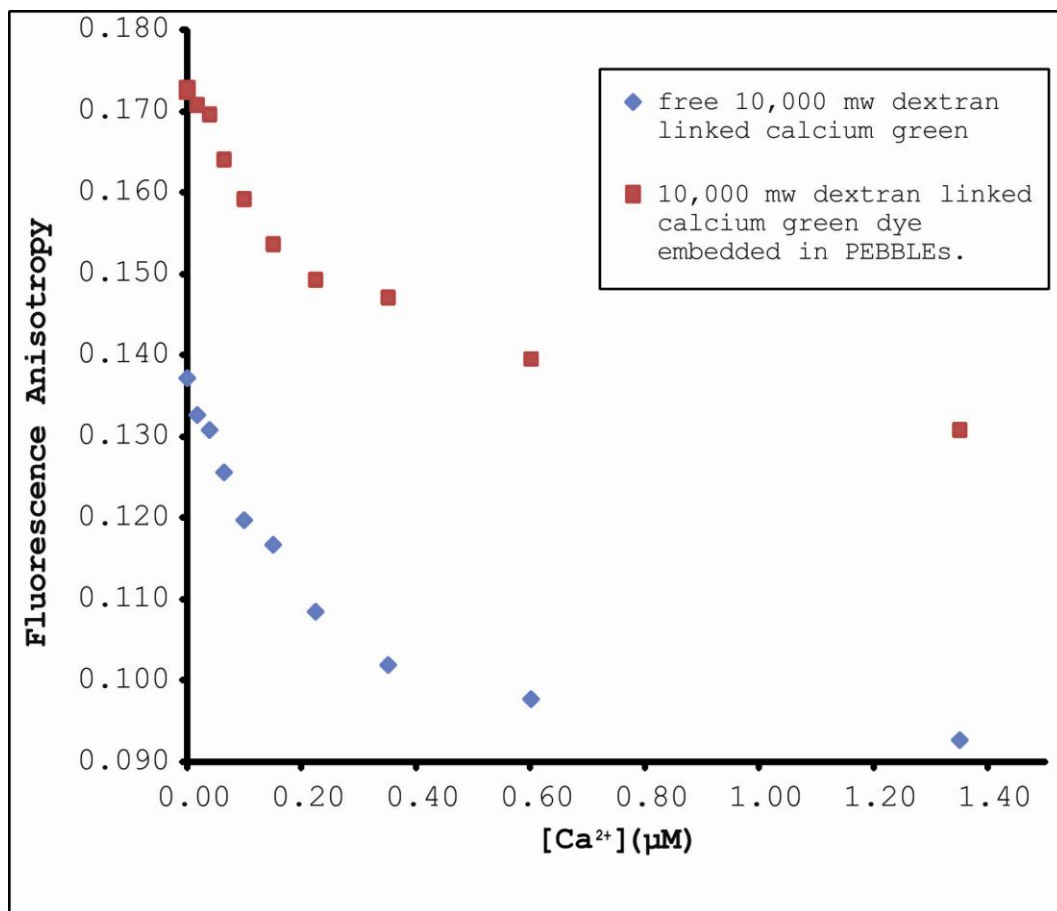
Figure 2.5: Anisotropy calibration curves for both Calcium Green PEBBLEs and the free dye. The error for each measurement was less than 2%, so the error bars are smaller than the markers for the data points.

It has been found in previous work that non-specific protein binding can interfere with free dye sensing[2,4]. A BSA interference study was performed on the Calcium Green-1 free dye, and calcium Green PEBBLE nanosensors, to measure the extent of protein interference in the steady-state fluorescent anisotropy of these sensors. As can be seen in Figure 2.6, the anisotropy does not change significantly

39

for the PEBBLEs with increasing BSA concentration. Conversely, a significant change in anisotropy resulted upon the addition of the BSA for the free dye measurement. These data indicate that the Calcium Green-1 dye is firmly embedded in the interior of the PEBBLE, where it is isolated from interferents such as BSA and other proteins, while still being accessible to the analyte. This experiment shows the critical role of the PEBBLE matrix in protecting the embedded molecular probe from the BSA interference, and demonstrates the significant advantage that PEBBLE nanosensors offer in making real-life analyte measurements within cellular matrices. The EGTA was added to complex any Ca^{2+} present in the suspension prior to measurement, so that the zero free Ca^{2+} is truly a zero point measurement. With the addition of an aliquot of $CaCl_2$ $_{(aq.)}$ stock, the final concentration of Ca^{2+} in the suspension was 60 μM, but the free Ca^{2+} concentration would be less due to an equilibrium established between free Ca^{2+} and EGTA chelated Ca^{2+} in the suspension.
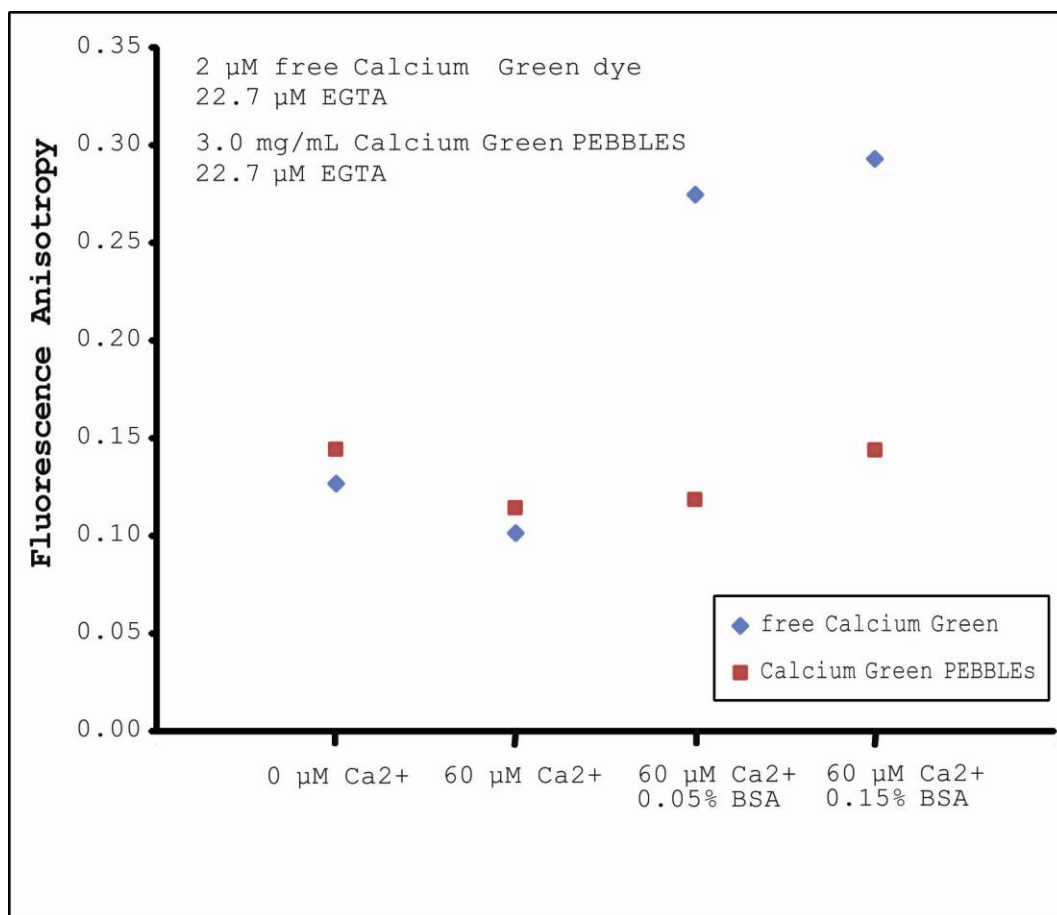
Figure 2.6: The effects of BSA on the steady-state fluorescence anisotropy for both the Calcium Green PEBBLEs and the free dye responses to calcium.

In order to investigate the flexibility of this approach, experiments were performed using another type of fluorescent probe. Ruthenium based dyes have a long-lived fluorescence, which is quenched in the presence of O_2 [4]. For the ruthenium sol-gel PEBBLE studies, a variation in the O_2 / N_2 ratio within the optical cell was used to probe the anisotropy changes exhibited by the dye.

The 23% O_2 measurement was made first because the sample was made at atmospheric conditions. Over the course of

this measurement, the optical cell was left open to the atmosphere so that air was allowed to diffuse into the PEBBLE suspension. Once the 23% O_2 measurement was completed, the optical cell was sealed with a cap and septum so that the suspension could be bubbled with pure N_2 or O_2. In order to measure the anisotropy for the samples without O_2, the PEBBLE nanosensors were present in a N_2 atmosphere. Sealing the optical cell with a rubber septum and bubbling N_2 through the sensor suspension for ½ hour generated this environmental change. For the 100% O_2 measurement, the optical cell containing the PEBBLE suspension was sealed with a septum and pure O_2 was bubbled into the suspension for ½ hour.

The results of these studies show an increase in the anisotropy with increasing O_2 concentration (see Figure 2.7). This trend is opposite the previous results because, as mentioned earlier, the lifetime of the ruthenium dye decreases in the presence of increased O_2 concentration. The fluorescence lifetime of the $[Ru(dpp)_3]^{2+}$ in an oxygen free environment is 3.61 μS. When the dye is in the presense of 100% dissolved O_2, the fluorescence lifetime decreases to 0.277 μS because of quenching of the excited state by O_2[27]. The anisotropy is higher because the dye

42

embedded in the PEBBLE matrix does not have as much time to rotate before emitting.
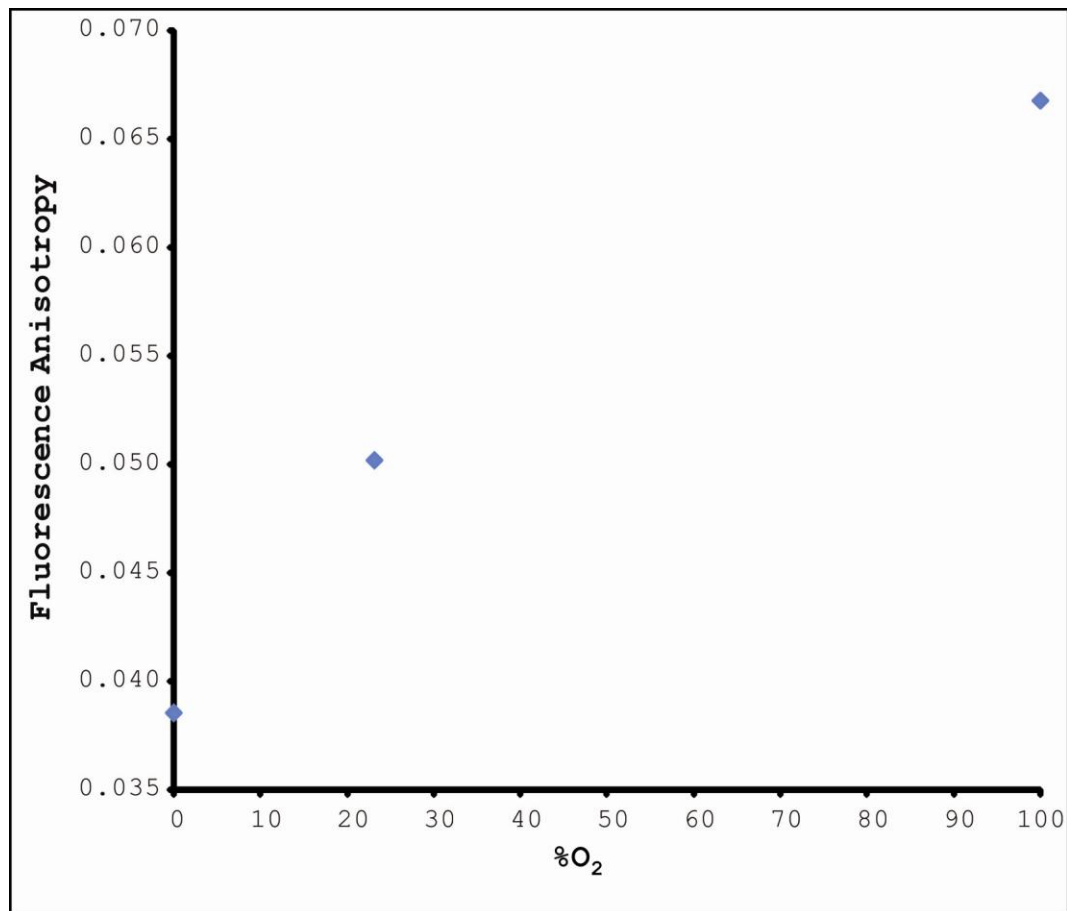
Figure 2.7: Anisotropic calibration curve for ruthenium PEBBLEs in N_2, air, and O_2 environments. The error for each measurement was less than 2%, so the error bars are smaller than the markers for the data points.

In conclusion, these data show that steady-state fluorescence anisotropy can be used to determine analyte concentrations, such as O_2, Ca^{2+}, and Zn^{2+}, when utilized in conjunction with fluorescence intensity-based probes embedded in PEBBLEs. These experiments show all the

43

advantages of PEBBLEs (i.e. mutual protection of the cellular organelles from the toxic probes, and a uniform rotational environment for the embedded probes) over the free dye. In this way PEBBLEs can also be utilized to quantitatively measure analyte concentration even without the aid of a reference dye. Although reference dyes were not used in these experiments, high anisotropy reference dyes could be embedded in PEBBLE nanosensors to potentially extend the dynamic range of the PEBBLE response, due to the additive nature of anisotropy[18,19]. Incidentally, there is no physical or chemical interference among different classes of PEBBLEs (in contrast to free dyes), only potential spectral overlap. The absence of reference dyes reduces such spectral overlap and opens the door towards simultaneous real-time chemical imaging inside a given live cell.

What is interesting in the Calcium Green and Newport Green PEEBLE studies is the loss of fluorescence anisotropic response when compared to the anisotropy of the free dyes (Calcium Green is actually attached to 10,000 g/mol dextran). Most likely this loss of anisotropic response is due to rotational correlation time of the PAA PEBBLEs used for this study. It is possible that the diameter of the particle (which directly effects the

44

rotational correlation time of the particle) is not the optimum size to maximize the anisotropy response of the embedded dye. This conjecture would have to be tested empirically with the synthesis of PAA PEEBLEs of different diameters. Alternatively, the rotational correlation time of the PEBBLE nanosensors may be altered by changing the temperature or viscosity of the suspending medium. Surface modification of the PEBBLE nanosensors could also change the rotational correlation time.

It would be prudent for any investigator extending this technique to cellular work to test the fluorescence anisotropy of the PAA PEBBLE nanosensors in a suspension that mimics the viscosity of cellular cytosol prior to testing this technique in cellular applications. The reason that the fluorescence anisotropy of the PAA Newport Green and Calcium Green PEBBLEs can be measured is that the nanosensors rotate very quickly. The increased viscosity of the cytosol could reduce the rotation to such a degree that the measured anisotropy response would diminish to such a degree that the sensor would not show a response to the presence of analyte.

2.5 ACKNOWLEDGEMENTS

2.6 REFERENCES

1. Clark, H.A., S.L.R. Barker, R. Kopelman, M. Hoyer, and M.A. Philbert, Subcellular optochemical nanobiosensors: probes encapsulated by biologically localized embedding (PEBBLEs)., *Sensors and Actuators B* **1998.** *51*: p. 12-16.

2. Clark, H.A., M. Hoyer, M.A. Philbert, and R. Kopelman, Optical nanosensors for chemical analysis inside single living cells. 1. Fabrication, characterization, and methods for intracellular delivery of PEBBLE sensors., Anal. Chem. **1999.** *71*(21): p. 4831-4836.

3. Brasuel, M., R. Kopelman, T.J. Miller, R. Tjalkens, and M.A. Philbert, Fluorescent Nanosensors for Intracellular Chemical Analysis: Decyl Methacrylate Liquid Polymer Matrix and Ion-Exchange-Based Potassium PEBBLE Sensors with Real-Time Application to Viable Rat C6 Glioma Cells., Anal. Chem. **2001.** *73*(10): p. 2221-2228.

4. Xu, H., J.W. Aylott, R. Kopelman, T.J. Miller, and M.A. Philbert, A Real-time Ratiometric Method for the Determination of Molecular Oxygen Inside Living Cells Using Sol-Gel-Based Spherical Optical Nanosensors with Applications to Rat C6 Glioma., Anal. Chem. **2001.** *73*(17): p. 4124-4133.

5. Lee-Koo, Y.E., Cao, Y., Kopelman, R., Koo, S.M., Brasuel,M.G., Philbert, M.A., Real-Time Measurements of Dissolved Oxygen Inside Live Cells by Organically Modified Silicate Fluorescent Nanosensors., Anal. Chem. **2004.** *76:*2498-2505.

6. Clark, H.A., R. Kopelman, R. Tjalkens, and M.A. Philbert, Optical nanosensors for chemical analysis inside single living cells. 2. Sensors for pH and calcium and the intracellular applications of PEBBLE sensors., Anal. Chem. **1999,** *71*(21): p. 4837-4843.

7. Brasuel, M., Kopelman, R., Miller, T.J., Tjalkens, R., Philbert, M.A., Fluorescent nanosensors for intracellular chemical analysis: decyl methacrylate liquid polymer matrix and ion-exchange-based potassium PEBBLE sensors with real-time application to viable rat C6 glioma cells., Anal. Chem. **2001,** *73*:2221-2228

8. Sumner, J.P., Aylott, J.W., Monson, E., Kopelman, R., A fluorescent PEBBLE nanosensor for intracellular free zinc., Analyst **2002,** *127*: 11-16.

9. Brausel, M. Kopelman, R., Kasman, I., Miller, T.J., Philbert, M.A., Ion concentrations in live cells from highly selective ion correlation fluorescent nano-sensors for sodium., Proceedings of IEEE sensors **2002,** *1*:288-292.

10. Park, E.J., Brasuel, M., Behrend, C., Philbert, M.A., Kopelman, R., Ratiometric optical PEBBLE nanosensors for real-time magnesium ion concentrations inside viable cells., Anal. Chem. **2003,** *75*:3784-3791.

11. Brasuel, M.G., Miller, T.J., Kopelman, R., Philbert, M.A., Liquid polymer nano-PEBBLEs for Cl- analysis and biological applications., The Analyst **2003,** *128*:1262-1267.

12. Barker, S.L.R., Kopelman, R., Fiber-Optic Nitric Oxide-Selective Biosensors and Nanosensors., Anal. Chem. **1998,** *70*(5):971-976

13. Hao, X., Aylott, J.W., Kopelman, R., Fluorescent nano-PEBBLE sensors designed for intracellular glucose imaging., The Analyst **2002,** *127*:1471-1477.

14. Buck, S.M., Koo, Y.E.L., Park, E., Xu, H., Philbert, M.A., Brasuel, M.A., Kopelman, R., Optochemical nanosensor PEBBLEs: photonic explorers for bioanalysis with biologically localized embedding., Current Opionion in Chemical biology **2004,** *8*:540-546.

15. Moffat, B.A., Reddy, G.R., McConville, P., Hall, D.E., Chenevert, T.L., Kopelman, R., Philbert, M., Weissleder, R., Rehemtulla, A., Ross, B.D., A Novel Polyacrylamide Magnetic Nanoparticle Contrast Agent for Molecular Imaging Using MRI., Mol. Imaging **2003,** *2*:324-332

16. Yan, F., Xu, H., Anker, J., Kopelman, R., Ross, B., Rehemtulla, A., Reddy, R., Synthesis and Characterization of Silica-embedded Iron Oxide Nanoparticles for Magnetic Resonance Imaging., J. Nanoscience and Nanotechnology **2004,** *4*:72-76.

17. Lippitch, M.E., Optical sensors based on fluorescence anisotropy., Sensors and Actuators B **1993,** *11*:499–502.

18. Lakowicz, J.R., Gryczynski, I., Grycznski, Z., and Dattelbaum, J.D., Anisotropy-Based Sensing with Reference Fluorophores., Anal. Biochem. **1999,** *267*:397-405.

19. Gryczynski, I., Gryczynski, Z., Rao, G., and Lakowicz, J.R., Polarization-based oxygen sensor., The Analyst **1999,** *124*:1041-1044.

20. Thompson, R.B., Fierke, C.A, and. Maliwal, B.P., Expanded Dynamic Range of Free Zinc Ion Determination by Fluorescence Anisotropy., Anal. Chem. **1998,** *70*:1749-1754.

21. Thompson, R.B., Fierke, C.A., Maliwal, B.P., Feliccia, V.L., and McCall, K., Determination of Picomolar Concentrations of Metal Ions Using Fluorescence Anisotropy: Biosensing with a "Reagentless" Enzyme Transducer., Anal. Chem. **1998,** *70*:4717-4723.

22. Hof, M., Fidler, V., Hutterer, R., (**2005**). Basics of Fluorescence Spectroscopy in Biosciences. Ed. Wolfbeis, O.S., Fluorescence Spectroscopy in Biology, New York, NY, Springer

23. Tsien, R., Pozzan, T., Measurement of cytosolic free Ca2+ with quin2., Methods Enzymol **1989,** *172*:230-262.

24. Thompson, R.B., Peterson, D., Mahoney, W., Cramer, M., Maliwal, B.P., Suh, S.W., Frederickson, C., Fierke, C., Herman, P., Fluorescent zinc indicators for neurobiology, J. Neuro. Meth. **2002,** *118*:63-75.

25. Yoshiki, K., Azuma, H., Yoshioka, M.H., Araki, T., Finding of Optimal Calcium Ion Probes for Fluorescence Lifetime Measurement, Optical Review **2005,** *12*: 415-419.

26. Martin, J.L., Stork, C.J., Li, Y.V., Determining zinc with commonly used calcium and zinc fluorescent indicators, a question on calcium signals, Cell Calcium **2006,** *40*:393-402.

27. Castellano, F.N., Lakowicz, J.R., A Water-Soluble Luminescence Oxygen Sensor, Photochemistry and Photobiology **1998,** *67*:179-183.

CHAPTER 3

**SILVER NANOPRISM COLLOIDS AS SURFACE-ENHANCED RAMAN
SCATTERING (SERS) SUBSTRATES**

3.1 INTRODUCTION

In 1928, Sir C.V. Raman and K.S. Krishnan experimentally
observed inelastically scattered photons of a modified
wavelength in many different transparent organic
solvents[1]. They collected sunlight using a 7-inch
refractor telescope, and filtered the solar radiation using
a Zeiss Cobalt Blue filter. The blue-violet components of
the solar spectrum transmitted through the filter were
focused into a tank that had a vial of a scattering medium.
Raman and Krishnan observed, through the use of a yellow-
green filter, a feeble green track of scattered and highly
polarized radiation along the track of elastically
scattered incident blue-violet light. Later that same
year, they utilized a monochromatic light source (435 nm
line from a mercury arc lamp) to measure the first
inelastically scattered modified wavelength spectrum for

several organic solvents including carbon tetrachloride and benzene[2]. They noted in this work that the secondary radiation was highly polarized, and not excited near an IR or UV absorption frequency for the scattering media used in the experiment. Therefore, the investigators had discovered a new form of secondary radiation that could not be attributed to fluorescence of the scattering materials. For this work, Sir C.V. Raman won the Noble Prize in 1930 and was honored by this effect being named after him[3].

In the early 1970's the electrochemical research community had started to look at the application of Raman spectroscopy to study electrochemical interactions at solid-liquid interfaces. This interest was steeped in the molecular specificity that the rich vibrational spectrum Raman scattering provides. The molecular specificity and environmental sensitivity inherent in Raman scattering can provide spectral information to elucidate the geometry of molecular interactions of a probed molecule with either surfaces or bulk solvent local to the molecule. In terms of vibrational spectroscopy of aqueous solutions, Raman spectroscopy is superior to IR absorption spectroscopy because the Raman scattering efficiency from water is weak, and it is in the visible region of the spectrum[4].

The model electrochemical system that was first studied using Raman scattering spectroscopy was the potential dependent interaction of the pyridine molecule with a roughened silver electrode reported in 1974[4]. The same electrochemical system was studied using Raman scattering spectroscopy twice more in 1977[5,6]. In all three publications the authors discussed the necessity of performing oxidation-reduction cycling to roughen the surface of the electrochemical electrode prior to making the Raman measurements of the pyridine. They also all reported that the pyridine molecule is adsorbed onto the electrode surface axially through the non-bonding electron pair from the hetero-nitrogen atom in the pyridine ring. The evidence of this configuration is the presence of a Very Strong (VS) Raman band at 1025 cm^{-1} that is not present in pure pyridine solvent, or in 50 mM pyridine solutions[4].

The two studies conducted in 1977 presented an alternative view for the mechanism of signal enhancement compared with the study from 1974. Originally, it was suggested that by roughening the silver electrode through electrochemical oxidation-reduction cycling, the overall surface area of the electrode is increased by a factor of ten[4]. This increased surface area of the electrode allowed for a larger concentration of the scattering

analyte to be absorbed onto the surface of the roughened electrode, thus providing the sensitivity to measure a near-monolayer of adsorbed pyridine. Jeanmaire *et al.* presented experimental data that showed a fifty-fold increase in the Raman signal from a sample of 50 mM pyridine in a 100 mM KCl electrolyte solution, with the presence of a roughened silver electrode, relative to a 50 mM pyridine solution, in the same electrolyte solution without the electrode[5]. Albrecht *et al.* presented a case where the signal from the ring-stretching modes from pyridine adsorbed on a roughened silver electrode were 5-times more intense than they were for a pure pyridine sample[6]. Both studies indicate that the Raman signal enhancement was not caused by an increased surface area of the electrode, but rather due to either an electromagnetic enhancement mechanism such as the electric field gradient on the order of $1 \times 10^{+6}$ V cm^{-1} local to the electrode surface[5], or by a first layer chemical enhancement mechanism such as Resonant Raman scattering effect, where the adsorbed molecule interacts with the surface plasmon of the metallic electrode[6].

In 1978 Creighton *et al.* reported a SERS study of pyridine performed on silver and gold hydrosols that have a particle diameter that is comparable to the wavelength of

the incident radiation[7]. In the silver sol experiment, strong SERS bands were found to be at 1038 cm^{-1}, 1010 cm^{-1}, and 228 cm^{-1} as was reported in the roughened silver electrode studies. For comparison, the intensity of the 1010 cm^{-1} ring breathing band for sample preparations of between 2 and 7 mM pyridine in the presence of a silver hydrosol suspended in a 100 mM KCl electrolyte solution is approximately 5 times the intensity of that for the normal Raman scattering of a 100 mM pyridine in a 100 mM KCl electrolyte solution under the same conditions.

In the first report of SERS on a gold hydrosol, strong SERS bands were observed at 1038 cm^{-1}, 1014 cm^{-1}, and 260 cm^{-1} [7]. It was found that the 1014 cm^{-1} ring stretching band for a 3 mM pyridine solution in the presence of the gold hydrosol suspended in 100 mM KCl electrolyte was approximately 3 times more intense than the 1003 cm^{-1} band in the normal Raman spectrum for 100 mM pyridine in a 100 mM KCl electrolyte solution using the 632.8 nm excitation of a He-Ne laser.

Since the discovery of the SERS phenomenon on roughened silver electrodes and both silver and gold hydrosols, there has been tremendous growth in the development of colloidal and core-shell based floatware SERS substrates[8], and flatware SERS substrates (e.g. nanolithography based

islands, and island films on microscope slides)[9]. A floatware substrate is a substrate that is suspended in a fluid, such as suspended colloidal dispersions that are free to translate, rotate, and aggregate in suspension. Although the substrate is free to move about the volume of liquid, the SERS effect takes place on solid-liquid interface between the analytes in the sample adsorbed onto or in close proximity (~10 nm) with the surface of the colloid. A flatware substrate is a SERS substrate that is deposited, attached, or etched onto a bounding surface, or embedded in a film such as silica gel or poly (acrylamide)[10-12]. With the flatware substrate the analyte of interest still interacts with the solid surface of the SERS substrate, but in this case the substrate could be used to sample solid, liquid, or gaseous interfaces.

The continued development and enhancement of these floatware and flatware SERS substrates has advanced the presence of optical based measurements in environmental science[13,14], biological and biomedical sciences[15-18], pharmaceutical science[19-21], and single molecule spectroscopy[22,23].

Recently, the attention of colloid scientists has been focused on the development of wet-chemical synthetic methods for aspherical colloidal particles with tunable

plasmonic resonances. To date, many aspherical silver colloids have been synthesized via wet-chemical methods including silver and gold nanorods and nanowires[24,25], silver and gold nanoprisms[26-34], silver nanotetrahedrons[35], silver nanocubes[36], and silver nanodisks[37,38]. It has also been discovered that utilizing a wet-chemical galvanic replacement reaction, the aspherical colloids already mentioned above, can be converted into a thin gold shells, with hollow interiors, that retain the same shape morphology as the silver nanoparticle templates[39,40]. In a study for the galvanic replacement of silver by gold for the nanoprism colloid, it was noted that the tetrachloroaurate ($HAuCl_4$) etching of the silver structure occurred on the [111] triangular facet of the silver nanoprism structure[31,41]. As a result of this reaction, a thin triangular gold nanoframe structure is synthesized instead of a hollow triangular nanoshell. It is thought that the narrow width (<10 nm) of the silver nanoprism, distance between the parallel triangular [111] facets for the nanoparticle, results in the formation of this gold nanoframe structure during the galvanic replacement reaction. The redox reaction for the galvanic replacement of silver by gold is as follows:

$$3 \ Ag_{(S)} + AuCl_4^-{}_{(aq.)} \rightarrow Au_{(S)} + 3Ag^+{}_{(aq.)} + 4 \ Cl^-{}_{(aq.)} \qquad Eq. \ 1$$
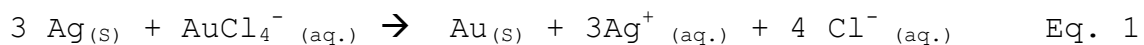
The thin gold shell is resultant of the stoichiometry of the redox reaction. The gold ion is in the 3^+ oxidation state in the aurate salt, therefore 3 silver atoms are oxidized to reduce one gold atom.

The silver nanoprism colloid is one of the most optically tunable and well characterized aspherical colloids to be synthesized via wet-chemical methods. The interest in the nanoprism colloid is based upon the tunability of the Localized Surface Plasmon Resonance (LSPR), and hence the optical properties of the nanostructure. The LSPR can be tuned by changing the edgelength of the triangular nanoparticle, degree of truncation of the triangular tips, or by changing the thickness of the nanoparticle[26,27]. In the UV-Vis extinction spectrum for the nanoprism colloid, the in-plane quadrapole and out-of-plane quadrapole plasmon resonances are found near 350 nm and 450 nm, respectively[26]. The dipolar plasmon resonance of the nanoprism colloid is tunable from 600 nm to approximately 1000 nm. As the edgelength of the nanoprism is increased, the dipolar plasmon resonance of the colloid is moved to the red. If the sharp edges of the nanoprism colloid are

truncated (as in a hexagonal plate), or rounded, then a blue shift of as much as 60 nm in the dipolar plasmon resonance is observed. Synthetic pathways described in the literature for the formation of the silver nanoprism colloid include both photo-mediated and thermal-mediated Ostwald Ripening reactions[42].

In the photo-mediated reactions[26,31,32,41], a spherical silver precursor colloid is synthesized (<10 nm diameter) by the reduction of silver nitrate ($AgNO_3$) solution in the presence of trisodium citrate by the addition of a sodium borohydride ($NaBH_4$) solution. Once the precursor colloid is synthesized, the conversion of the spherical colloid into the aspherical colloidal structure is guided by an organic capping agent such as poly(vinyl pyrrolidone) (PVP). It is thought that the PVP works by capturing, and holding the precursor colloid in close proximity so that Ostwald ripening of the nanoprism colloid can take place.

The conversion process, within the synthetic reaction, is driven by illuminating the sample with a monochromatic light source for a period of approximately 50 hours. When a single wavelength of light is used for the synthesis, a bimodal size distribution of the nanoprisms is evident when the particles are imaged with electron microscopy, and with the presence of an additional dipolar plasmon peak that is

measured in the NIR portion of the electromagnetic spectrum (~1000 nm)[26]. The bimodal size distribution is based on the photo-induced fusion of four smaller type 1 nanoprism colloids in an end-on configuration forming a much larger type 2 nanoprism (See Figure 3.1).
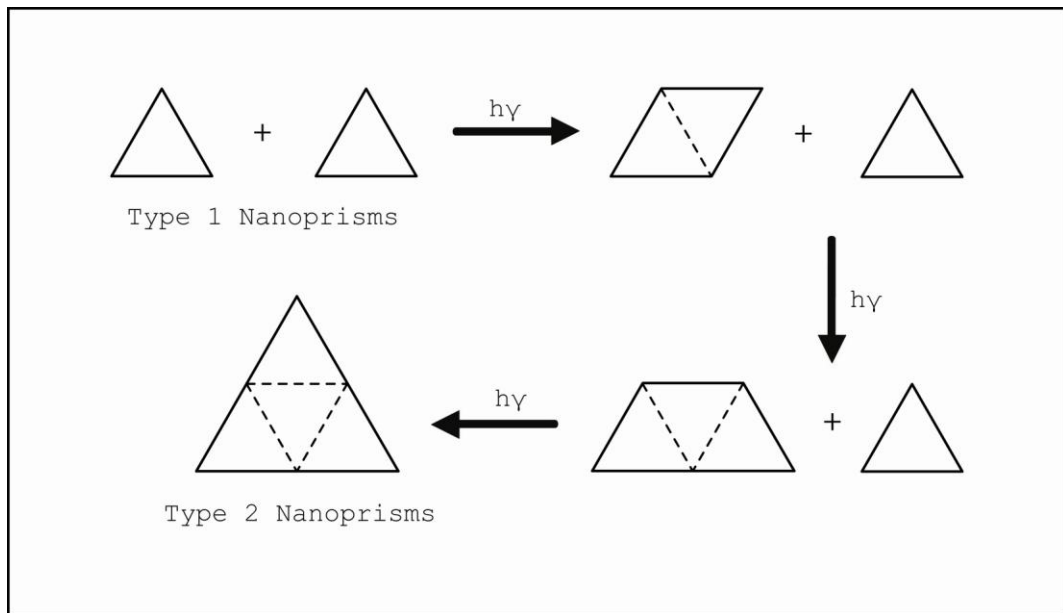
Figure 3.1: Schematic of how a bimodal distribution of nanoprisms forms in suspension under illumination in resonance with the dipolar plasmon of the nanoparticle. This figure adapted from reference 26.

This occurs when the dipolar plasmon of the smaller nanoprism structures are in resonance with the excitation for the photo-lysis reaction. A method was devised to synthesize a monodisperse nanoprism size distribution by driving the conversion of the spherical precursor colloid into the nanoprism colloid using a dual wavelength excitation approach[32]. The first wavelength chosen is used

60

to excite either the in-plane or the out-of plane quadrapole plasmon resonance of the Type 1 nanoprisms to prevent end-on fusion of these smaller nanoprisms. The second wavelength is used to selectively tune the dipolar plasmon resonance of the nanoprism.

The thermal synthetic methods rely on heat imparted either by external heating or generated by reagents in solution to drive the formation of the nanoprism structure[27,29,33,34]. The work presented by Métraux *et al.*, outlines a thermal synthetic method for producing nanoprisms with unimodal size distribution in terms of edgelength, and of a tailorable particle thickness[27]. This method of synthesis allows for rational control over the nanoprism plate thickness, and thus the dipolar plasmon resonance. It has been shown in the dual-beam, photo-induced synthetic method for nanoprisms that the rational control of the edgelength for the nanostructure allowed the tuning the dipolar plasmon by up to 60 nm[32]. The thermal synthetic method provides a rational control of nanoprism thickness, and thereby allowing for the tuning of the dipolar plasmon resonance by up to 200 nm[27]. The dual-beam synthetic pathway requires up to 50 hours of illumination to complete the nanoprism synthesis where the thermal

method take approximately 30 minutes to complete the reaction.

3.2 EXPERIMENTAL BACKGROUND

It has been experimentally discovered that there are two components to the SERS enhancement mechanism that occur either in contact with, or in close proximity to, a metallic substrate surface. The electromagnetic enhancement mechanism is based on an electromagnetic field enhancement local to a metallic substrate because of the LSPR of the conduction electrons near the surface of the metallic substrate. This electromagnetic effect is a proximity effect that has a $(1/d)^{12}$ distance dependence from the substrate surface[43]. The second Raman enhancement mechanism is described as a first layer chemical enhancement mechanism and results from an adsorbed molecule on the surface of a roughened bulk metallic substrate or a nanoscale metallic colloid.

A model for the enhanced Stokes-shifted SERS signals for analyte molecules local to metallic colloids in suspension has been described by Kneipp *et al.* that encompasses both mechanisms[43], and is defined as:

$$P^{SERS}(\nu_s) = N' * \sigma_{ads}^{R} * G_{em}(\nu_S) * I(\nu_L) \hspace{2cm} \text{Eq.2}$$

Where the Stokes shifted SERS signal is designated as P^{SERS} (ν_s), and N' is the number of molecules adsorbed onto the colloidal surface, or in proximity of the enhancing substrate (~10 nm for colloidal particles). The chemical enhancement mechanism term is the σ_{ads}^{R}, and it represents the increased Raman Scattering cross-section for the molecule. The enhancement factor for the chemical mechanism is typically reported to be a $10-10^2$ enhancement over normal Raman scattering. The $G_{em}(\nu_S)$ term represents the electromagnetic enhancement mechanism for the increased electromagnetic field local to the colloid particle because of the LSPR, and has been reported as high as an enhancement of 10^{12} to the Raman cross-section of the analyte for single molecule SERS experiments.

In a sample with suspended metallic colloidal particles, the electromagnetic enhancement term is a direct result of the scattering molecule's proximity (0-10 nm) to colloids or fractal colloidal structures in suspension or on a surface in the presence of a driving electromagnetic field. The electromagnetic enhancement near the metallic nanoparticle is the result of a plasma of coherently oscillating conduction electrons moving about the lattice

of metallic atoms, in fixed position, that consist of nuclei and core electrons. This LSPR phenomenon occurs in free-electron metals such as alkali metal, Mg, Al, and the coinage metals. These quantized oscillations of the conduction electron gas account for the polarizability of the metallic nanoparticle in the presence of the electromagnetic field, allowing the metallic nanoparticle to behave like an electronic dipole. These oscillations are known as dipolar Surface Plasmons that oscillate at a frequency known as the plasma frequency. This plasma frequency is defined for a bulk metal with infinite size scale in all three dimensions as[44]:

$$\omega_p = \left(\frac{Ne^2}{\varepsilon_o m_e}\right)^{1/2}$$

Eq.3

Where N is the metal specific number density of conduction electrons, ε_o is the dielectric constant of a vacuum, e is the charge on an electron, and m_e is the reduced mass of an electron. In nanoscale metallic colloids, below the Rayleigh limit (diameter $\ll \lambda$), a boundary condition that defines a resonant frequency for the LSPR (in vacuum) is $\omega_p/\sqrt{3}$. When the frequency of the electromagnetic field is in resonance with the LSPR of the metallic colloid, the electromagnetic field is strongly scattered, strong SP

absorption bands occur, and the electromagnetic field local to the colloid is enhanced[45].

The electromagnetic enhancement term, $G_{em}(v_S)$, in Eq. 2 describes the enhancement of the electromagnetic fields for both the driving field of the laser, and the scattered fields from the stokes shifted Raman scattering from the analyte near the surface of a metallic colloid, and is defined as[43]:

$$G_{em}(v_S) = |A(v_L)|^2 |A(v_S)|^2 \sim \left|\frac{\varepsilon(v_L) - \varepsilon_o}{\varepsilon(v_L) + 2\varepsilon_o}\right|^2 \left|\frac{\varepsilon(v_S) - \varepsilon_o}{\varepsilon(v_S) + 2\varepsilon_o}\right|^2 \left(\frac{r}{r+d}\right)^{12} \qquad \text{Eq. 4}$$

Where $A(v_L)$ is the field enhancement term for the laser field, and $A(v_S)$ is the field enhancement term for the Stokes scattered field. The terms $\varepsilon(v_L)$ and $\varepsilon(v_S)$ are the complex dielectric constants of the metallic colloid at the frequencies of the driving field and the scattered field, respectively. The term ε_o is the dielectric constant for the medium the colloid is suspended in. The field enhancement terms for a metallic sphere are resonant at the frequency for which real part of the dielectric constant for the metal equals two times the dielectric constant of the medium, or $Re(\varepsilon) = 2*\varepsilon_o$. For a metal to be a strong enhancement substrate, the density of the conduction electrons in the free-electron metal has to be large, and

the imaginary part of the dielectric constant of the metal, $\text{Im}(\varepsilon)$, needs to be small. The terms r and d represent the radius of the colloidal particle and the distance of the molecule to the surface of the colloid, respectively.

Although it is difficult to experimentally isolate the chemical enhancement contribution from the overall SERS enhancement, there have been several experimental observations that have provided evidence for the existence of the chemical enhancement mechanism when analytes are adsorbed onto the surface of roughened electrodes and nanoscale colloids[43,49]. Evidence for the chemical enhancement mechanism is present in the data presented for the original SERS studies of pyridine adsorbed onto electrochemically roughened electrodes[5,6]. In these original works, the authors studied the SERS intensity response as a function of electrode potential for adsorbed pyridine molecules. It was observed in these experiments that when the wavelength of the laser excitation is held constant, broad resonances are measured when the electrode potential is swept.

Several different mechanisms have been described in the literature for the first layer chemical enhancement mechanism. In all cases, the molecule has to be adsorbed onto the surface of the metallic colloid. One such

mechanism describes an electronic coupling between the adsorbate-metal complex that results in an increased Raman cross section for the complex relative to the analyte free in solution[49,50]. A second potential chemical enhancement mechanism is based on a resonant Raman effect where the electronic levels of the analyte are broadened due to the adsorption of the molecule on the metallic surface because of metal and analyte molecular orbital mixing between the molecule-metal complex[43,49]. This energy level broadening would allow for new electronic transitions in the molecule-metal complex. A third potential mechanism is known as a dynamical charge transfer mechanism that can be described in four steps[43,51]. An incident photon is annihilated with the corresponding excitation of an electron from below the Fermi level of the metal-molecule complex to above the Fermi level. Once this electron is in the excited state, it transfers into the Lowest Unoccupied Molecular Orbital (LUMO) of the adsorbed molecule. When the electron falls back into the hole below the Fermi level for the complex, and the molecule is in an excited vibrational state, a Stokes shifted photon is created from the interaction of the metal and molecule in a complex.

3.3 EXPERIMENTAL SETUP

The Raman system consisted of an Olympus BX 60 upright microscope fitted with a Holoprobe VPT® system and Hololab 1000® Raman spectrometer system (Kaiser Optical Systems, Ann Arbor, MI, USA). Encompassed in the Hololab 1000 system is a He-Ne laser with emission at 633 nm. Light from the excitation source, from within the Hololab 1000 system is coupled to the VPT system using an optical fiber. The light from the excitation source is focused into the sample using a 10x objective with NA 0.25. The Raman emission was collected in a backscattered configuration by the same objective used for focusing the excitation. Dispersion of the collected Raman emission was performed by a holographic Holospec F/1.8i volume transmissive grating with the range of 400 to 3650 cm^{-1}. The Raman spectrum is then detected by a 1024 x 64 Hamamatsu MPP CCD camera. Operational control of the microscope, and data acquisition of the experimental sample were provided by the HoloGRAMS® software package (Kaiser Optical Systems, Ann Arbor, MI, USA).

3.4 EXPERIMENTAL METHODS

3.4.1 4-Mercaptopyridine (4-MPy) studies

After searching the literature, the 4-MPy molecule was chosen as an analyte for testing the SERS enhancing capability of the silver nanoprism colloid because of its well characterized SERS spectrum, and its known orientation of interaction with a silver surface[46-48]. It has been experimentally determined that the 4-MPy molecule is adsorbed onto a silver surface through the thiol moiety with the plane of the pyridine ring oriented perpendicular to the silver surface. This adsorption geometry makes the nonbonding pair of electrons on the hetero-nitrogen (Lewis base) available for Lewis Acid-Base interactions with hydronium ions in solution. This Lewis acid-base interaction provides for interesting pH dependent SERS signals. Therefore, if a Stokes-shifted SERS signal could be acquired for the nanoprism colloid in combination with the 4-MPy molecule, a SERS based pH sensor would be plausible. As the pH of a sample of 4-MPy is lowered from neutral, the thiol-to-thione tautomerization will shift equilibrium towards the thiol structure, and the N-protonation SERS bands for the hetero-nitrogen atom in the

pyridine ring will blueshift by up to 40 cm^{-1} [48] (see Figure 3.2). The primary pH dependent SERS marker band (8a$_1$ – ν(CC)) for hetero-nitrogen protonation for the 4-MPy molecule shifts from 1624 cm^{-1} (cationic thiol tautomer, ~ pH 1) to 1580 cm^{-1} (anionic thiolate form, ~ pH 12) (see Figure 3.3) [46,48]. At intermediate pH, both bands are present in equal proportion to the population of cationic thiol versus the anionic thiolate tautomer. A calibration curve for the relative ratios for the intensities of these two bands would provide a SERS based method for determining pH for a sample. A second N-protonation SERS band (9a – β(CH)/δ(NH)) shifts from 1202 cm^{-1} when protonated to 1220 cm^{-1} when deprotonated [46,48]. The following study was conducted to explore the potential of the silver nanoprism colloid to act as a SERS enhancing substrate. If a SERS spectrum for 4-MPy could be acquired, the possibility of creating a SERS-based silver nanoprism pH sensor would be investigated.
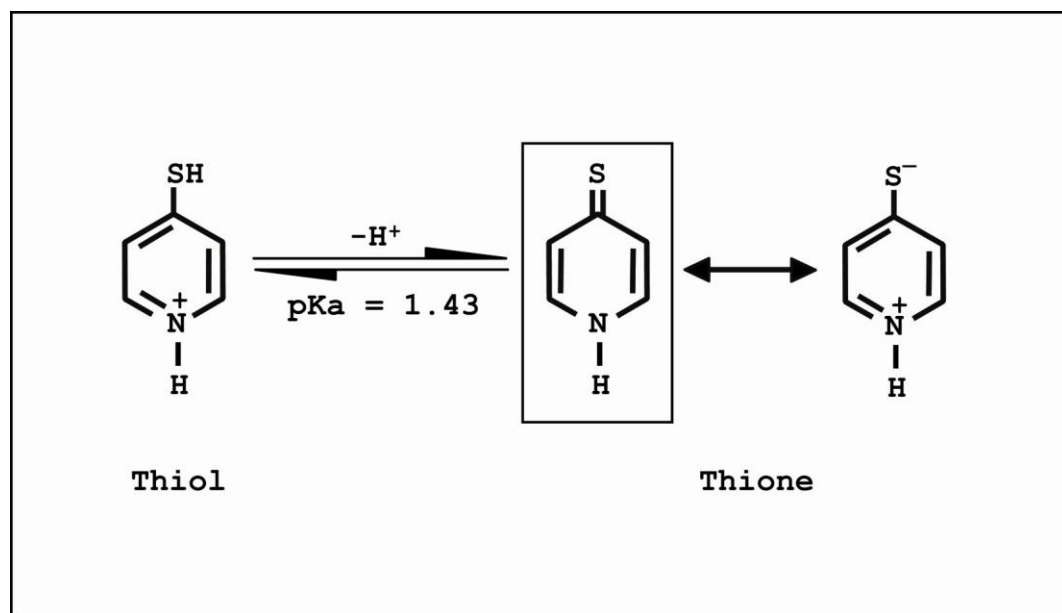
Figure 3.2: Thiol-thione tautormerization of the 4-MPy structure based on pH of sample. The resonance hybrid structure for the 4-MPy molecule at neutral pH is indicated in the box. Figure adapted from references 46-48.

The sample solution of 4-MPy (95% crystalline, Sigma-Aldrich, St. Louis, MO, USA) was prepared by making a saturated solution of analyte in 18 MΩ deionized (DI) water purified with a Barnstead 1 Thermolyne Nanopure II system (Barnstead International, Dubuque, IA, USA). More specifically, this sample was produced by adding 0.57 g of 4-MPy to a glass scintillation vial along with 10 mL of 18 MΩ DI water, and sonicated for one hour to dissolve the material. When sonication was complete, the vial was placed on the benchtop to allow the undissolved 4-MPy crystals to settle to the bottom of the vial. The saturated 4-MPy solution had a deep yellow color that was

slightly cloudy due to the small particles of 4-MPy still suspended. A plastic pipette was used to draw off the saturated 4-MPy supernatant solution, leaving the large undissolved crystals on the bottom of the vial. The solution was transferred to a 4 mL quartz cuvette, sealed and placed on the Raman microscope stage. The HoloGRAMS software was configured so that the acquisition time was set for one minute, with only one trial. The software was also set to subtract off the dark current image from the CCD image. The acquired spectrum is shown in Figure 3.3.
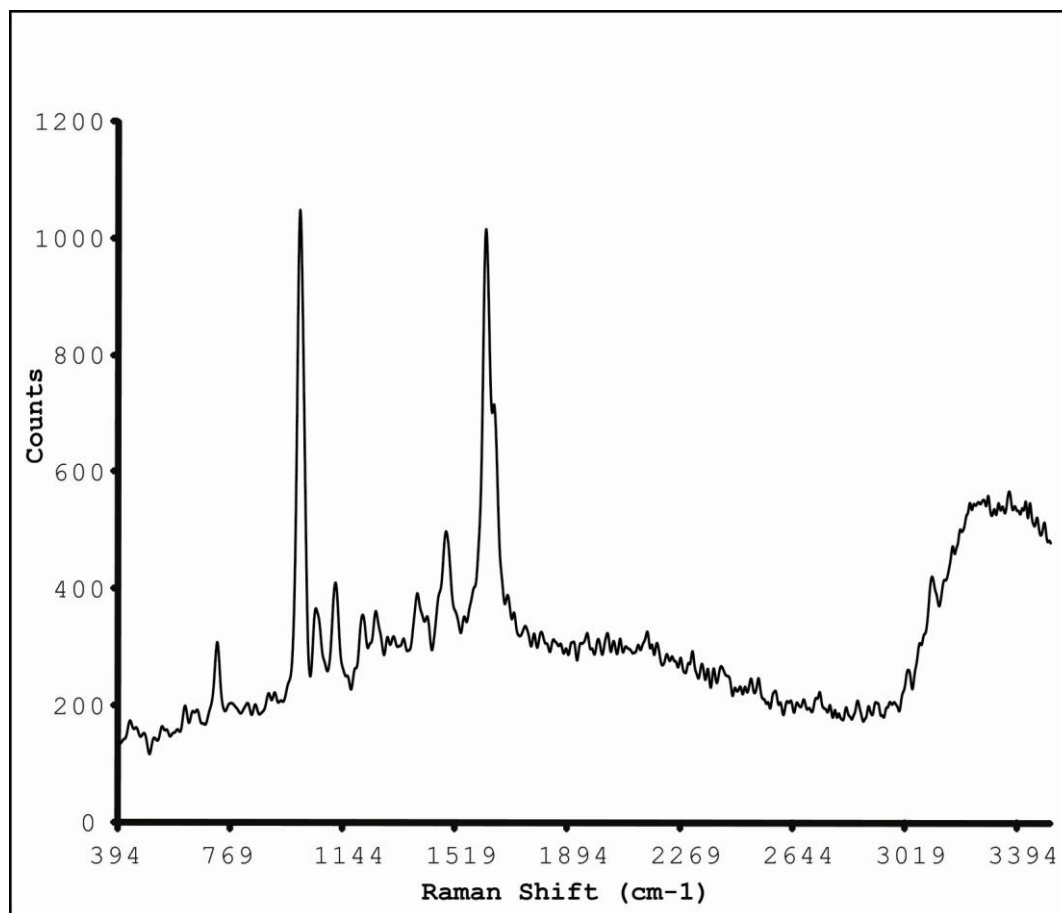
Figure 3.3: The Raman spectrum acquired for a saturated solution of 4-MPy in water.

3.4.2 Nanoprism Synthesis via Thermal Methods

G.S. Metraux *et al.*, presents a thermal synthetic method for creating nanoprisms with a unimodal size distribution, sharp triangular morphology, and a tunable thickness[27]. These characteristics, and especially the thickness of the nanoprism, allow for dipolar resonance tuning capabilities. This method involves varying the amounts of $NaBH_4$ added to

the reaction mixture in its initial stages (See Figure 3.4), to alter nanoprism thicknesses.

At the beginning of the experiment, all reagents were prepared fresh, and three round bottom flasks were cleaned with concentrated H_2SO_4 (Sigma-Aldrich, St. Loius, MO, USA) in order to remove all deposits from the glassware. The glassware was then rinsed with copious amounts of DI water to remove the acid. Each flask was fixed, using a metal clamp, so that they were held on the surface of stir plates in the hood. A 1 cm magnetic stir bar that had been cleaned with alconox was added to each flask.

A 25 mL aliquot of a 0.1 mM $AgNO_3$ (aq.) stock solution was added to each of three round bottom flasks and stirred at 1300 rpm. To the stirred $AgNO_3$ solution in each of the flasks, a 1.5 mL aliquot of a 30.1 mM trisodium citrate (aq.) (Alfa Aesar, Ward Hill, MA, USA) stock solution and a 1.5 mL aliquot of a 0.759 mM PVP (aq.) (Mw = 29,000 g/mol, Sigma-Aldrich, St. Louis, MO, USA) stock solution were added. Next, a 60 µL aliquot of a 30% H_2O_2 (aq.) (GFS Chemical, Powell, OH, USA) solution was added to each flask. In order to initiate the nanoprism synthesis reaction, and create varying nanoprism colloid thicknesses, a different volume of a 96 mM $NaBH_4$ (aq.) (99.99% pellet, Sigma-Aldrich, St. Louis, MO, USA) stock solution was added to each flask,

respectively. After adding the NaBH$_4$ aliquot, each solution turned a very light yellow color as the silver colloid suspension formed. Each flask was covered with a sheet of aluminum foil, for the duration of the synthesis, in order to block light from the fluorescent lighting in the lab. After allowing 30 minutes for the nanoprism synthesis to complete, the colloid suspension that had 87.5 μL of 96 mM NaBH$_4$ stock solution added had a deep burgundy color, the other two colloidal suspensions were deep blue in color. The UV-Vis extinction spectra for each of the colloidal suspensions were measured using a Shimadzu UV-1601 UV-Vis spectrophotometer (See Figure 3.4). It has been shown experimentally that the reagents do have a viable lifetime, so all the reagents should to be made fresh before each nanoprism synthesis.

In order to prepare this suspension of particles for the TEM imaging, the samples were pre-concentrated by centrifugation at 12,000 rpm for 30 minutes in order for the nanoprism colloid to settle out of suspension. When the centrifugation was completed, the supernatant was drawn off with a pipette, and the remaining suspension was sonicated for several minutes to resuspend the particles. A 10 μL droplet of the concentrated nanoprism colloid suspension was dropped onto a copper with Formvar® and

carbon reinforced TEM Grid (Structure Probe, Inc., West Chester, PA, USA).
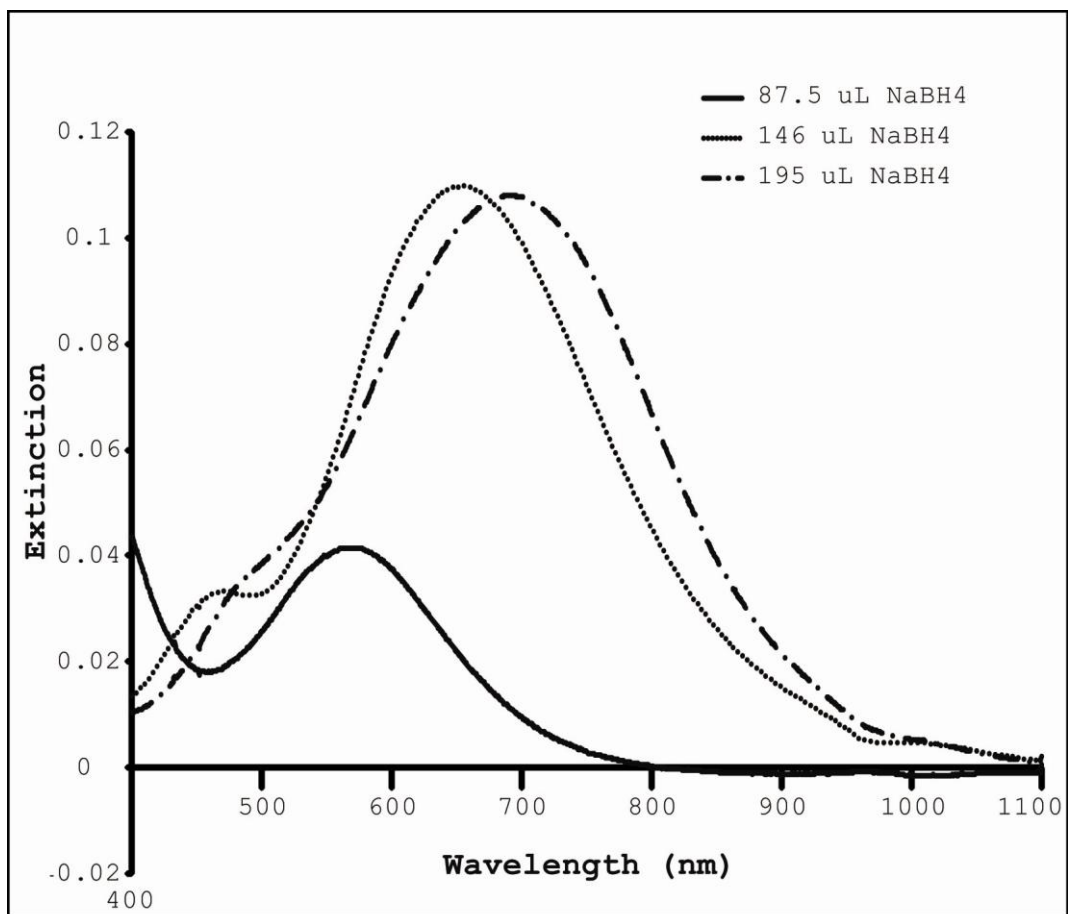
Figure 3.4: UV-Vis Extinction spectra for the thermally synthesized nanoprisms as a function of $NaBH_4$ (aq.) concentration.

TEM microscopy shows that the primary colloidal structure in suspension is the nanoprism colloid, having a triangular shape without corner truncation. The sharp colloidal corners cause a red-shifting of the dipolar plasmon (See Figure 3.5 (a.)). The Figure 3.5(b.) shows a stack of the nanoprism colloid from which the average

thickness of the 124 colloidal particles was measured to be

5.28 nm with a standard deviation of 0.91 nm. These images

were acquired using the ITEM® software on the Phillips CM-

12 TEM/STEM electron microscope, and the thickness

measurements were made on the TEM images using the magic

wand utility on the ITEM software.
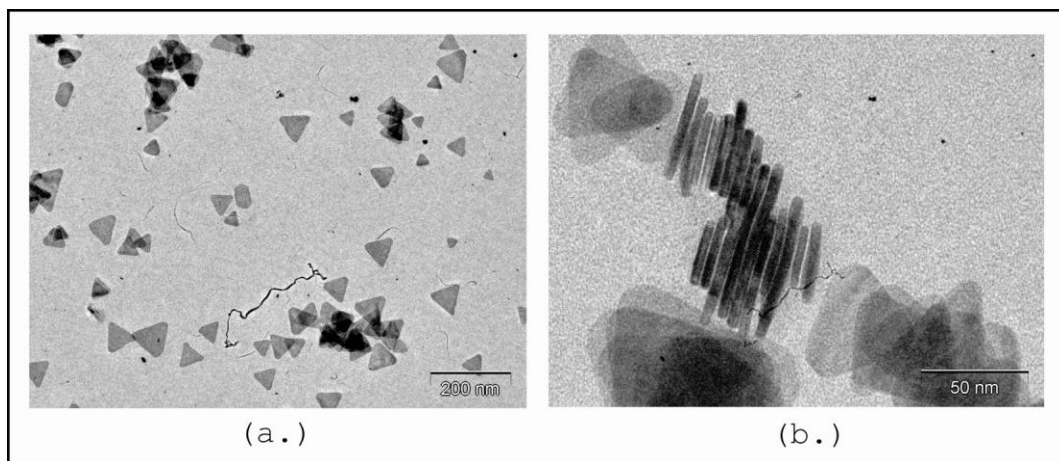
Figure 3.5: (a.) Image of nanoprisms produced using the
thermal synthetic pathway. (b.) Image of a stack of
nanoprisms that are standing perpendicular to the TEM grid
surface.

3.4.3 4-Mercaptopyridine (4-MPy) SERS Spectra on Spherical Silver Colloid

With the successful measurement of the Raman spectrum

for the 4-MPy analyte, the next step was to measure a SERS

spectrum for 4-MPy analyte adsorbed onto a spherical Ag

colloid.   Commercially available 20, 40, 60, and 80 nm

spherical silver colloid suspensions were purchased to perform this study (Ted Pella, Inc., Redding, CA, USA). Before the SERS samples were prepared, the extinction spectra for all of the purchased colloidal suspensions were measured using a Shimadzu UV-1601 UV-Vis spectrophotometer. The raw extinction spectrum for the bare 40 nm Ag colloidal suspension before sample preparation is illustrated in Fig. 3.6. All of the colloidal suspensions exhibited a strong dipolar plasmon resonance around 410 nm, which is expected based on literature values for this resonance for a spherical silver colloidal nanoparticle.

The first step in preparing the SERS samples for the four different colloidal particle suspensions was to add 0.4 mL of 1.0 M KCl electrolyte solution to a 3.6 mL aliquot of each of the commercial colloidal suspensions, so that the spherical colloids were suspended in a 100 mM KCl electrolyte solution. The chloride anion in the electrolyte solution acts to aggregate the colloidal suspension to produce SERS "hot spots", and is also known to activate the surface of the colloidal particles for SERS. Next, an 8 µL aliquot of a 9.9 mM 4-MPy stock solution was added to each of the four electrolyte colloidal suspensions to give a final analyte concentration of 20 µM 4-MPy per sample. The pH of the four colloidal

suspensions was measured to be 4.5 prior to the addition of the analyte and salt. Soon after the addition of the salt and the 4-MPy analyte, the color of the colloid suspension dramatically changed as the colloidal particles aggregated and the analyte self-assembled on the colloidal surface. The extinction spectrum for the 40 nm spherical colloid suspension with the 100 mM KCl and 20 μM 4-MPy is shown in Figure 3.6.
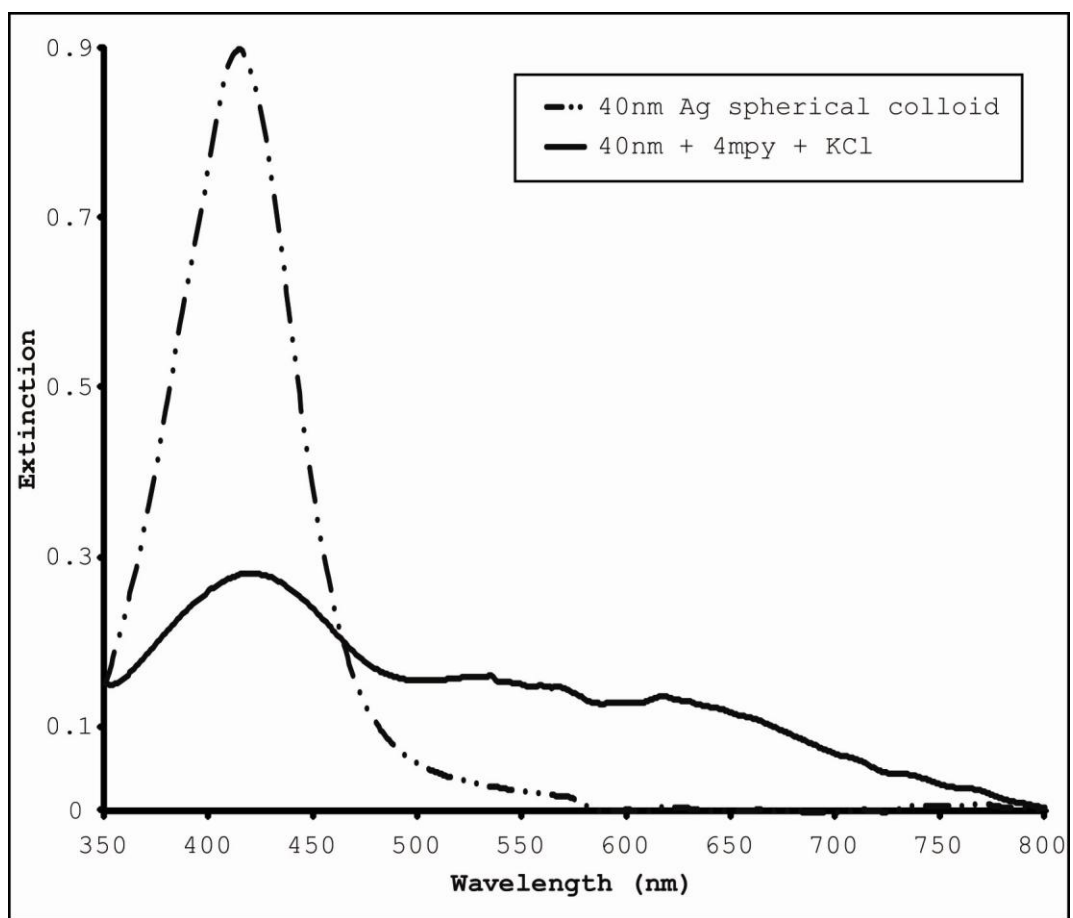
Figure 3.6: Extinction comparison for a 40 nm colloid suspension, and the suspension with 20 μM 4-MPy and 100 mM KCl. Notice the sizable increase in the extinction of the mixture at 633 nm, the emission of the He-Ne laser.

After the color shift for the LSPR for the four SERS samples seemed to stabilize, the proper working distance for the 10 x objective on the Raman microscope was determined using the focus function on the HoloGRAMS software. This was performed by repeating five second acquisitions of the Raman spectrum for a pure isoproponal (IPA) sample while adjusting the focus of the microscope. When the most intense Raman peaks for the IPA were acquired, the focus function was ceased, and the first sample was transferred to a 4 mL quartz cuvette, and sealed with a plastic cap that contained a septum. The quartz cuvette was placed on its side on the microscope stage, and the HoloGRAMS software was set so that the SERS spectrum was acquired for 1 minute, and the signal was averaged over 5 trials. The dark current acquisition and subtraction functions were selected so that the dark current for the CCD camera would be subtracted off of the acquired Raman spectrum for each trial. The SERS spectra for the four samples are presented in Figure 3.7.
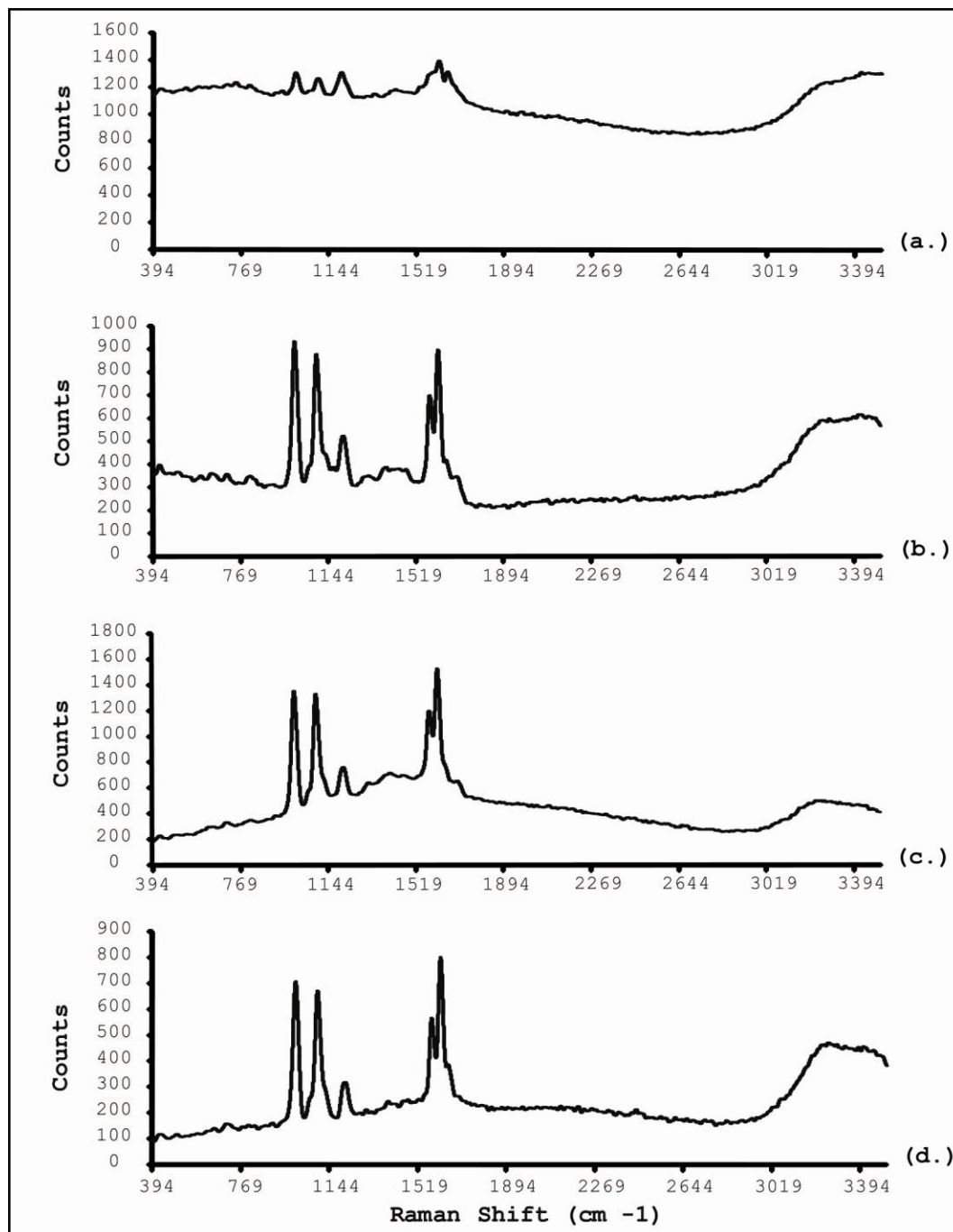
Figure 3.7: SERS spectral comparison for Spherical Ag colloid with 20 μM 4-MPy and 100 mM KCl. The acquisition time for the spectra was 1 min, and 5 trials per experiment. Sample a.) 20 nm spherical silver colloid, B.) 40 nm spherical silver colloid, c.) 60 nm spherical silver colloid, d.) 80 nm spherical silver colloid.

The results of the experiment show that all of the commercially available spherical colloidal particles tested, that included diameters of 20, 40, 60, and 80 nm particles, provided a SERS spectrum. The SERS spectrum of the 20 nm colloidal particles had the highest background and the weakest SERS enhancement. The 60 nm particles seemed to have the best SERS enhancement of the lot.

3.4.4 Nanoprism Solution Phase SERS Experiments

The silver nanoprism colloid that was synthesized with the addition of an 87.5 µL aliquot of the 96 mM NaBH$_4$ had a dipolar plasmon resonance with the He-Ne laser system, so it was used as the colloid substrate for the SERS studies (see Section 3.4.2 for the description of the synthesis). For this study, a 16.1 mM 4-MPy stock was made by dissolving the appropriate amount of solid material in 0.1 M H$_2$SO$_4$ (aq.). The sample was made at a final concentration of 16.1 µM 4-MPy with 2 mM KCl in the 2.00 mL of nanoprism colloidal suspension. For comparison purposes, the SERS spectrum for the commercially available 60 nm spherical silver colloid suspended in 100 mM KCl electrolyte with 20 µM 4-MPy was used as a comparison (See Figure 3.7 (c.)).

The parameters for the SERS experiment for the silver nanoprism sample were 30 second spectral acquisitions averaged over five trials, the acquisition parameters for the 60 nm spherical colloid SERS spectrum were 1 minute acquisitions averaged over 5 trials. The working distance for the 10 x objective on the Raman microscope was focused using the focus function in the HoloGRAMS software with an acquisition time of five seconds, and the test solvent was IPA. For the experiment, the software was set to acquire and subtract a new dark background for the CCD on each trial. See Figure 3.8 for the experimental comparison results.

There was a signal that was acquired from the 16.1 uM 4-MPy sample with the nanoprisms, however it did not look like the 4-MPY SERS spectrum acquired on 60 nm Spherical gold colloid in the past (See Figure 3.7 c., and Figure 3.8). It was noted during the acquisition of the data for the nanoprism SERS experiment that the curtain was letting in some light from laboratory. After adjusting the curtain surrounding the Raman microscope to block the light from the laboratory, the peaks for the silver nanoprism spectrum went away. This spectrum shows the peaks from the fluorescent bulbs in the laboratory.
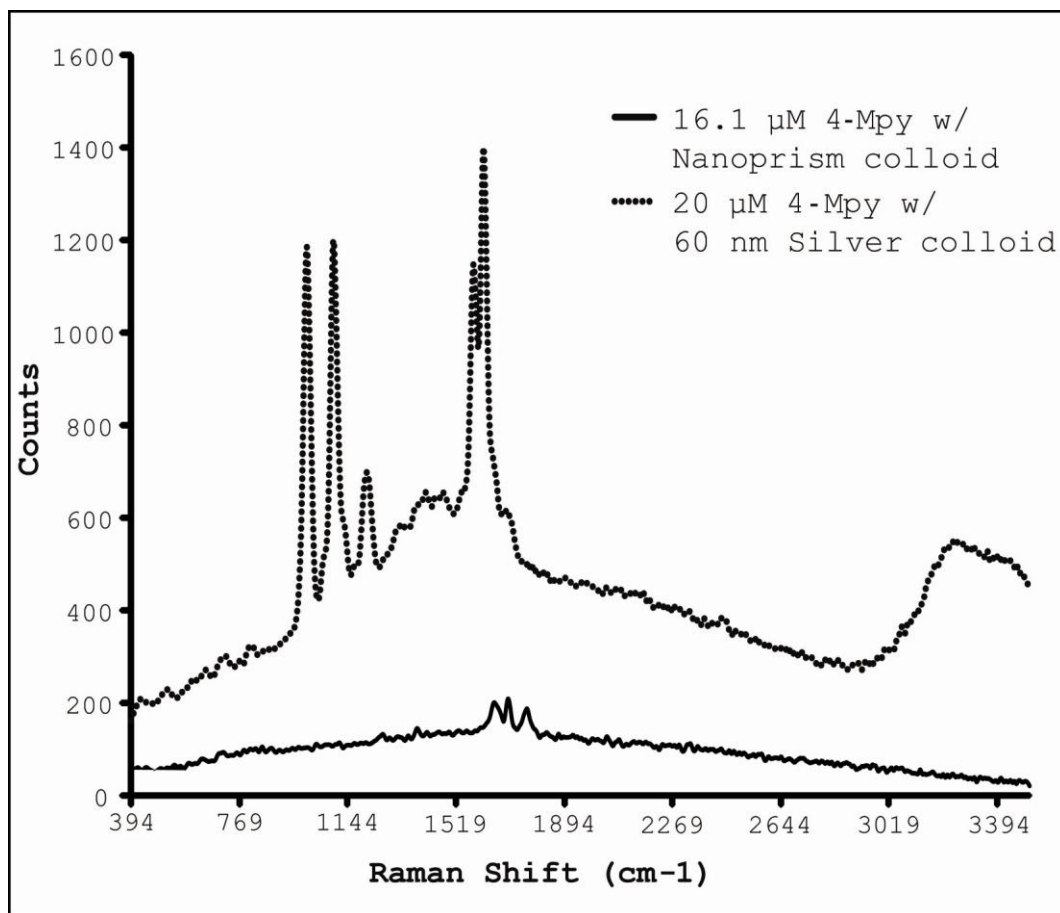
Figure 3.8: Comparison for a sample of 60 nm spherical silver colloid suspended in 100 mM KCl $_{(aq.)}$ electrolyte solution with 20 μM 4-MPy analyte as compared with a sample made of nanoprisms suspended in 2 mM KCl $_{(aq.)}$ electrolyte solution with 20 μM 4-MPy analyte concentration.

3.4.5 Nanoprism SERS Interference Experiment with polyvinyl pyrrolidone (PVP)

After analyzing the results presented in Figure 3.7, a study was performed to look at the potential of the PVP polymer, used in the synthesis of the nanoprism colloid, as an interferent in the acquisition of a SERS spectrum for 4-

84

MPy in a sample of nanoprism colloid. For this interference study, two SERS samples were prepared using commercially available 60 nm spherical silver colloids as the SERS enhancing substrates. Both samples were prepared by adding an aliquot of KCl electrolyte solution so that 60 nm colloids in both samples were suspended in 2 mM KCl electrolyte solution. The first sample preparation was without PVP polymer, so an aliquot of the 10 mM 4-MPy stock in 0.1 M H_2SO_4 was added to the sample, and the sample was vortexed for 30 seconds at 2000 RPM. The sample to study the interference of the PVP polymer had 2.6 mg of PVP (Mw = 29,000 g/mol) added to a 2.0 mL suspension of 60 nm colloid suspended in 2 mM KCl electrolyte solution. This quantity of PVP polymer was added to the second sample to mimic the amount of PVP present in the flask during the synthesis of the nanoprism colloid. The sample was then vortexed for 30 seconds at 2000 rpm. An aliquot of the acidic 4-MPy stock was then added so that a final analyte concentration of 10 µM was present in the sample.

The Raman microscope was focused utilizing the same procedure described in this body of work. The experimental parameters in the HoloGRAMS software were set to acquire the SERS spectrum from each sample for 2 minutes, and the signal was averaged over 5 trials. The dark current for

the CCD was acquired and subtracted for each trail. The experimental parameters and the focus for the 10 x objective on the Raman microscope were not altered for the acquisition of both SERS spectra (see Figure 3.9).

With the acquisition parameters of the HoloGRAMS software being exactly the same, the SERS band at 1094.7 cm^{-1} for the 4-MPy sample without PVP was on the order of 13 times more intense than the same SERS band for the sample with the PVP polymer added. This data shows that the organic capping agent does interfere, to a large degree, with the SERS spectrum using commercially available 60 nm spherical silver colloid for the 4-MPy molecule. The mechanism of the interference is not known for this simple experiment. It is possible that the PVP molecule disrupts the adsorption the 4-MPy molecule onto the colloidal surface thus disrupting any chemical enhancement mechanism that could occur on the surface of the colloid (10 to 10^{+2} contribution to the overall enhancement). A second potential mechanism is that the polymer encapsulates the analyte and does not allow the analyte molecule to get close in proximity to the colloidal aggregates (>10 nm from the surface).
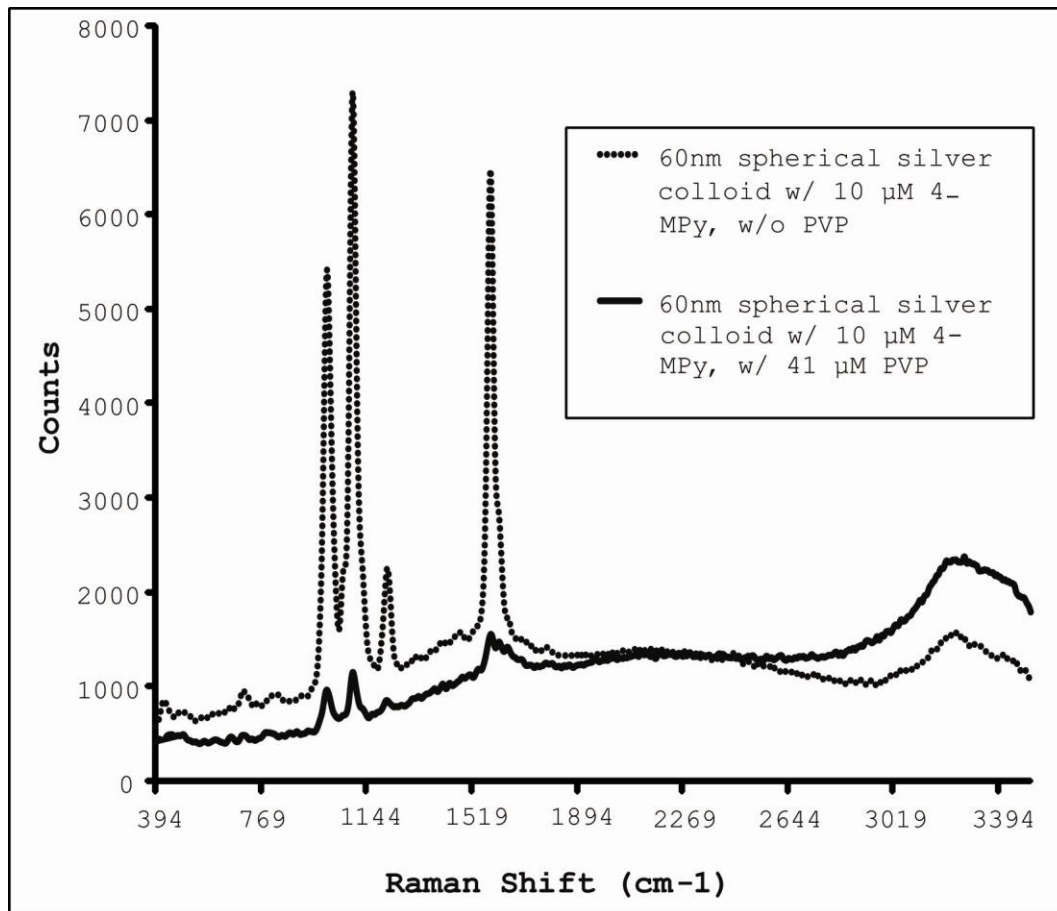
Figure 3.9: Comparison for the SERS spectrum for two similarly prepared samples with the exception that one of the samples contained the organic capping agent PVP polymer.

3.5 RESULTS AND DISCUSSION

Normal Raman spectra were acquired for a saturated aqueous 4-MPy sample, and SERS spectra were acquired for the 4-MPy analyte with commercial colloids of 20, 40, 60, and 80 nm diameter suspended in KCl electrolyte solutions.

87

Although all of these Raman spectra were successfully acquired using the Raman microscope system described in this body of work, a SERS spectrum for 4-MPy with the nanoprism substrate was not detected. Experiments that were performed on two samples of commercially available 60 nm spherical silver colloid show that the organic capping agent, PVP polymer, used to synthesize the nanoprism colloid interferes with the acquisition of the SERS spectrum on the 60 nm spherical silver colloid purchased from Ted Pella, Inc. In that experiment, two samples were prepared exactly the same with the exception that one sample had PVP added. The SERS spectra show that the Intensity of the 1094.7 cm^{-1} band is approximately 13 times more intense for the sample without the PVP capping agent.

In 2007, Tiwari *et al.* published study reports that a SERS comparison has been made for a 10^{-3} M rhodamine 6G solution on silver nanorods, silver nanoprisms, and silver nanospheres suspended in electrolyte solution[52]. The data shows that the 1577 cm^{-1} SERS band for the nanoprism substrate is 3-4 times the 1577 cm^{-1} band for the spherical silver colloid substrate, and 10-20 times more intense than the 1577 cm^{-1} band for the nanorods substrate. The authors attribute the large enhancement of the nanoprism colloid to morphology effects that cause chemical enhancement. They

also attribute the large enhancement effect to the lightening rod affect[53]. The authors do not specifically list the organic capping agent that they used to synthesize the nanoprism colloid. They do list cetyltrimetylammonium bromide in the materials portion of the paper, so this capping agent would need to be investigated.

In 2006, Bishnoi *et al*. reported the development of a SERS based pH sensor that was developed to measure pH of a nanoenvirionment. The measurement is based on the ratio of the 1702 cm^{-1} (C=O stretch) and the 1394 cm^{-1} (COO- stretch) SERS bands for p-mercaptobenzoic acid adsorbed on a surface of a gold shell nanoparticle[54]. The sensor is reported to be capable of measuring pH in the vicinity of the nanoparticle over the range of 5.80 to 7.60 pH units with an accuracy of ± 0.10 pH units in the operating range of the sensor.

The results of these two studies show that the idea of a SERS based pH sensor utilizing the nanoprism colloid as the enhancing substrate was at the least plausible. With some investigation of other organic capping agents the goal of measuring pH with the 4-MPy attached to the surface of the nanoprism colloid substrate could be utilized as a SERS based pH sensor.

3.6 ACKNOWLEDGEMENTS

3.6 REFERENCES

1. Raman, C.V., Krishnan, K.S., A New Type of Secondary Radiation, Nature **1928,** *3048*:501-502.

2. Raman, C.V., Krishnan, K.S., The Production of New Radiations by Light Scattering-Part. I., Proc. Roy. Soc. Lon. A. **1929,** *122*:23-25.

3. Raman, C.V., The molecular scattering of light, Nobel Lecture, Dec. 11, 1930.

4. Fleischmann, M., Hendra, P.J., McQuillan, A.J., Raman Spectra of Pyridine Adsorbed at a Silver Electrode, Chem. Phys. Lett. **1974,** *26*:163-166.

5. Jeanmaire, D.L., Van Duyne, R.P., Surface Raman Spectroelectrochemistry: Part I. Heterocyclic, Aromatic, and Aliphatic Amines Adsorbed on the Anodized Silver Electrode, J. Electroanalyt. Chem. **1977,** *84*:1-20.

6. Albrecht, M.G., Creighton, J.A., Anomalously Intense Raman Spectra of Pyridine at a Silver Electrode, J. Amer. Chem. Soc. **1977,** *99*:5215-5217.

7. Creighton, J.A., Blatchford, C.G., Albrecht, M.G., Plasma Resonance Enhancement of Raman Scattering by Pyridine Adsorbed on Silver or Gold Sol Particles of Size Comparable to the Excitation Wavelength, J. Chem. Soc., Faraday Trans. 2. **1979,** *75*:790-798.

8. Penn, S.G., He, L., Natan, M.J., Nanoparticles for bioanalysis, Curr. Opin. Chem. Bio. **2003,** 7:609-615.

9. Hulteen, J.C., Treichel, D.A., Smith, M.T., Duval, M.L., Jensen, T.R., Van Duyne, R.P., Nanosphere Lithography: Size-Tunable Silver Nanoparticle and Surface Cluster Arrays, J. Phys. Chem. B. **1999,** *1 03*:3854-3863.

10. Maruszewski, K., Jasiorski, M.A., Hreniak, D., Strek, W., Hermanowicz, K., Heiman, K., Raman Spectra of Molecules Adsorved on Ag Centers in Sol-Gel Matrices., J. Sol-Gel Sci. and Tech. **2003,** *26*:83-88.

11. Zhu, M., Qian, G., Hong, Z., Wang, Z., Fan, X., Wang, M., Preperation and characterization of silica-silver core-shell structural submicrometer spheres, J. of Phys. And Chem. Of Solids **2005,** *66*:748-752.

12. Bell, S.E.J., Sirimuthu, N.M.S., Rapid, quantitative analysis of ppm/ppb nicotine using surface-enhanced Raman scattering from polymer-encapsulated Ag nanoparticles(gel-colls), The Analyst **2004,** *129*:1032-1036.

13. Bao, L., Mahurin, S.M., Haire, R.G., Dai, S., Silver-Doped Sol-Gel Film as a Surface-Enhanced Raman Scattering Substrate for Detection of Uranyl and Neptunyl Ions, Anal. Chem. **2003,** *75*:6614-6620.

14. Kim, M.S., Kang, J.S., Park, S.B., Lee, M.S., Surface-enhanced Raman Spectroscopy of Quinomethionate Adsorbed on Silver Colloids, Bull. Korean Chem. Soc. **2003,** *24*:633-637.

15. Cao, Y.C., Jin, R., Mirkin, C.A., Nanoparticles with Raman Spectroscopic Fingerprints for DNA and RNA detection, Science **2002,** *297*:1536-1539.

16. Haes, A.J., Stuart, D.A., Nie, S., Van Duyne, R.P., Using Solution-Phase Nanoparticles, Surface-Confined Nanoparticle Arrays and Single Nanoparticles as Biological Sensing Platforms, J. Fluor. **2004,** *14*:355-367.

17. Yonzon, C.R., Haynes, C.L., Zhang, X., Walsh, J.T., Van Duyne, R.P., A Glucose Biosensor Based on Surface-Enhanced Raman Scattering: Improved Partition Layer, Temporal Stability, Reversibility, and Resistance to Serum Protein Interference, Anal. Chem. **2004,** *76*:78-85.

18. Kneipp, J., Kneipp, H., McLaughlin, M., Brown, D., Kneipp, K., In-vivo molecular probing of cellular compartments with gold nanoparticles and nanoaggregates, Nano Letters **2006,** *6*:2225-2231.

19. Wang, Y., Li, Y.S., Zhang, Z., An, D., Surface-enhanced Raman scattering of some water insoluble drugs in silver hydrosol, Spectrochimica Acta Part A **2003,** *59*:589-594.

20. Pinzaru, S.C., Pavel, I., Leopold, N., Kiefer, W., Identification and characterization of pharmaceuticals using Raman and surface-enhanced Raman scattering, J. Raman Spec. **2004,** *35*:338-346.

21. Fabriciova, G., Sanchez-Cortes, S., Garcia-Ramos, J.V., Miskovsky, P., Joint application of micro-Raman and surface-enhanced Raman spectroscopy to the interaction study of the antitumoral anthraquinone drugs danthron and quinizarin with albumins, J. Raman Spec. **2004,** *35*:384-389.

22. Nie, S., Emory, S.R., Probing Single Molecules and Single Nanoparticles by Serface-Enhanced Raman Scattering, Science **1997,** *275*:1102-1106.

23. Kneipp, K., Wang, Y., Kneipp, H., Perelman, L.T., Itzkan, I., Dasari, R.R., Single Molecule Detection Using Surface-Enhanced Raman Scattering (SERS), Phys. Rev. Lett. **1997,** *78*:1667-1670.

24. Sun, Y., Xia, Y., Large-Scale Synthesis of Uniform Silver Nanowires Through a Soft, Self-Seeding, Polyol Process, Adv. Mater. **2002,** *14*:833-837.

25. Jana, N.R., Gearheart, L., Murphy, C.J., Wet chemical synthesis of silver nanorods and nanowires of controllable aspect ratio, Chem. Commun. **2001,** 7:617-618.

26. Jin, R., Cao, Y., Mirkin, C.A., Kelly, K.L., Schatz, G.C., Zheng, J.G., Photoinduced Conversion of Silver Nanospheres to Nanoprisms, Science **2001,** *294*:1901-1903.

27. Metraux, G.S., Mirkin, C.A., Rapid Thermal Synthesis of Silver Nanoprisms with Chemically Tailorable Thickness, Adv. Mater. **2005,** *17*:412-415.

28. Junior, A.M., de Oliveira, H.P.M., Gehlen, M.H., Preparation of silver nanoprisms using poly(N-vinyl-2-pyrrolidone) as a colloid-stabilizing agent and the effect of silver nanoparticles on the photophysical properties of cationic dyes, Photochem. Photobiol. Sci. **2003,** *2*:921-925.

29. Sun, Y., Mayers, B., Xia, Y., Transformation of Silver Nanospheres into Nanobelts and Triangular Nanoplates through a Thermal Process, Nano Letters **2003,** *3*:675-679.

30. Pastoriza-Santos, I., Liz-Marzan, L.M., Synthesis of Silver Nanoprisms in DMF, Nano Letters **2002,** *2*:903-905.

31. Sun, Y., Xia, Y., Triangular Nanoplates of Silver: Synthesis, Characterization, and Use as Sacrificial Templates For Generating Triangular Nanorings of Gold, Adv. Mater. **2003,** *15*:695-699.

32. Jin, R., Cao, C., Hao, E., Metraux, G.S., Schatz, G.C., Mirkin, C.A., Controlling anisotropic nanoparticle growth through plasmon excitation, Nature **2003,** *425*:487-490.

33. Chen, S., Carroll, D.L., Synthesis and Characterization of Truncated Triangular Silver Nanoplates, Nano Letters **2002,** *2*:1003-1007.

34. Chen, S., Carroll, D.L., Silver Nanoplates: Size Control in Two Dimensions and Formation Mechanisms, J. Phys. Chem. B **2004,** *108*:5500-5506.

35. Wiley, B., Herricks, T., Sun, Y., Xia, Y., Polyol Synthesis of Silver Nanoparticles: Use of Chloride and Oxygen to Promote the Formation of Single-Crystal, Truncated Cubes and Tetrahedrons, Nano Letters **2004,** *4*:1733-1739.

36. Sun, Y., Xia, Y., Shape-Controlled Synthesis of Gold and Silver Nanoparticles, Science **2002,** *298*:2176-2179.

37. Chen, S., Fan, Z., Carroll, D.L., Silver Nanodisks: Synthesis, Characterization, and Self-Assembly, J. Phys. Chem. B. **2002,** *106*:10777-10781.

38. Hao, E., Kelly, K.L., Hupp, J.T., Schatz, G.C., Synthesis of Silver Nanodisks Using Polystyrene Mesospheres as Templates, J. Am. Chem. Soc. **2002,** *124*:15182-15183.

39. Sun, Y., Mayers, B., Xia, Y., Metal Nanostructures with Hollow Interiors, Adv. Mater. **2003,** *15*:641-646.

40. Sun, Y., Xia, Y., Mechanistic Study on the Replacement Reaction between Silver Nanostructures and Chloroauric Acid in Aqueous Medium, J. Am. Chem. Soc. **2004,** *126*:3892-3901.

41. Metrauz, G.S., Cao, Y.C., Jin, R., Mirkin, C.A., Triangular Nanoframes Made from Gold and Silver, Nano Letters **2003,** *3*:519-522.

42. Wiley, B., Sun, Y., Chen, J., Cang, H., Li, Z.-Y., Li, X., Xia, Y., Shape-Controlled Synthesis of Silver and Gold Nanostructures, MRS Bulletin **2005,** *30*:356-361.

43. Kneipp, K., Kneipp, H., Itzkan, I., Dasari, R.R., Feld, M.S., Surface-Enhanced Raman scattering and biophysics, J. Phys.: Condens. Matter. **2002**, *14*:R597-R624.

44. Xia, Y., Halas, N.J., Shape-Controlled Synthesis and Surface Plasmonic Properties of Metallic Nanostructures, MRS Bulletin **2005**, *30*:338-343.

45. Hutter, E., Fendler, J.H., Exploitation of Localized Surface Plasmon Resonance, Adv. Mater. **2004**, *16*:1685-1706.

46. Hu, J., Zhao, B., Surface-Enhanced Raman Spectroscopy on the structure changes of 4-mercaptopyridine adsorbed on silver substrates and silver colloids, Spectrochimica Acta Part A. **2002**, *58*:2827-2834.

47. Baldwin, J.A., Vlćková, B., Andrews, M.P., Butler, I.S., Surface-Enhanced Raman Scattering of Mercaptopyridines and Pyrazinamide Incorporated in Silver Colloid-Adsorbate Films, Langmuir **1997**, *13*:3744-3751.

48. Jung, H.S., Kim, K., Kim, M.S., Raman spectroscopic investigation of the adsorption of 4-mercaptopyridine on a silver-sol surface, Journal of Molecular Structure **1997**, *407*:139-147.

49. Campion, A., Kambhampati, P., Surface-enhanced Raman scattering, Chem. Soc. Rev. **1998**, *27*:241-250.

50. Otto, A., Mrozek, I., Grabhorn, H., Akemann, W., Surface-enhanced Raman scattering, J. Phys.: Condens. Matter **1992**, *4*:1143-1212.

51. Persson, B.N.J., On the theory of Surface-Enhanced Raman Scattering, Chem. Phys. Lett. **1981**, *82*:561-565.

52. Tiwari, V.S., Oleg, T., Darbha, G.K., Hardy, W., Singh, J.P., Ray, P.C., Non-resonance SERS effects of silver colloids with different shapes, Chem. Phys. Lett. **2007**, *446*:77-82.

53. Mohamed, M.B., Volkov, V., Link, S., El-Sayed, M.A., The 'lightning' gold nanorods: fluorescence enhancement of over a million compared to the gold metal, Chem. Phys. Lett. **2000**, *317*:517-523.

54. Bishnoi, S.W., Rozell, C.J., Levin, C.S., Gheith, M.K., Johnson. B.,R., Johnson, D.H., Halas, N.J., All-optical Nanoscale pH Meter, Nano Letters **2006**, *6*:1687-1692.

CHAPTER 4

APPLICATION OF RATIOMETRIC PHOTOACOUSTIC SENSING OF pH

4.1 INTRODUCTION

In 1881, Alexander Graham Bell discovered that audible tones were generated from thin disks of different substances while being illuminated by an intermittent beam of sunlight[1]. The device that was used to detect these emitted sounds was called the photophone. The device utilized a test tube as a sample cell, in which the material to be studied was placed. A piece of rubber tubing was affixed to the throat of the test tube, with the opposite end of the tubing attached to an ear piece. The intermittent beam of sunlight was then focused on-to the substance in the tube, and the observer would listen to the sounds emanating from the sample with the earpiece. Using this device, Bell was able to hear sounds generated from crystals of potassium bichromate, crystals of copper sulphate, tobacco smoke, and lampblack pigment.

Since the discovery of the photoacoustic phenomenon, it has been applied to many biomedical applications, as varied as analytical chemistry[2-7], early cancer screening and detection *in vivo*[8-10], and both *in vitro* and *in vivo* imaging of vasculature and tissue[11-13].
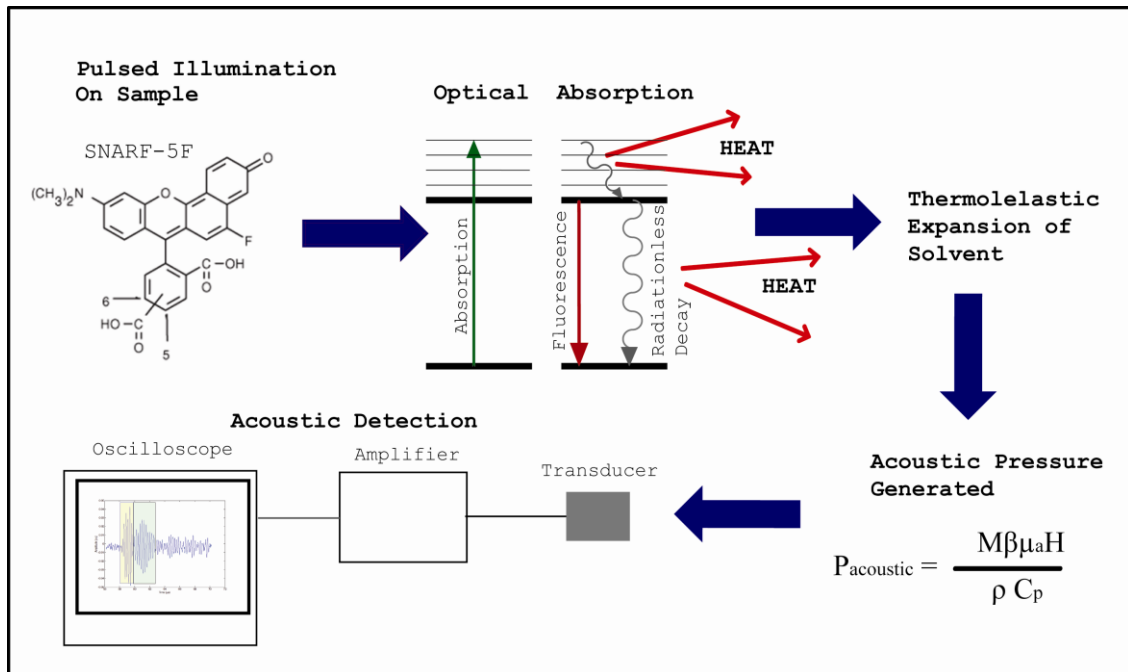

Figure 4.1: Diagram for photoacoustic generation and detection using a transducer.

With the advent of high power pulsed lasers, photoacoustic sensing and imaging has developed as a sensitive analytical technique that can be used where traditional spectroscopic techniques are limited. See

figure 4.1 for a diagram of how photoacoustic signals are generated by absorption of photons in a sample.

Current interest in the application of the photoacoustic effect, such as an *in vivo* imaging modality, has increased due to the nature of the effect. The imaging contrast of the photoacoustic effect is based on the distribution of optical absorption, while the spatial resolution is based on ultrasound resolution. Both the imaging resolution of ultrasound detection, and image reconstruction, are the result of the coefficient of scattering for ultrasound being approximately two orders of magnitude smaller than the coefficient of optical scattering of traditional spectroscopic methods. Acoustic waves are detected and used to reconstruct the distribution of light absorption within the sample; therefore, the photoacoustic effect is insensitive to light scattering. It has been reported in the literature that photoacoustic imaging (@ 800 nm) has produced sub-millimeter image resolution at an imaging depth of 5.2 cm deep in tissue when optically matched contrast agents (i.e. Indocyanine Green dye) are used to enhance the photoacoustic signal of embedded objects in tissue[14]. When compared to traditional absorption measurements in highly scattering samples, photoacoustic spectroscopy has a distinct advantage. The result measured

is an effective absorption power spectrum based on an effective absorption coefficient (μ_{eff}) given in equation 4.1.

$$\mu_{eff} = \sqrt{3 * \mu_{abs} * ((1 - g) * \mu_{sca})} \qquad \text{Eq. 4.1}$$

In this equation, μ_{abs} is the absorption coefficient of the absorbers in the medium. The $((1-g)* \mu_{sca})$ is known as the reduced scattering coefficient, and the g term is known as the scattering anisotropy and is equal to the $<\cos \theta>$, where θ is the scattering angle. Finally, μ_{sca} is the scattering coefficient of the medium. In traditional absorption based spectroscopies, an extinction spectrum is produced that is based on both absorption and scattering (μ_{abs} + μ_{sca}).

The absorption based generation of an acoustic wave, from within the sample, is a measure of the internal conversion of absorbed electromagnetic energy to thermal energy. The thermal energy produced in the sample, under specific conditions, produces acoustic waves within the sample that can be used to reconstruct the distribution of light absorption within the sample.

Traditionally, fluorescent dye indicators have been widely used in biological research for exploring analytes

in cells, tissues, and small animals. Specific fluorescent dye indicators have been developed for probing analytes such as: H^+ [15], Ca^{2+} [16], K^+ [17], Na^+ [18], Zn^{2+} [19], Mg^{2+} [20], Cl^- [21], NO [22], O_2 concentration [23], cellular membrane potential [24], and enzyme activity utilizing Fluorescence Resonance Energy Transfer (FRET) [25].

The potential benefit of combining photoacoustic based imaging with fluorescent based indicators is the enhanced capability of making bio-analytical measurements of analyte concentrations in both *in vivo* and *in vitro* samples. In these measurements, the fluorescent indicator molecule acts as a sensor for the analyte of interest. The effect of the analyte on the fluorescent based indicator causes a change to the absorption of light, fluorescence of light, or both. These changes in the optical properties of the indicator affect the heat locally generated in the sample, thus changing the acoustic signal near the indicator within the sample. The change of the optical properties of the fluorescent indicator as a function of analyte concentration across the depth profile of the sample acts as a photoacoustic contrast agent. Therefore, the indicator acts as a "sonophore", i.e. a molecular indicator whose sonic response is dependent on analyte concentration.

The goal of this research project is to show an improvement upon a photoacoustic pH measurement method reported by Schlageter *et al.*[6], while moving toward an imaging modality by which pH can be measured in intact tissue. The following experiment was designed around a ratiometric optical system that lends itself to *in vitro* cellular measurements of pH using the photoacoustic detection of an organic pH indicator dye. To translate to *in vivo* systems, an indicator dye that absorbs light in the NIR (~ 750 nm) where biological tissue and hemoglobin do not absorb, is selected.

For this work, the fluorescent pH indicator dye, seminaphthorhodafluors-5F (SNARF-5F) (Invitrogen, Inc., Eugene, OR, USA) was used to photoacoustically sense pH in a series of pH buffers. The SNARF-5F dye lends itself perfectly to be used as a ratiometric pH sonophore because of the pH insensitive isosbestic point of the indicator dye near 532 nm (wavelength of the double YAG laser), and the pH sensitive absorption peak near 580 nm (excited with the emission of a dye laser system). We show that this dye is a viable candidate for a pH sensitive contrast agent, enabling ratiometric intracellular photoacoustic imaging.

4.2 EXPERIMENTAL BACKGROUND

The diagram in Figure 4.1 illustrates the process of how pulsed illumination on the SNARF-5F sonophore produces a thermoelastic pressure wave that can be detected as an acoustic signal. With the absorption of photons, electrons in the dye molecules are excited to higher electronic states. As the vibrational energy of this excited electronic state decays, it transitions to lower vibrational energy states within the excited electronic state of the molecule producing heat in the surrounding solvent. When the electron in the excited state of the sonophore undergoes radiationless decay, which is the transition of the electron from the electronically excited state back to the ground state without the emission of a photon, heat is produced. Therefore, it can be expected that a condition that alters the absorption or fluorescence (change in quantum yield) of a sonophore will result in a change in the acoustic response of the molecule.

In order for this localized heating of the solvent to produce a thermoelastic pressure wave, the effect of local heating due to the absorption of electromagnetic radiation must be thermally confined. This condition is met when the laser pulse duration is much shorter than the thermal

diffusion time[26]. Therefore, as the energy of the absorbed photons is converted into heat, the heat is confined to the irradiated area, resulting in the maximum increase of the temperature of the irradiated area. The increase in temperature of the solvent local to the sonophore is given by the relation[27]:

$$\Delta T = \left(\frac{\mu_{eff} H}{\rho C_p} \right) \qquad \text{Eq. 4.2}$$

Where μ_{eff} is the absorption coefficient of the sonophore in the sample (defined in eq. 4.1), and H [J/m^2] is the radiant exposure of the sample. The density of the environment is given as ρ [kg/m^3], and the heat capacity of the medium, at constant pressure, is given by C_p [J/kg°C]. The temperature gradient within this thermally confined volume produces a strain within the medium when it is irradiated with the short laser pulse. This strain is calculated using the following equation:

$$Strain = \beta \Delta T = \beta \left(\frac{\mu_{eff} H}{\rho C_p} \right) \qquad \text{Eq. 4.3}$$

Where β [°C^{-1}] is defined as the thermal expansion coefficient of the medium for which the sonophore is located.

The strain that was imparted in the material because of the internal conversion of electromagnetic radiation to thermal energy, imparts a stress in the material. This stress, confined to the irradiated area of the sample, causes an expansion of the medium. This expansion generates acoustic pressure waves in the sample, and is described as:

$$P_{amplitude} = M * Strain = \left(\frac{M \beta \mu_{eff} H}{\rho C_p} \right)$$ Eq. 4.4

Where M [Pa] is the bulk modulus of the material environment in which the sonophore is located. This acoustic pressure wave is measured using a piezoelectric transducer that is acoustically coupled with the sample being probed.

4.4 EXPERIMENTAL SETUP

A frequency doubled Surelite I10 Continuum® Nd:YAG laser (420 mJ, 10 Hz repetition rate, Continuum Inc., Santa Clara, CA, USA) at 532 nm emission (see Fig. 4.2(a.)) was used as the pump laser for the dye laser set up. The laser was operated at maximum power output with a Q-switch delay of 220 µS.

The dye laser system used for this experiment was a Lambda Physik, Lasertechnik Scanmate® dye laser (Coherent Inc., Santa Clara, CA, USA). The laser dye that was used for the experiment was rhodamine 590 chloride (Exciton Inc., Dayton, OH, USA), which was dissolved in methanol (Sigma-Aldrich, St. Louis, MO, USA) and excited at 532 nm. The emission from the dye laser was set at 564 nm, in order to excite the pH sensitive region of the absorption spectrum of the SNARF-5F dye. To excite the pH insensitive isosbestic point near 532 nm, that acted as the internal reference for each sample, a set of repositionable mirror mounts were positioned to redirect the 532 nm emission of the pump laser along the same path as the 564 nm light from the dye laser system (see Figure 4.2(a.)).

The system was set up using two transducers, one for detection and the other for normalization. A glass slide was placed in the beam path of both lasers, so that reflections from both beams are used to normalize the laser emission (see Figure 4.2(a.)). The normalization transducer (5 MHz, flat face) was used for normalizing the signals from both lasers by detecting thermo-acoustically generated waves induced by light absorption on its front face.

The experimental system was based on a sample flow cell

107

constructed using a piece of glass tubing as a sample window with two pieces of nylon tubing attached to each end (see Figure 4.2(b.)). One side of the nylon tubing was fitted with a plastic insert that was used to attach a syringe for sample introduction. The other end of the tubing was left long enough to allow for transport of waste out of the acoustic tank. During set up, a solution of red food coloring was pushed into the sample cell and illuminated with the pulsed laser excitation. The detection transducer's (3.5 MHz, 1.9 cm aperture, 10 cm focal length, Aerotech) position was then adjusted until the photoacoustic signal from the food coloring was maximized on the oscilloscope.
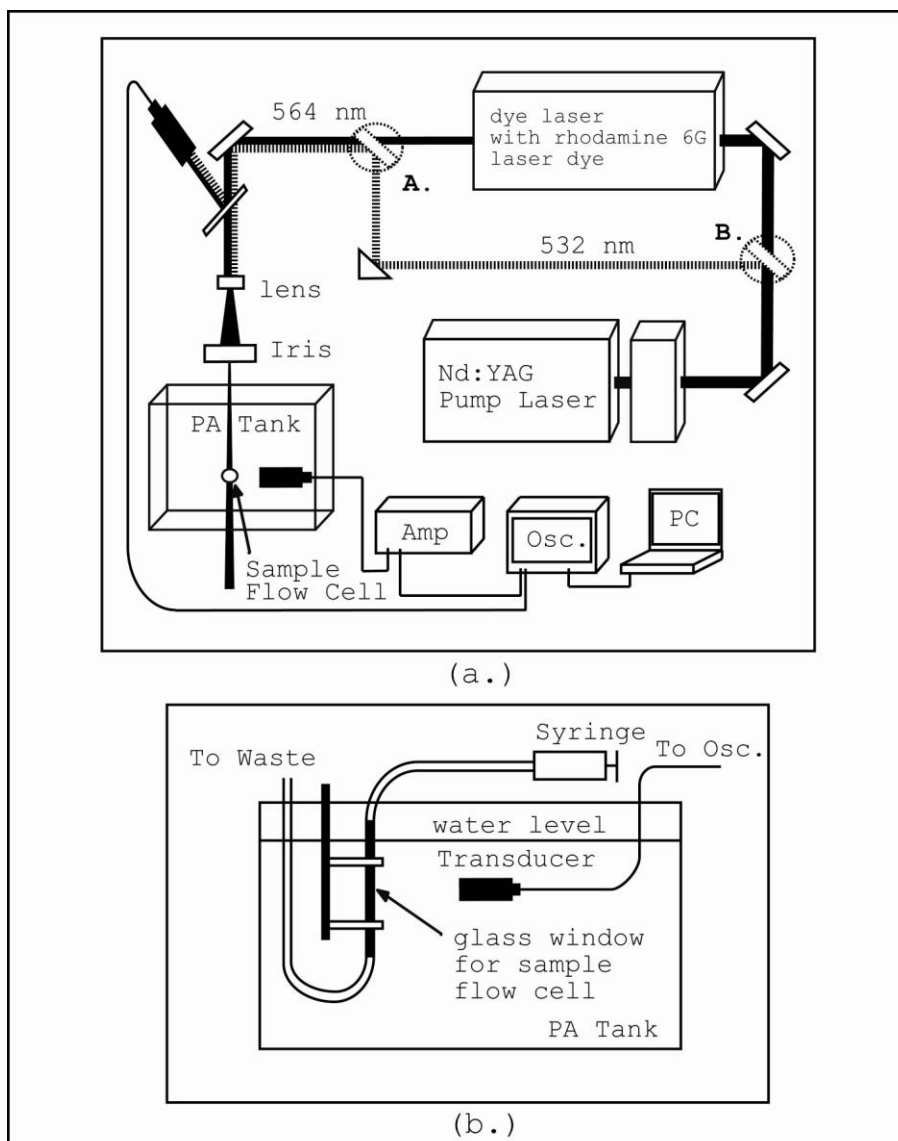
Figure 4.2: (a.) Laser set up for the Photoacoustic sensing of pH using the pH sensitive sonophore SNARF-5F. The movable mirror mounts used in this system are designated with A. and B. (b.) The Photoacoustic tank set up for conducting the pH measurements using SNARF-5F indicator dye.

A glass tubing sample window was added to the flow cell after preliminary tests with food coloring dye had shown that the dye laser emission had burned the nylon tubing.

These black burn spots on the nylon tubing contribute to an increasing photoacoustic signal of the food coloring dye over the course of the measurement. The increasing photoacoustic signal is a result of the continued burning of the nylon tubing with each successive laser pulse.

The signal from the detection transducer was amplified with a Panametrics Squarewave 5077PR Pulser/Reciever. The signal amplification was set to 50 dB, with both the high pass (1 MHz) and the low pass (10 MHz) filters operating. The amplified signals, from both the detection transducer and the normalization transducer, were collected using a LeCroy Wavesurfer 432, 350 MHz Oscilloscope. Channel one was set to 10 mV/Division, DC 50 Ω coupling, and 20 MHz bandwidth. Channel two was set to 100 mV/Division, DC 50 Ω coupling, and 20 MHz bandwidth. Both channels were set to take an average of 20 acquisitions. The time setting for the oscilloscope was set to 10 µS/Division.

4.5 SNARF-5F Sample Preparation

Once confident with the experimental set up and preliminary red food coloring test results, we concentrated on measuring the photoacoustic response of the SNARF-5F sonophore. The pH indicator dye SNARF-5F 5-(and-6)-

carboxylic acid (product number S-23922, Invitrogen Inc., Eugene, OR, USA) was chosen due to its known isosbestic point near 530 nm, making it ideal for internally referenced, dual wavelength photoacoustic measurements. The samples were prepared in pH buffers ranging from pH 6 to pH 9 (Fisher Scientific Inc., Waltham, MA, USA). A pH 6 buffer solution was used to make the original dye stock. The pH samples for extinction and fluorescence analysis were prepared at a final 10 μM dye concentration. The extinction spectra for the pH samples were measured using a Shimadzu UV-1601 UV-Vis spectrophotometer (see Figure 4.3, Note the Isosbestic point near 530 nm).

The photoacoustic samples were prepared again for pH 6 through pH 9 buffers by diluting the appropriate volume of SNARF-5F dye stock (pH 6) to a final dye concentration of 43.2 μM. This concentration was chosen so that the absorption of the dye at 580 nm was similar to the absorption of a red food coloring solution that was used to test the experimental set up during the preliminary studies.
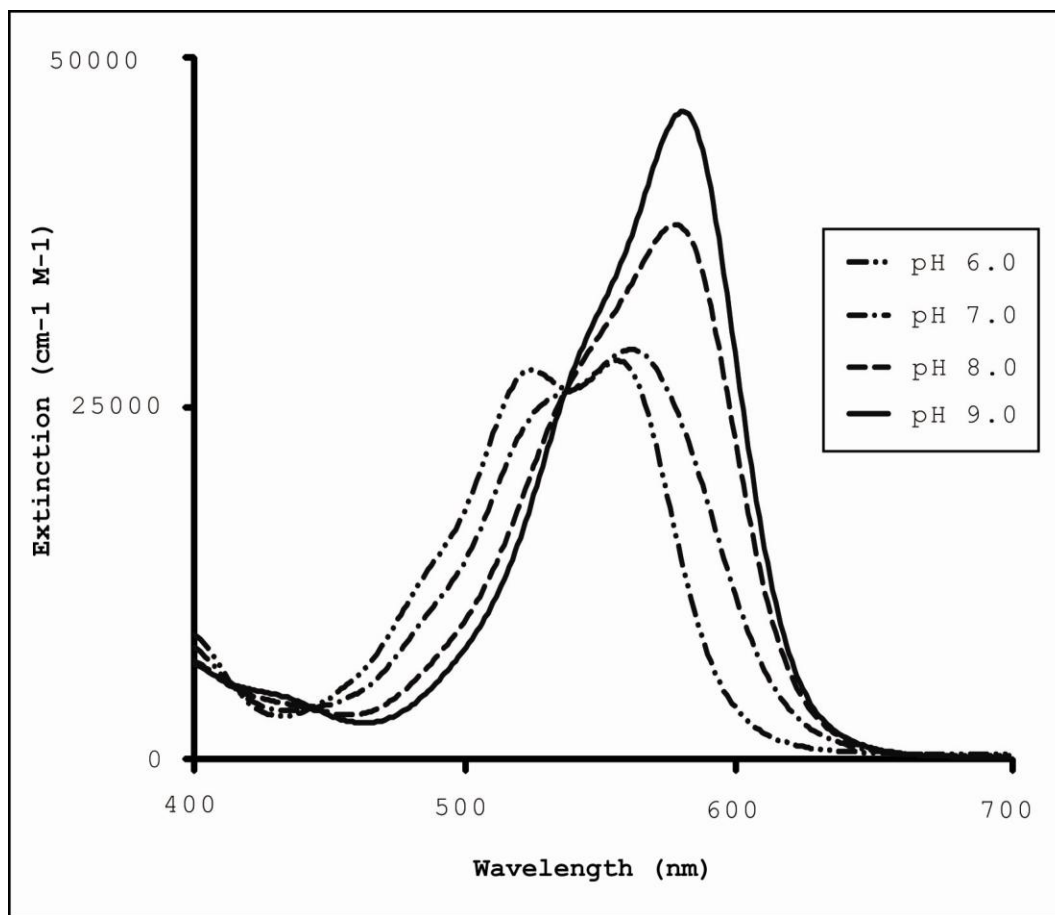
Figure 4.3: Extinction spectra for the 10 µM SNARF-5F dye solution in buffers for pH 6 thru pH 9.

The photoacoustic response was measured for each pH solution by aliquotting four samples for each solution. Each measurement of the photoacoustic response, for each specific sample, was an average of 20 acquisitions of the acoustic response of the sonophore indicator dye in order to reduce the noise in the measurement (see Table 4.1 and 4.2). The order of the measurements for the 16 total trials was performed in random order to observe the

112

reproducibility of the measurements for each pH. The photoacoustic pH measurements were conducted by injecting 0.5 mL of the sample solution into the sample flow cell and adjusting the position of the sample solution plug with an air bubble that was pushed into the tubing with the syringe. When the sample reached the glass sample window on the flow cell, its motion through the tube was stopped and the measurement was taken.

It was noted during setup and tuning of the photoacoustic system that the glass sample window gave a photoacoustic signal. The red food coloring was flushed out of the system, and the signal from the sample cell was located on the oscilloscope. After locating this signal, another red food coloring sample was introduced into the glass sample cell. The arrival times of the two signals at the detection transducer could be resolved; therefore the signal from the glass sample window could be disregarded with respect to the signal from the column of sample within the glass tubing (see Figure 4.4)
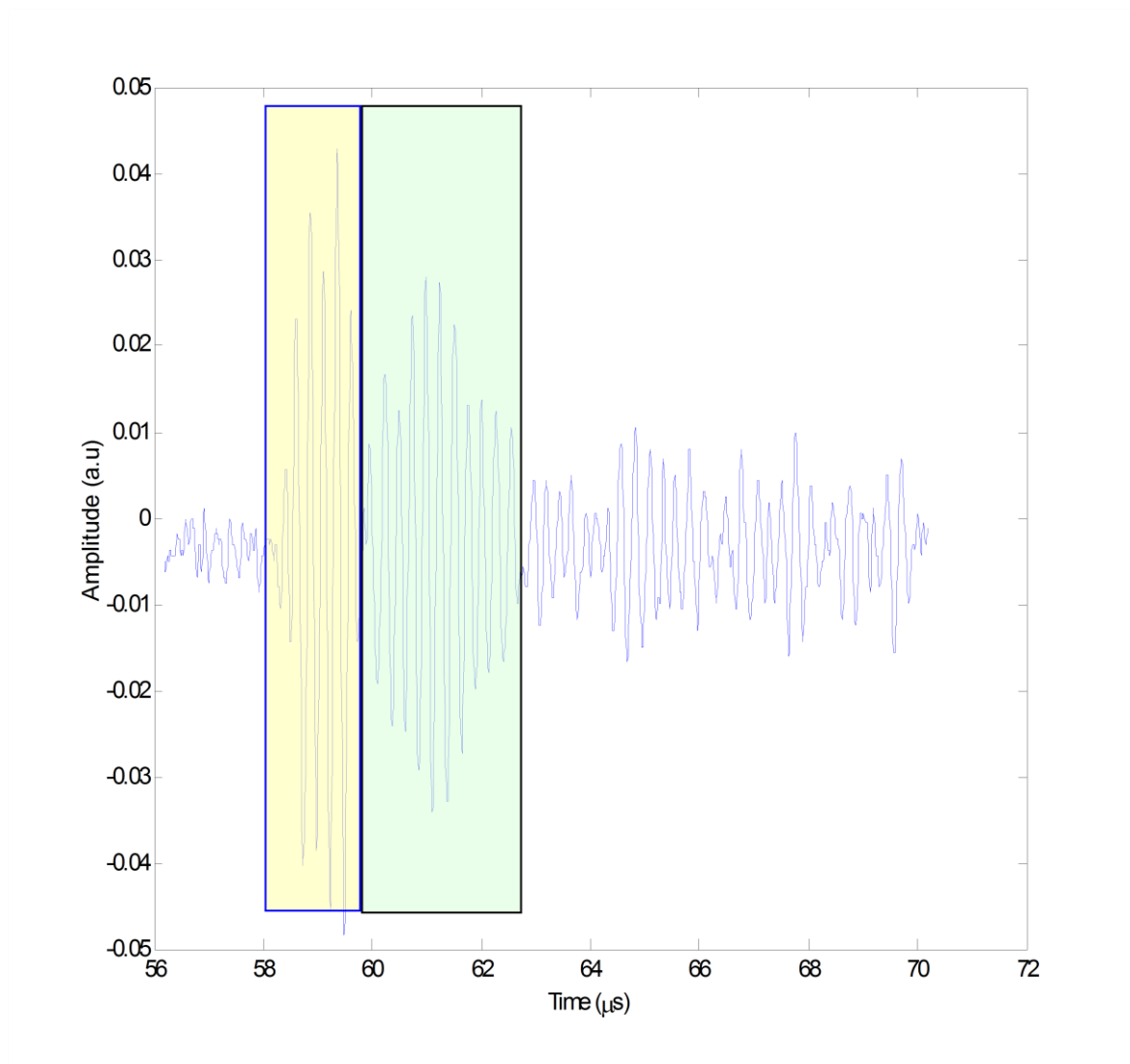
Figure 4.4: Raw signal recorded on the oscilloscope that was measured from the detection transducer in the acoustic tank. The first region in time represents the signal from the glass sample window. The second region represents the signal from the SNARF-5F sample.

The data for the pH insensitive isosbestic point are plotted in Figure 4.5. This plot of the mean photoacoustic response for the four independent measurements shows relative stability for the SNARF-5F dye as a function of pH

114

at 532 nm excitation. The data plotted in Figure 4.6 shows an increasing photoacoustic response as the sample pH increases when the sonophore is excited with 564 nm light. This trend in the data is validated when comparing to the enhanced absorption of SNARF-5F at increasing pH (see Figure 4.3 for the absorption spectra).
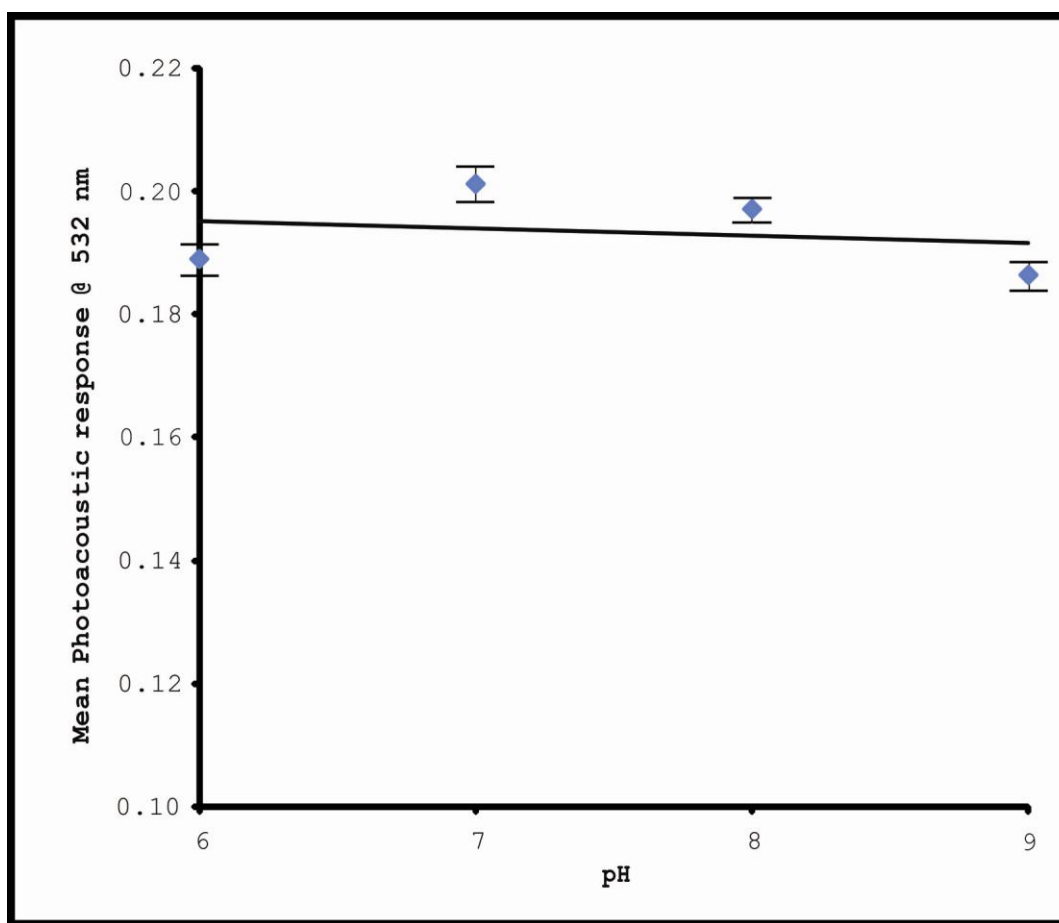

Figure 4.5: The photoacoustic response for 43.2 µM SNARF-5F sonophore dye solution, at 532 nm excitation, in pH 6 through pH 9 buffered solutions. The error bars represent the standard deviation calculated for these data points.

		PA Response @532 nm			
		Mean 1	Mean 2	Mean 3	Mean 4
pH 6	6	0.1905	0.1915	0.186	0.1876
pH 7	7	0.1985	0.2005	0.2052	0.2004
pH 8	8	0.1936	0.1959	0.1981	0.2006
pH 9	9	0.1832	0.1858	0.1879	0.1883

Table 4.1: Mean photoacoustic data over the course of four randomized measurements for four different pH buffered solutions.
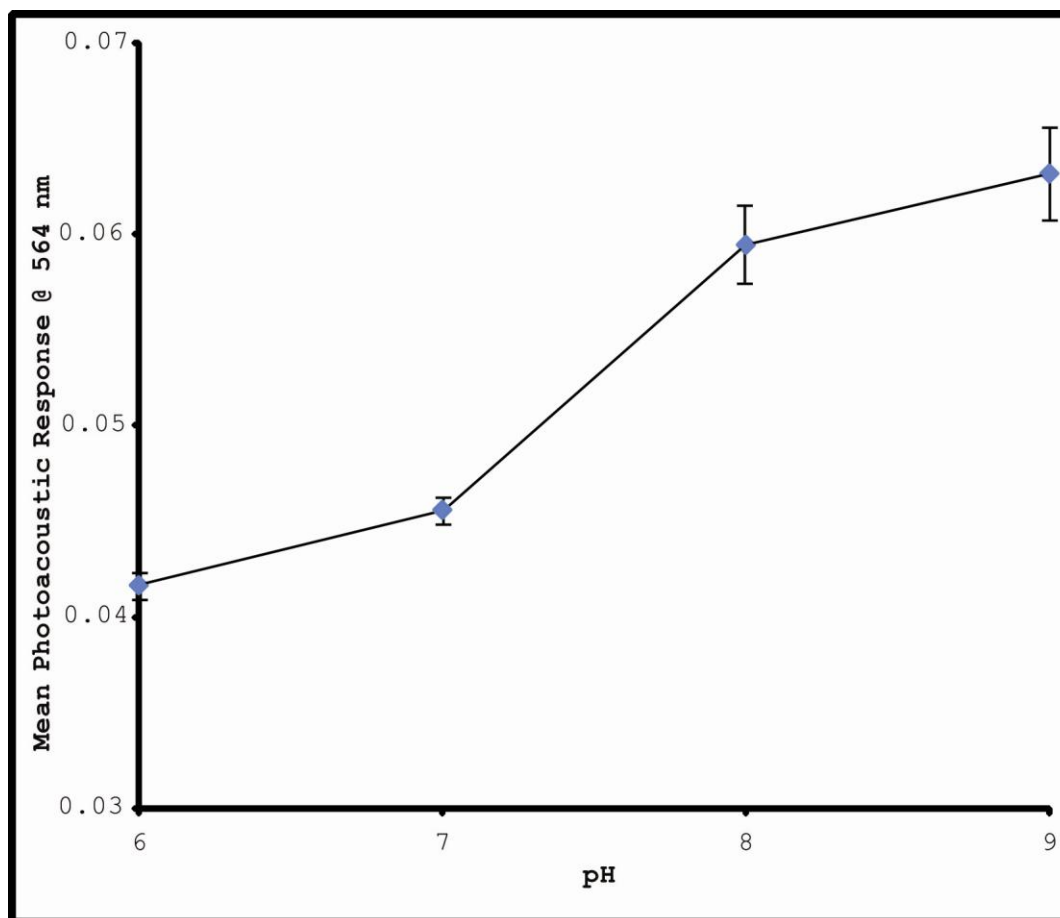

Figure 4.6: The photoacoustic response for 43.2 µM SNARF-5F sonophore dye solution, at 564 nm excitation, in pH 6 through pH 9 buffered solutions. The error bars represent the standard deviation calculated for these data points.

		PA Response @564 nm			
		Mean 1	Mean 2	Mean 3	Mean 4
pH 6	6	0.0414	0.0408	0.0418	0.0425
pH 7	7	0.0451	0.0449	0.0459	0.0464
pH 8	8	0.0578	0.0577	0.0617	0.0607
pH 9	9	0.0597	0.0636	0.0653	0.0642

Table 4.2: Mean photoacoustic data over the course of four randomized measurements for four different pH buffered solutions.

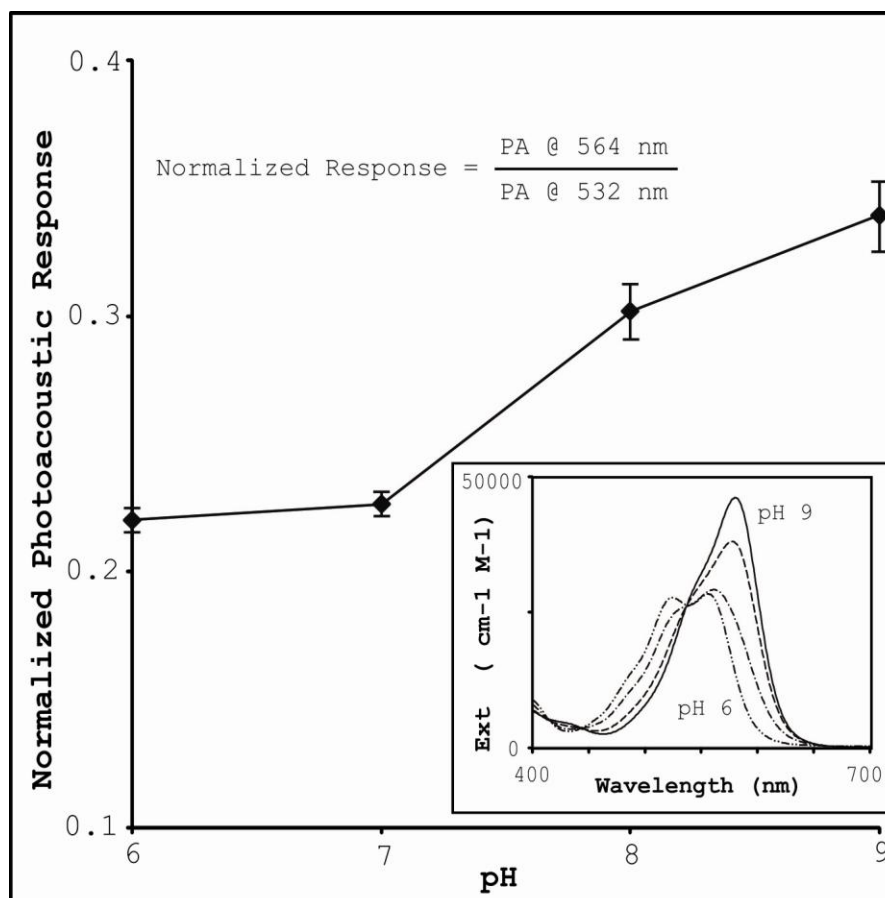Figure 4.7: Normalized photoacoustic response calibration plots for the SNARF-5F pH sonophore dye solution. The error bars represent the relative error propagated for the ratio of the photoacoustic response at 564 nm with respect to that of the photoacoustic response at 532 nm for the four independent measurements. Inset is the normalized Extinction spectra for tSNARF-5F sonophore as a function of pH.

4.6 RESULTS AND DISCUSSION

The results in figure 4.7 show that the ratiometric, photoacoustic response of the pH sensitive sonophore, SNARF-5F, is a monotonic function of pH with highest sensitivity in the 7-8 pH range. When illuminating the dye samples with the 532 nm pump laser excitation, near the isosbestic point of the dye, the overall photoacoustic response was relatively constant over the course of all the measurements. When the dye was excited at 564 nm, the photoacoustic response increased as a function of pH, which matches the expected result because the pH indicator dye SNARF-5F exhibits an increase in absorption as the pH of the solution increases (see Figure 4.7 inset).

In conclusion, it has been shown that when using SNARF-5F as a pH sensitive sonophore, organic indicator dyes can be used as photoacoustic sensor/contrast agents for pH sensing and imaging. These measurements show proof-of-principle for chemical measurements based on photoacoustic imaging, and also show potential for *in-vivo* biochemical imaging. In order to utilize this method for *in vivo* pH imaging deep in tissue, NIR absorbing dyes will have to be utilized to increase penetration depth in tissue. This method can also be generalized to be used with

nanoparticle "PEBBLE" sensors[28,29], to cover a wider range of analytes and to enable targeting to specific in-vivo locations[30].

It would have to be investigated to see if a different optical setup could be utilized to extend the photoacoustic response across the dynamic range between pH 7 and pH 8 for this system. The acoustic tank set up utilized a small piece of glass tubing for a sample window. Based on the acoustic impedence of glass, just 7% of the available sound escaped through the glass tubing. At the time of the experiment the glass tubing had to be used because of the optical burning of the Tygon plastic tubing that occured with each pulse of the dye laser system. The current transducer arrangement may not be optimal for the acquisition of sonophore signal changes in sensing applications. These measurements were proof-of-concept measurements to see if the photoacoustic effect could be extended to making chemical measurements, and ultimately to see if chemical indicator dyes could be extended to use as sensing contrast agents for photoacoustic imaging *in vivo*.

4.7 ACKNOWLEDGEMENTS

4.8   REFERENCES

1.   Bell,A.G.,   Production   of   sound   by   radiant   energy.,
     Phil. Mag. **1881,** *11*:156-158.

2.   Adelhelm,   K.,   Faubel,   W.,   Ache,   H.J.,   Laser   induced
     photoacoustic   spectroscopy   in   liquid   samples:
     temperature   and   solvent   effects.,   Fresenius   J.   Anal.
     Chem. **1998,** *338*:259-264.

3.   Karabutov,   A.A.,   Savateeva,   E.V.,   Oraevsky,   A.A.,   Real-
     Time   Optoacoustic   Monitoring   of   Substance   Penetration   in
     Tissue.,   Proc.   SPIE,   Biomedical   Optoacoustics   II   **2001,**
     4256:61-70.

4.   Zhao,   Z.,   Myllylä,   R.,   Photoacoustic   determination   of
     glucose   concentration   in   whole   blood   by   a   near-infrared
     laser   diode.,   Proc.   SPIE,   Biomedical   Optoacoustics   II
     2001, *4256*:77-83.

5.   Sawada,   T.,   Oda,   S.,   Shimizu,   H.,   Kamada,   H.,   Laser-
     Induced   Photoacoustic   Spectroscopy   of   Some   Rare   Earth
     Ions   in   Aqueous   Solutions.,   Anal.   Chem.   **1979,** *51*:688-
     690.

6.   Schlageter,   B.,   Pörting,   Straßburger,   J.,   Moreno-Bondi,
     M.C.,   Braslavsky,   S.E.,   Oliveros,   E.,   Braun,   A.M.,
     Development   of   an   Optoacoustic   sensor   module   for   pH
     and/or CO2 determination in aqueous solutions.,   Sensors
     and Actuators B. **1997,** *38-39*:443-447.

7.   Adams,   M.J.,   Beadle,   B.C.,   King,   A.A.,   Kirkbright,
     G.F.,   Analytical   Optoacoustic   Spectrometry.,   Analyst
     1976, *101*:553-561.

8. Oraevsky,   A.A.,   Karabutov,   A.A.,   Solomon,   S.V.,
     Savateeva,   E.V.,   Andreev,   V.G.,   Gatalica,   Z.,   Singh,   H.,
     Fleming,   R.D.,   Laser   optoacoustic   imaging   of   breast

cancer *in vivo.*, Proc. SPIE, Biomedical Optoacoustics II **2001,** *4256*:6-15.

9. Manohar, S., Vaartjes, S.E., van Hespen, J.C.G., Klaase, J.M., van den Engh, F.M., Thé, A.K.H., Steenbergen, W., van Leeuwen, T.G., Region-of-breast studies using the Twente Photoacoustic Mammoscope (PAM)., Proc. SPIE, Optoacoustics, and Acousto-optics. **2007,** *6437*:643702-1 – 643702-9.

10. Oraevsky, A.A., Andreev, V.A., Karabutov, A.A., Fleming, D.R., Gatalica, Z., Singh, H., Esenaliev, R.O., Laser Opto-Acoustic Imaging of the Breast: Detection of Cancer Angiogenesis., Proc. SPIE **1999,** *3597*:352-363.

11. Konstantin, M., Wang, L.V., High-resolution photoacoustic vascular imaging in vivo using a large-aperture acoustic lens., Proc. SPIE, Photons Plus Ultrasond: Imaging and Sensing **2005,** *5697*:7-14.

12. Li, L., Zemp, R.J., Lungu, G., Stoica, G., Wang, L.V., Photoacoustic imaging of lacZ gene expression *in vivo.*, Journal of Biomedical Optics **2007,** *12*:020501-1-020504-3.

13. Kim, G., Huang, S.W., Day, K.C., O'Donnell, M., Agayan, R.R., Day, M.A., Kopelman, R., Ashkenazi, S., Journal of Biomedical Optics **2007,** *12*:044020-1-044020-8.

14. Ku, G., Wang, L.V., Deeply penetrating photoacoustic tomography in biological tissues enhanced with an optical contrast agent., Opt. Lett. **2005,** *30*:507-509.

15. Liu, J., Diwu, Z., Leung, W.Y., Synthesis and Photophysical Properties of New Fluorinated Benzo[C]xanthenes Dyes as Intracellular pH Indicators., Bioorganic & Medicinal Chemistry Letters **2001,** *11*:2903-2905.

16. Eberhard, M., Erne, P., Calcium Binding to fluorescent calcium indicators: Calcium Green, Calcium Orange and Calcium Crimson., Biochem. Biophys. Res. Commun. **1991**, *180*:209-215.

17. Meuwis, K., Boens, N., De Schryver, F.C., Gallay, J., Vincent, M., Photophysics of the Flourescent K+ Indicator PBFI., Biophys. J. **1995**, *68*:2469-2473.

18. Minta, A., Tsien, R.Y., Fluorescent Indicators for cytosolic sodium., J. Biol. Chem. **1989**, *264*:19449-19457.

19. Sensi, S. L., Ton-That, D., Weiss, J.H., Rothe, A., Gee, K.R., A new mitochondrial fluorescent zinc sensor., Cell Calcium **2003**, *34*:281-284.

20. Raju, B., Murphy, E., Levy., L.A., Hall, R.D., London, R.E., A fluorescent indicator for measuring cytosolic free magnesium., Am. J. Physiol. **1989**, *256*:C540-C548.

21. Verkman, A.S., Development and biological applications of chloride-sensitive fluorescent indicators., Am. J. Physiol. **1990**, *256*:C375-C388.

22. Kojima, H., Nakatsubo, N., Kikuchi, K., Kawahara, S., Kirino, Y., Nagoshi, H., Hirata, Y., Nagano, T., Detection and imaging of nitric oxide with novel fluorescent indicators: diaminofluoresceins., Anal. Chem. **1998**, *70*:2446-2453.

23. O'Riordan, T.C., Fitzgerald, K., Ponomarev, G.V., Mackrill, J., Hynes, J., Taylor, C., Papkovsky, D.B., Sensing intracellular oxygen using near-infrared phosphorescent probes and live-cell fluorescence imaging., Am. J. Physiol. Regul. Integr. Comp. Physiol **2007**. *292*:R1613-R1620.

24. Plásek, J., Sigler, K., Slow fluorescent indicators of membrane potential: A survey of different approaches to probe response analysis., J. Photochem. Photobiol. B **1996**, *33*:101-124.

25. Baruch, A., Jeffery, D.A., Bogyo, M., Enzyme activity – it's all about image., Trends in Cell Biology **2004**, *14*:29-35.

26. Wang, L.V., Ultrasound-mediated biophotonic imaging: A review of acousto-optical tomography and photo-acoustic tomography., Disease Markers **2003-2004**, *19*:123-138.

27. Jacques, S.L., Paltauf, G., Modeling pressure waves generated by pulsed laser irradiation of irregularily shaped absorbing objects within media., Proc. SPIE, Biomedical Optoacoustics II **2001**, *4256*:90-100.

28. Buck, S.M., Koo, Y.E.L., Park, E., Xu, H., Philbert, M.A., Brasuel, M.A., Kopelman, R., Current Option in Chemical Biology **2004**, *8*:540

29. Koo, Y.E.L., Agayan, R., Philbert, M.A., Rehemtulla, A., Ross, B.D., Kopelman, R., New Approaches in Biomedical Spectroscopy, ed. Kneipp, K., Aroca, R., Kneipp, H., and Wentrup-Byrne, E., **2007**, ch. 13, pp. 200-218.

30. Reddy, G.R., Bhojani, M.S., McConville, P., Moody, J., Moffat, B.A., Hall, D.E., Kim, G., Koo, Y.E.L., Woolliscroft, M.J., Sugai, J.V., Johnson, T.D., Philbert, M.A., Kopelman, R., Rehemtulla, A., Ross, B.D., Clin. Cancer Res. **2006**, *12*:6677.

CHAPTER 5

SUMMARY AND FUTURE WORK

Chapter 1 offers a brief background into nanotechnology and the development of PEBBLE nanosensors. Also introduced in Chapter 1 is the basis for this body of work that included fluorescence anisotropy based measurements of analytes in solution, photoacoustic sensing of pH using the pH "sonophore" SNARF-5F indicator dye, and the attempt to create a SERS based PEBBLE using an amine functionalized silica-silver nanoprism core-shell based nanoplatform.

Chapter 2 details the fluorescence anisotropy based experiments conducted for the Newport Green based Zn^{2+} sensor nano-PEBBLEs. The fluorescence anisotropy based calibration shows a decreasing fluorescence anisotropy response with increasing $Zn^{2+}_{(aq.)}$ concentration. This is the response one would expect because of the increased excited state lifetime of the dye in the presence of the $Zn^{2+}_{(aq.)}$ analyte. The calibration curve shows an anisotropy

decrease of 0.060 anisotropy units over a usable dynamic range of approximately 0 to 10 μM zinc. For the free dye, an anisotropy decrease of approximately 0.1 anisotropy units is exhibited over a dynamic range of 0 to 15 μM zinc. The overall sensitivity of the PEBBLEs was somewhat less than the Newport Green free dye (see Figure 2.4).

The Calcium Green nano-PEBBLE studies also exhibit an increase in the excited state lifetime in the presence of $Ca^{2+}_{(aq.)}$. The anisotropy decrease in the dextran linked Calcium Green dye is approximately 0.045 anisotropy units is exhibited across the usable dynamic range from 0 to 1.5 μM calcium. For the calcium Green PEBBLEs, the drop in the anisotropy exhibited across the same dynamic range is approximately 0.040 anisotropy units. (see Figure 2.5).

An interesting and important result was observed in a study of the interference effects of Bovine Serum Albumin (BSA). The overall change in the fluorescence anisotropy of an ensemble of Calcium Green PEBBLEs with 60 μM $Ca^{2+}_{(aq.)}$ and 0.05% BSA showed almost no increase in the fluorescence anisotropy. Conversely, when the 10,000 Mw dextran Calcium Green "free" dye was tested with the 60 μM $Ca^{2+}_{(aq.)}$ and 0.05% BSA, the fluorescence anisotropy increased from about 0.12 to about 0.28. The EGTA was added to complex any Ca^{2+}

present in the suspension prior to measurement, so that the zero free Ca^{2+} is truly a zero point measurement. With the addition of an aliquot of $CaCl_2$ $_{(aq.)}$ stock, the final concentration of Ca^{2+} in the suspension was 60 μM, but the free Ca^{2+} concentration would be less because an equilibrium was established between free Ca^{2+} and EGTA chelated Ca^{2+} in the suspension. These data show that the dextran bound Calcium Green dye is firmly embedded in the interior of the PEBBLE and therefore protein interference such as BSA cannot alter the fluorescence anisotropy based measurements (see Figure 2.6). This clearly elucidates the advantages of PEBBLE nanosensors for biomedical studies.

A third experiment measuring the fluorescence anisotropy response of ruthenium based sol-gel PEBBLEs in response to $O_{2(g)}$ concentration also showed positive results. When ruthenium chelate is in the excited state, the presence of $O_{2(g)}$ will quench the excited state and the long-lived excited state will shorten. Thus one would expect the fluorescence anisotropy of the $O_{2(g)}$ sensing PEBBLEs to increase as more $O_{2(g)}$ is introduced into the system as is indeed observed (see Figure 2.7).

Chapter 3 discusses the progress for the development of a SERS based PEBBLE that would be based on an aminated silica-silver nanoprism core-shell nanoplatform.

Experimental conditions were optimized on the Raman microscope so that SERS spectra were acquired for a 20 μM 4-MPy sample that was prepared for four different commercially available spherical silver colloid suspensions that were 20, 40, 60, and 80 nm in diameter. These colloidal suspensions were suspended in 100 mM KCl electrolyte solution (purchased from Ted Pella, Inc.).

After having produced a null result on many attempts at acquiring a SERS spectrum for 4-MPy on the Ag nanoprism colloid, it was suspected that the organic capping agent poly(vinyl pyrrolidone) was interfering with the acquisition of the signal. This suspicion was tested by performing an experiment on two samples of 60 nm colloid suspended in 2 mM KCl electrolyte solution with 10 μM 4-MPy. One of the samples had 41 μM of poly (vinyl pyrrolidone) (PVP, Mw = 29,000 g/mol) added in order to mimic the PVP concentration present in nanoprism synthesis (see Figure 3.9). A significantly weaker SERS spectrum was observed from the sample with the PVP dissolved in it. It is thought that PVP, at the concentration present in the nanoprism synthesis either inhibits the adsorption of the 4-MPy analyte onto the surface of the nanoprism colloid, or the PVP sequesters the 4-MPy and will not allow it to get

into close proximity to the silver nanoprisms in suspension.

Work published late in 2007 performs a comparison of the non-resonant SERS enhancement for silver nanoprisms, silver nanorods, and spherical silver colloid. The SERS enhancement was much stronger than the enhancements for the nanorods or spherical colloid. The authors attribute the increased enhancement of the nanoprism colloid due to a chemical enhancement mechanism exhibited by the colloid, and to a lightening rod effect due to the particles shape morphology. The authors mention that they used a photo-mediated method to synthesize the nanoparticles, but in the materials section of the publication they do not specifically mention which capping agent was used to synthesize the nanoprism colloid.

Chapter 4 discusses the development of a photoacoustic sensing based laser system in order to measure the photoacoustic response of the sonophore SNARF-5F as a function of pH (see Figure 4.7). In the experiment, the photoacoustic response increased as a function of an increasing pH from 6 to 9. This is the trend that one would expect based on the absorption shift of the SNARF-5F dye as a function of pH. These measurements show proof-of-principle for chemical measurements based on photoacoustic

imaging, and also show potential for *in-vivo* biochemical imaging.

In order to utilize this method for *in vivo* pH imaging deep in tissue, NIR absorbing dyes will have to be utilized to increase penetration depth in tissue. This method can also be generalized to be used with nanoparticle PEBBLE sensors, to cover a wider range of analytes and to enable targeting to specific in-vivo locations. Research areas of interest where this experimental technique would be directly applicable would be analytical biochemistry measurements of pH in whole intact tissue or in *in vivo* animal models. With careful selection of sonophores, this technique could apply to the detection and diagnosis of disease states that alter the pH, or that alter other analytes of interest, in tissue or biological fluids. Specific examples include cancer, inflammation and diseases associated with gastric acidity.

FUTURE WORK

In order for the photoacoustic sensing method described in Chapter 4 to be utilized for sensing or imaging *in vivo* pH, a new NIR absorbing dye will have to be utilized that absorbs where tissue is optically transparent (> 750 nm). Currently, these NIR pH sensitive dyes are not commercially available, and experience with collaborations has proven to be plagued with problems in synthetic reproducibility. If such an elusive dye can be purchased, synthesized, or isolated from a natural source, then a PEBBLE pH sensor/contrast agent could be developed for *in vivo* imaging.

APPENDIX A

PHOTOACOUSTIC MEASUREMENT OF Ca^{2+} CONCENTRATION WITH THE RHOD-5N SONOPHORE

A.1 Introduction

With the proof-of-concept photoacoustic sensing experiment described in Chapter 4 for the pH sensitive sonophore SNARF-5F, the Rhod-5N dye (Invitrogen, Eugene, OR, USA) was investigated to see if it could be used to photoacoustically measure Ca^{2+} concentrations in neat solutions. In the case of the SNARF-5F sonophore, the change in the photoacoustic signal was a result of an increase in the absorption of the dye at the probed wavelength of 564 nm, that was a function of an increase in the pH of the samples. This increased absorption of the indicator dye lead to an increase in the heat evolved in the solvent, and thus an increase in the amplitude of the pressure wave launched from the thermoelastic expansion of the solvent. This effect resulted in an increasing photoacoustic response as the pH of each sample was increased.

In the case of the Rhod-5N indicator, the absorption of the dye does not change as a function of the analyte concentration (See Figure A.1); therefore the change in the fluorescence response of the dye is due to a change in the fluorescence quantum yield of the dye (See Figure A.2). With the change in the quantum yield as a function of the analyte concentration, one would expect that the photoacoustic response would decrease as a function of analyte concentration for Rhod-5N. This decrease in the photoacoustic response would be due to the proportion of excited state electrons in the population of dye molecules that undergo transition to the ground electronic state from the excited electronic state via fluorescence instead of radiationless decay mechanisms. So an increase in the fluorescence of the dye reduces the radiationless decay of the dye; therefore reducing the heat evolved in the solvent, and reducing the photoacoustic response of the dye.
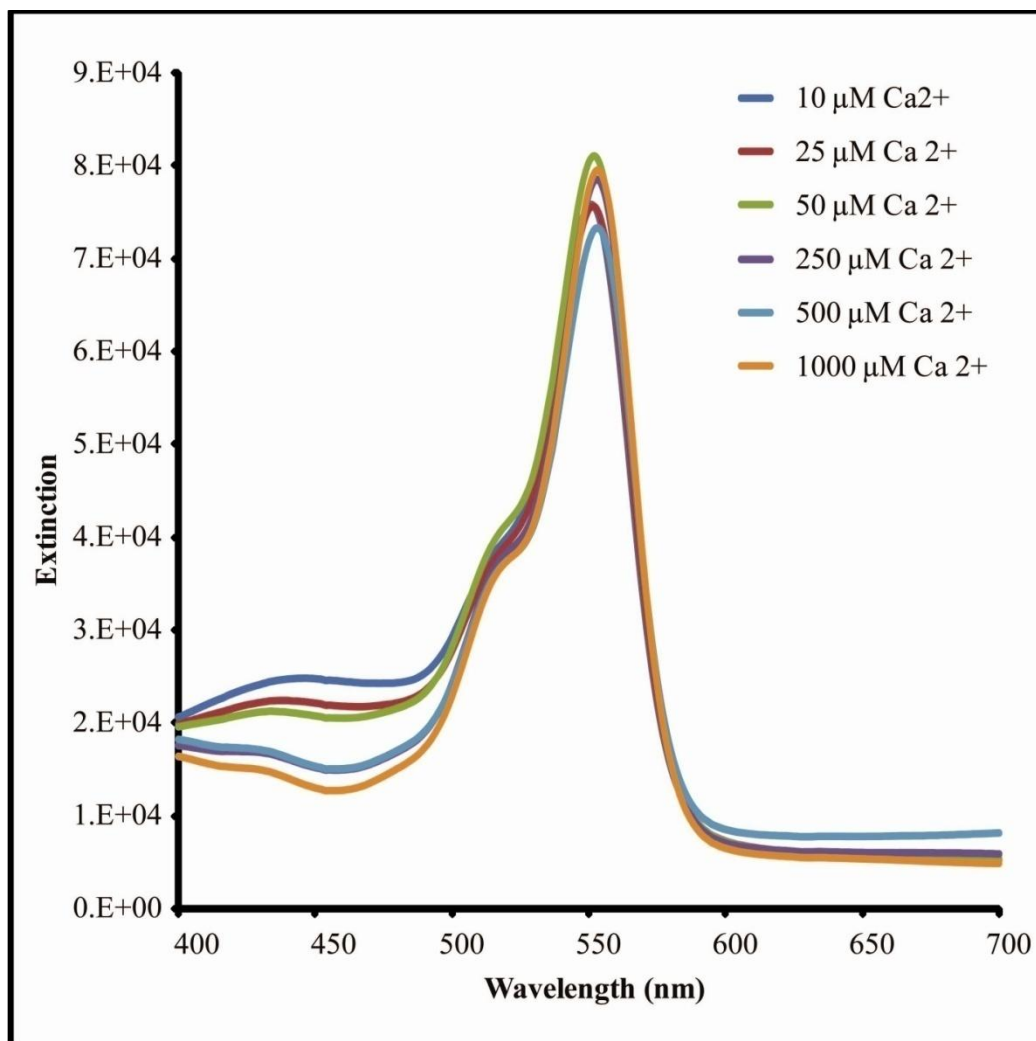
Figure A.1: The UV-Vis Extinction spectra for 10 µM Rhod-5N dye samples with varying concentrations of Ca^{2+}.
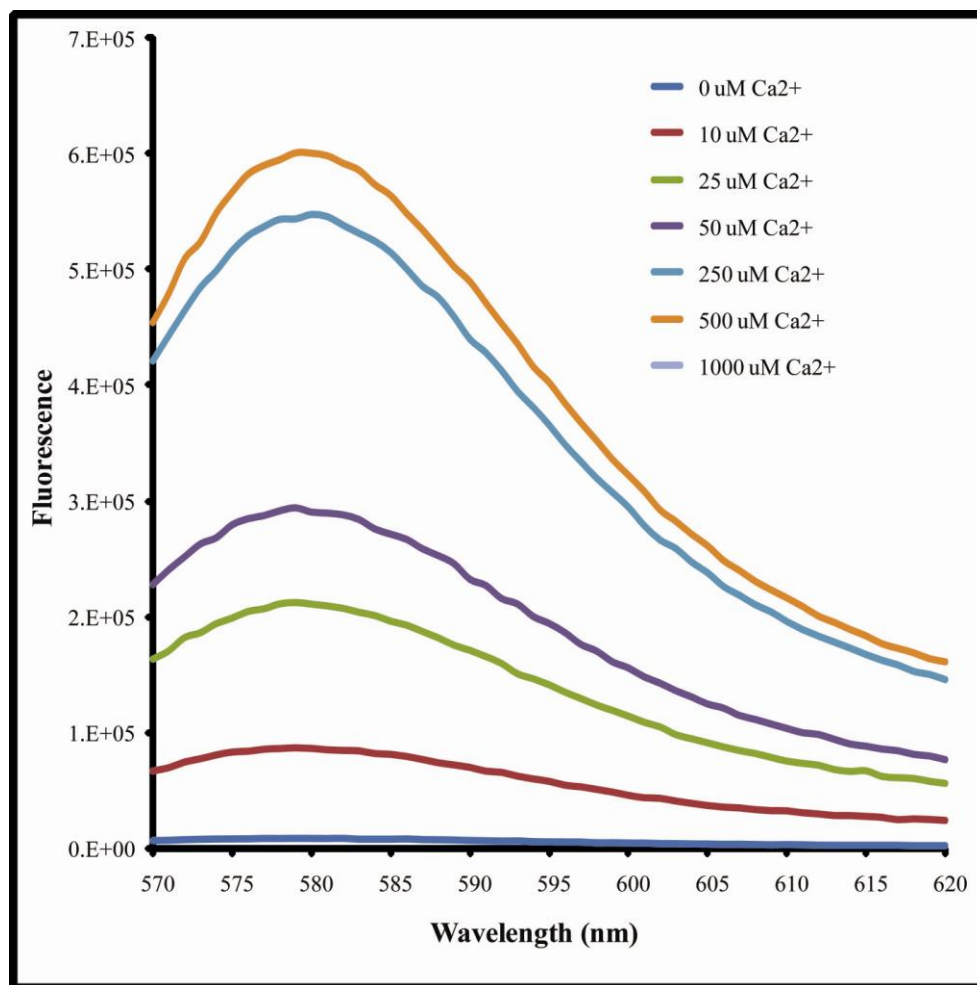
Figure A.2: Fluorescence spectra for 10 μM Rhod-5N dye samples with varying concentrations of Ca^{2+}.

A.2 EXPERIMENTAL SET UP

An optical set up was used that was similar to the work described in Chapter 4 for the photoacoustic pH sensing experiments (See Figure A.3 (a.)). A frequency doubled Surelite I10 Continuum® Nd:YAG laser (420 mJ, 10 Hz repetition rate, Continuum Inc., Santa Clara, CA, USA) at 532 nm emission was used as the pump laser for the dye

laser set up. The laser was operated with a Q-switch delay of 320 µS.

The dye laser system used for this experiment was a Lambda Physik, Lasertechnik Scanmate® dye laser (Coherent Inc., Santa Clara, CA, USA). The laser dye that was used for the experiment was rhodamine 590 chloride (Exciton Inc., Dayton, OH, USA), which was dissolved in methanol (Sigma-Aldrich, St. Louis, MO, USA) and excited at 532 nm. The emission from the dye laser was set at 564 nm, in order to excite the Rhod-5N Ca^{2+} indicator dye in the samples. The first pre-amplifier (shown in figure A.3 (b).) was used to increase the signal (+30 dB) for the sample absorption and photoacoustic signals from the Rhod-5N dye in the sample. The sample absorption was measured by measuring the photoacoustic response from absorption from the black rubber on the face of the transducer active element. The second amplifier was used to decrease the signal (-10 dB) from the photoacoustic response for the normalization transducer that was generated on the front face of the active element for the transducer. The amplitude of the signal was reduced so that it was on the same scale as the fluorescence signal that would be measure on the same channel of the oscilloscope. The LeCroy WaveSurfer 350 MHz oscilloscope was set so that channel 1 averaged 20

acquisitions with the scale set to 50 mV/Division, and this channel was used to acquire the signal from the absorption and photoacoustic response from the dye using the detection transducer. Channel 2 was set to average 20 signal acquisitions for the amplified (-10 dB) normalization signal and the unamplified fluorescence signal. The vertical scale for this channel was set to 20 mV/Division.

The sophisticated sample cell was set up for this experiment so that the photoacoustic response, dye absorption, normalization signal, and fluorescence from the dye could be monitored while the sample was stirred (with a magnetic stir bar). The sample block was machined from a block of Lexan, that had a small channel (~ 40 mL in total volume) machined into the block to act as a sample well (See Figure A.3 (b)). A port was machined into the front of the sample block so that a quartz window could be glued into place on the block to allow the incident laser light to enter the sample block. Another hole was machined on the other side of the sample block so that the detection transducer could be glued into place in the sample block in order to be in contact with the sample. When the block was fixed in place, a beam expander was put in the incident light from the laser to diffuse the beam to prevent photobleaching of the sample. A beam splitter was also put

in the path of the beam just before the sample window. It split a portion of the beam off so that the laser emission could be monitored by the normalization transducer (5 MHz, flat face transducer). The portion of the beam that went through the splitter excited the Rhod-5N dye and the photoacoustic response was measured by the detection transducer(). When the Rhod-5N fluoresced, a certain portion of light hit the beam splitter and was reflected in the opposite direction of the normalization transducer. This fluorescence was captured by a lens, and the Rayleigh scattered light was filtered with a 570 nm cutoff filter. The fluoresecence was measured with a photo-diode detector.

The photoacoustic cell was designed so that temperature control and termperature monitoring could be incorporated into the measurements (see Figure A.3 (b)). The heater coil was simply a "knot" of coated wire that was dropped into the sample well. The two ends of the wire were connected to a Hewlett Packard, E3630A Triple Output Power Supply that was set to 6.71 volts and 0.59 Amps. A Thermistor was dropped into the sample cell to monitor the temperature fluctuations over the course of the measurement. The thermistor was attached to a voltmeter, and the system was allowed to reach thermal equilibrium with the addition of the sample heating coil. The

voltmeter registered 0.905 Volts for the length of the measurement. A magnetic stir bar was added to the sample cell to re-circulate the sample in the well, and to ensure complete mixing when the analyte was added. The magnetic stir plate was mounted on the bottom of the aluminum support plate that held the sample block at the correct height for the laser illumination.
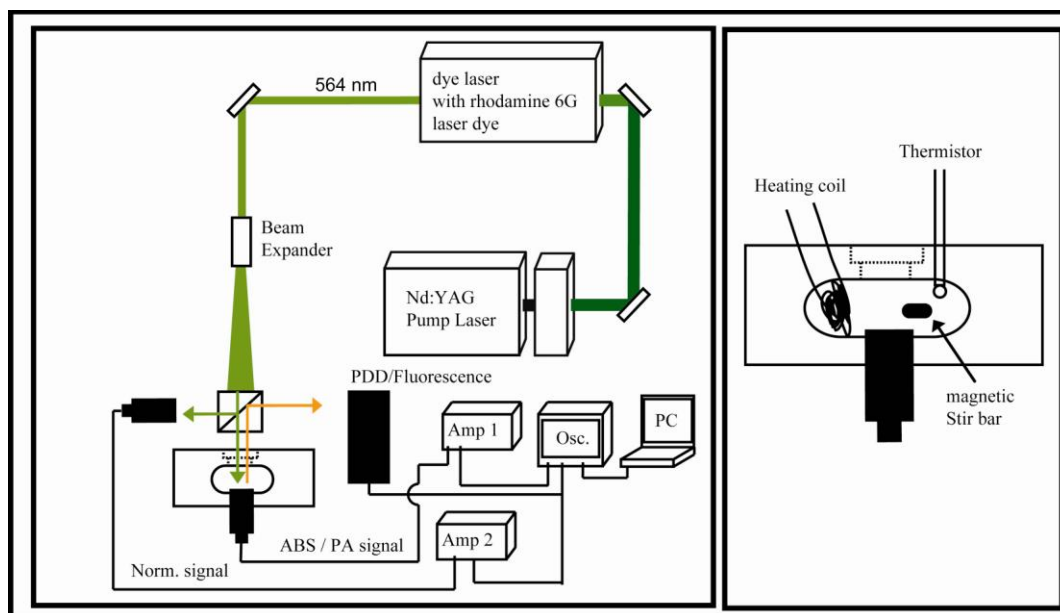

Figure A.3 (a.) The optical set up for the Rhod-5N experiments. (b.) A blow up of the photoacoustic cell showing the magnetic stir bar for sample circulation, the heating coil for thermal control, and a thermistor to monitor the temperature.

A.3 Sample Preparation

The photoacoustic sample was prepared in a metal free plastic vial. To the vial, a 39.96 mL of a 10 mM metal free pH 7.38 buffer was added to the vial. Present in the buffer was 138 mM NaCl, so no salt was added. An aliquot of a dye stock was added so the final dye concentration in the sample was 1 µM. In order to have a true 0-point Ca^{2+} measurement, A 40 mL aliquot of 10 mM EGTA solution was added to the sample well, with the heating coil, the thermistor, and the stir bar present. The EGTA solution was allowed to set in the well overnight so that all of the free Ca^{2+} in the system would be chelated. Before the Rhod-5N sample was added, the chelation solution was removed from the sample well, and the well with the heating coil, thermistor, and the stir bar was triple rinsed with 18 MΩ Deionized water.

A.4 Experiment

The laser system was turned on and allowed to operate for a period of 30 minutes to reach equilibrium. The Rhod-5N sample was poured into the sample well, and the power supply for the heating coil and the voltmeter for the thermistor were both switched on so that thermal equilibrium within the sample could be reached. The sample

sat idle for approximately 1 hour so that thermal equilibrium could be reached.

The measurement was started at zero free calcium, and the measurement was acquired for approximately 100 data points before the addition of an aliquot to make the final concentration of Ca^{2+} in the sample 1 mM. Each data point is representative of the photoacoustic response, normalization response, or fluorescence based on an average of 20 acquisitions. It was noted at the start of the experiment that the normilazation signal (see Figure A.4), photoacoustic response (see Figure A.5), and the fluorescence (see Figure A.6) were all stable prior to starting the experiment.
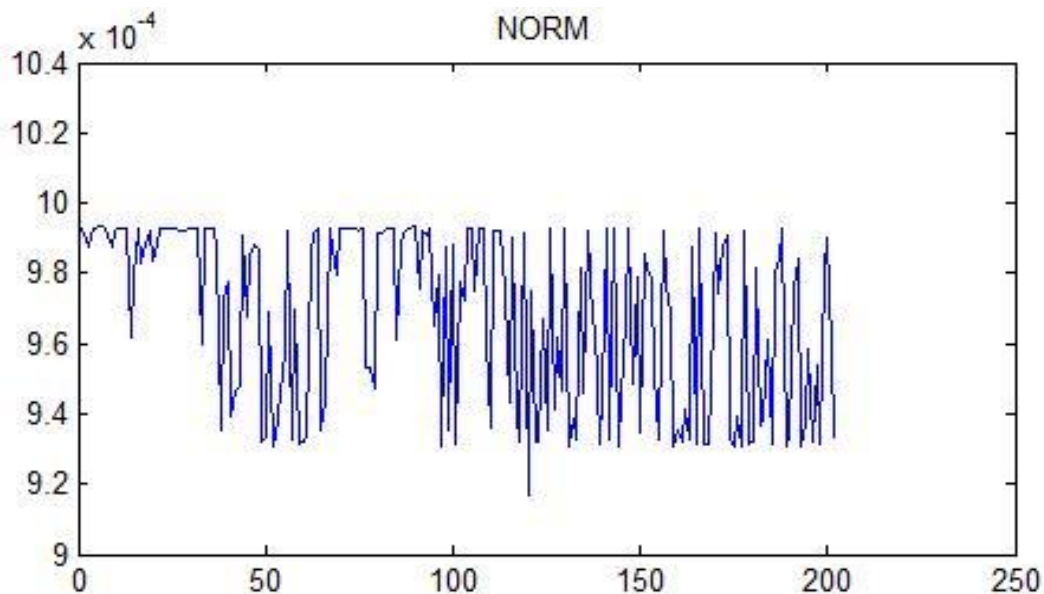
Figure A.4: The normalization signal for the experiment showing that the laser system was stable before making the measurement.
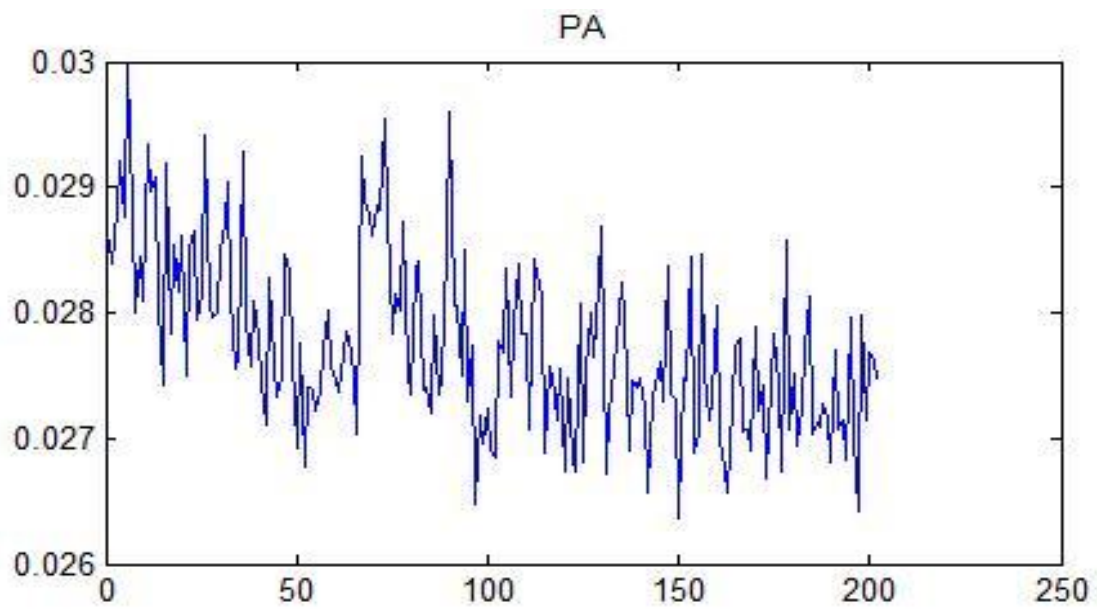
Figure A.5: The photoacoustic response for the Rhod-5N dye sample. Note that there is no change in the Response near the 100 data point.
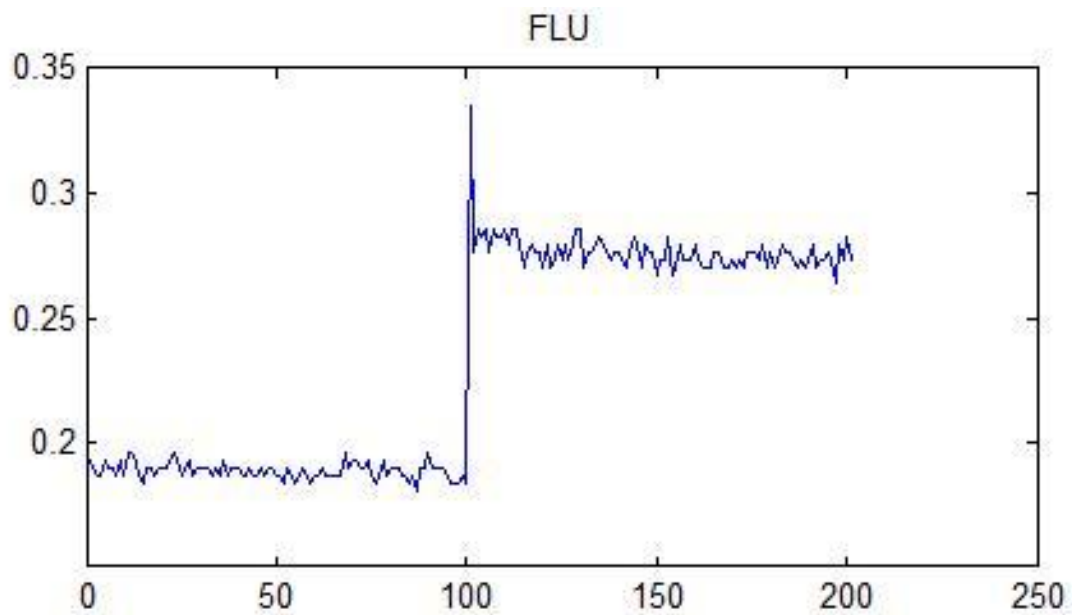

Figure A.6: The fluorescent response of Rhod-5N with the addition of Ca^{2+}.

A.5 Result

The results for this experiment was that after approximately 100 data points had been acquired, an aliquot of a Ca^{2+} stock was added so that the final analyte concentration was 1 mM in the sample. The addition of the Ca^{2+} caused the fluorescent signal to double, but there was no corresponding change in the photoacoustic response of the dye. The conclusion was made that the overall change in the quantum yield for the Rhod-5N must be to small to observe a change in the photoacoustic response with the current photoacoustic sensing set up.

A.6 Acknowledgements